

# Preview Control for Wind Turbines

A DISSERTATION  
SUBMITTED TO THE FACULTY OF THE GRADUATE SCHOOL  
OF THE UNIVERSITY OF MINNESOTA  
BY

Ahmet Arda Ozdemir

IN PARTIAL FULFILLMENT OF THE REQUIREMENTS  
FOR THE DEGREE OF  
Doctor of Philosophy

Professor Gary J. Balas  
Professor Peter J. Seiler

August, 2013

© Ahmet Arda Ozdemir 2013

Section 5.4: © 2013 IEEE. Reprinted, with permission, from  
Ahmet Arda Ozdemir, Peter Seiler, Gary J. Balas,  
Design Tradeoffs of Wind Turbine Preview Control,  
IEEE Transactions on Control Systems Technology, July, 2013

ALL RIGHTS RESERVED

# Acknowledgements

I would like to express my endless gratitude for my advisers Gary Balas and Pete Seiler. They have been exceptional guides throughout my graduate studies. They taught me how to think. What I have learned from them is above and beyond what is contained in this thesis. I have been very lucky to have them as my advisers. They will remain as my role models as I progress beyond my graduate studies. I will strive to live up to their high standards.

I would like to thank my thesis committee members Mihailo R. Jovanovic and Demoz Gebre-Egziabher. I learned a great deal from their excellent classes. Their feedback on my research and my thesis was very valuable.

The current and past members of the Lab 309, or formerly Lab 15 as I prefer to call it, have enriched my graduate school experience with their sincere friendship and knowledge. I would like to acknowledge Paul, Andrei, Claudia, Abhijit, Arnar, David, Will, Shu and Bin. We spent countless hours talking about many topics ranging from control theory to random bits of life during our lunch breaks, happy hours and the ‘I am stuck on my research’ breaks we had throughout the day. It was time well spent: I owe my sanity to those moments.

No less important are my friends Kamran, Pietro, Kyung-Hoon, Eyoab and Davide. I have shared countless memories with them that made my time in Minneapolis a special chapter in my life. I would also like to thank Miao for her support during the initial years of my studies.

I am very grateful for the patience and understanding of Briahna. This thesis took away many hours of my time from her. I especially thank her for bearing with the boring me while I was busy writing all the time. I deeply appreciate her support.

Last but not least, I would like to thank my parents for their unwavering love.

*Dedicated to my parents: Zümral and Nutullah Ozdemir*

## Abstract

The success of wind power as a renewable energy source depends on its cost of energy. Wind turbine control has attracted much attention in the controls community due to its potential impact on the cost of wind power. However, novel methods in the literature have not transitioned well to industry. This is because the potential cost benefits of these methods are not well understood. There is a need for basic research to address this issue.

This thesis is one step toward transitioning of advanced control methods in literature to the industry. Particularly, we aim to understand the limits of performance. The potential performance improvements of the advanced methods should be large enough to justify their cost and complexity. We investigate the optimal trade-offs between multiple turbine performance goals. We also explore the use of a novel wind preview sensor in closed-loop control laws. The impact of this novel sensor on the optimal turbine performance is investigated.

The specific contributions of this thesis can be grouped in three categories. First, we present a preliminary, nonlinear optimization based controller design and analysis framework. This framework can simplify the design of the advanced multivariable controllers for nonlinear systems. It can also be used to investigate the optimal design trade-offs between nonlinear performance constraints and objectives. Second, engineering insight is provided into turbine design trade-offs. Third, we provide mathematical tools that quantify the limits of turbine performance in presence of preview wind measurements. Optimization tools that can analyze the trade-off between preview time and operating condition dependent turbine performance objectives are presented. In low wind speeds, our results show that simultaneous power capture improvements and structural load reductions can be obtained. In high wind speeds, a short amount of preview wind information can be used to overcome the fundamental performance limitations imposed by actuator rate constraints. We provide analytical formulas that quantify these preview time requirements and performance limitations. A convex optimization framework is also presented for the analysis of extreme operating conditions that are defined by deterministic wind disturbance trajectories.

# Contents

<b>Acknowledgements</b>	<b>i</b>
<b>Abstract</b>	<b>iii</b>
<b>List of Tables</b>	<b>vii</b>
<b>List of Figures</b>	<b>viii</b>
<b>1 Introduction</b>	<b>1</b>
1.1 Thesis Overview . . . . .	3
1.2 Thesis Contributions . . . . .	5
<b>2 Background</b>	<b>7</b>
2.1 Introduction . . . . .	7
2.2 Types of Turbine Designs . . . . .	8
2.3 Basics of Horizontal-Axis Turbine Operation . . . . .	10
2.4 Current Approaches and Challenges . . . . .	12
<b>3 Wind Turbine Modeling</b>	<b>16</b>
3.1 Introduction . . . . .	16
3.2 Overview of Turbine Modeling . . . . .	17
3.3 Lower Fidelity Models . . . . .	21
3.4 Medium Fidelity Models . . . . .	22
3.4.1 Turbine Dynamics . . . . .	22
3.4.2 Actuator Dynamics . . . . .	25

3.4.3	LIDAR Sensor Dynamics . . . . .	26
3.5	Linear System Approximations . . . . .	27
3.5.1	Linear Time Varying via Linearization . . . . .	28
3.5.2	LTI Approximation and Multiblade Coordinate Transformation . . . . .	30
<b>4</b>	<b>Multivariable Control Design</b>	<b>34</b>
4.1	Introduction . . . . .	34
4.2	Multivariable Control Design Framework . . . . .	36
4.2.1	Problem Formulation . . . . .	36
4.2.2	Design Process . . . . .	39
4.2.3	Auto-Tuning Framework . . . . .	43
4.3	Example Problem: Turbine Region 3 Controllers . . . . .	45
4.3.1	Linear Model and Input-Measurement Transformations . . . . .	47
4.3.2	$H_\infty$ Design Interconnection and the Initial Design . . . . .	49
4.3.3	Cost and Constraint Functions . . . . .	52
4.3.4	Gradient-based Optimization . . . . .	54
4.4	Example Problem Results . . . . .	54
4.5	Conclusions and Recommendations . . . . .	59
<b>5</b>	<b>Preview Control</b>	<b>61</b>
5.1	Introduction . . . . .	61
5.2	Related Work . . . . .	63
5.3	Region 2 Preview Control . . . . .	64
5.3.1	Problem Formulation . . . . .	65
5.3.2	Power Capture versus Drivetrain Loads Trade-off . . . . .	71
5.4	Region 3 Preview Control . . . . .	76
5.4.1	Analytical Results for One-State Turbine Model . . . . .	77
5.4.2	Validation with $H_\infty$ Preview Controllers . . . . .	87
5.5	Preview Control for Extreme Events . . . . .	99
5.5.1	Problem Formulation . . . . .	101
5.5.2	Analysis of a 50-Year Gust . . . . .	104
5.5.3	Generalizations . . . . .	108
5.6	Conclusions . . . . .	109

<b>6 Conclusions and Recommendations</b>	<b>111</b>
<b>References</b>	<b>116</b>

# List of Tables

4.1	Optimization Results . . . . .	55
5.1	Atmospheric parameters used in TurbSim for generating turbulent wind data . . . . .	80
5.2	Summary of results for $a = 0$ . . . . .	86
5.3	Weights for $H_\infty$ Preview Control Design . . . . .	93
5.4	Values of gain K used in actuator penalty weight $W_{act}$ . . . . .	93

# List of Figures

2.1	Turbine System Components [1] . . . . .	11
2.2	Clipper Liberty turbine [2] (left) and power curve (right) . . . . .	12
2.3	Performance: PID and state-space controller [3] . . . . .	14
3.1	Sub-components of a turbine modeling problem . . . . .	17
3.2	Diagram of a rigid body turbine rotor model . . . . .	21
3.3	The Controls Advanced Research Turbine (CART3) at the NWTC site at Golden, CO. Photo courtesy of Benjamin Sanderse from Energy Research Centre of the Netherlands. . . . .	24
4.1	Nonlinear, classical feedback diagram . . . . .	37
4.2	Controller implementation on the nonlinear plant . . . . .	38
4.3	Linear, classical feedback interconnection . . . . .	39
4.4	$H_\infty$ -optimal controller design interconnection . . . . .	40
4.5	LFT representation for controller design . . . . .	42
4.6	MBC application and Approximate LTI Turbine Model . . . . .	48
4.7	System Interconnection for $H_\infty$ Region 3 Controller Design . . . . .	50
4.8	Bode plot from wind perturbations to rotor speed error. . . . .	56
4.9	Bode plot from wind perturbations to collective blade bending moments. . . . .	57
4.10	Bode plot from wind perturbations to blade bending moments in tilt direction. . . . .	58
4.11	Power spectral densities of the blade bending moments in non-rotating coordinates. . . . .	58
4.12	Bode plot from wind perturbations to tower fore-aft bending. . . . .	59
5.1	Control of the CART3 for the maximum power capture . . . . .	67
5.2	Pareto optimal performance trade-off with different preview times . . . . .	72

5.3	Time-domain plots of the standard control law and the model predictive controller . . . . .	73
5.4	$C_p$ versus $\lambda$ data for the CART3 . . . . .	74
5.5	Pareto optimal performance trade-off with a fixed preview time of 15 (s) . . . . .	75
5.6	Frequency spectrum of the hub-height average speed of the turbulent wind conditions . . . . .	79
5.7	Time responses of rotor speed error ( $\delta_{\omega_r}(t)$ ) for “small” preview times. The wind gust occurs at $t = 0$ for all responses . . . . .	82
5.8	Time responses of rotor speed error ( $\delta_{\omega_r}(t)$ ) and optimal pitch command ( $\delta_{\beta}(t)$ ) for “moderate” preview times. The wind gust occurs at $t = 0$ for all responses . . . . .	84
5.9	Performance versus preview time predictions from analytical results . . . . .	86
5.10	Fundamental preview time versus trim wind speed . . . . .	88
5.11	System Interconnection for $H_{\infty}$ Collective Pitch Controller Design . . . . .	89
5.12	Closed-loop response of the CART3 FAST model to a 2.5 $m/s$ step uniform wind gust. The wind gust occurs at $t = 0$ for all responses . . . . .	95
5.13	Peak rotor speed error vs. preview time for step and turbulent wind for $H_{\infty}$ controllers on FAST simulations. Ideal three point measurements of the wind field is used. . . . .	95
5.14	Normalized, average blade DELs vs. preview time for step and turbulent wind for $H_{\infty}$ controllers on FAST simulations. Ideal three point measurements of the wind field is used. . . . .	96
5.15	Performance metrics vs. preview time for $H_{\infty}$ controller simulations in turbulent wind and realistic LIDAR sensor models on FAST . . . . .	98
5.16	A 50-year extreme gust as defined by IEC-61400-1 . . . . .	106
5.17	Peak Positive Rotor Speed Error with varying preview wind amounts . . . . .	107

# Chapter 1

## Introduction

The control of utility-scale wind turbines is considered in this thesis. This control problem has recently attracted much attention in the literature due to an increasing worldwide demand for renewable energy resources. Wind power is a strong candidate for this demand with its cost of energy approaching competitive levels with non-renewable energy resources. As a result, the global installed wind power capacity increased by 21% (199*GW* to 241*GW*) in 2011 [4]. However, this rapid growth is still not sufficient to reach the aggressive renewable energy goals set by many governments. One such example is the U.S. Department of Energy's goal to supply 20% of the nation's electrical energy by wind power by 2030 [5]. Achieving these aggressive goals requires further reductions in the cost of wind power.

The cost of wind power mainly depends on three factors: The efficiency of the power capture, the costs associated with initial installation and the recurring maintenance costs. Turbine controllers have an impact on all three factors. Improved control algorithms have the potential to extract a larger portion of the energy from the wind. These controllers can also reduce the loads on the turbine structures. Load reduction allows use of cheaper materials to lower the initial installation cost and less frequent maintenance due to reduced wear and tear.

Wind turbines offer many interesting control challenges. The control objectives depend on the operating conditions: low and high wind speeds. Optimal power capture, the control objective in low wind speeds, is achieved when the rotation speed of the turbine rotor is a constant multiple of the wind speed. There are two challenges associated

with this problem. First, there are no reliable wind measurements available in current commercial wind turbines. Second, the large rotor inertia of utility-scale turbines prevents rapid control of the rotor speed in response to rapid wind fluctuations. The control objective during high wind speeds is to reduce the loads on the turbine structure while maintaining a constant power production or constant rotor speed. There is a trade-off between the load reduction and the rotor speed regulation goals. The pitch angles of the turbine blades are controlled to achieve these objectives. However, blade pitch actuators' rate of response is constrained due to large blade inertia. Actuator rate constraints place fundamental constraints on performance. The turbine control problem in both wind conditions is further complicated by the periodic effects due to rotor rotation as well as the variations in the nonlinear turbine model based on the wind speed.

Recent research in the turbine control literature focused on two approaches to address these challenges. First, a preview wind sensor can be used to obtain a reliable wind speed measurement for the closed-loop controllers. This measurement can be used to address challenges associated with wind speed tracking, large rotor inertia and blade pitch rate limits. Second, advanced multiple-input multiple-output (MIMO) controllers can be used. Industrial turbine control is still, for the most part, based on classical, SISO designs. These SISO controllers yield sub-optimal performance since they ignore the coupling between multiple actuators, sensors and multiple performance goals. MIMO control algorithms take advantage of this coupling to achieve the optimal trade-off between rotor speed regulation and structural reduction objectives. Moreover, MIMO control design methodologies offer straightforward methods to make use of the preview wind measurements.

Unfortunately it has proven difficult to successfully transition the advanced MIMO controllers and the novel sensing solutions to the industry. The advanced MIMO design methodologies can deliver superior performance and reduced structural loads but they tend to have significantly more tunable design parameters. Multivariable control techniques also optimize performance with respect to mathematical cost functions that can be difficult to relate to the actual turbine performance objectives. Hence tuning of advanced multivariable controllers can be significantly more time consuming as well as requiring specific expertise in the particular design methodology. Increased performance

and reduced failures comes at the price of increased design time and cost, both of which are critical in an industrial setting. There are many questions and challenges before the transitioning of the MIMO controllers and preview wind sensors to the industry. Particularly, there are no clear answers to the following questions: Can the design of multivariable controllers be simplified? Is it possible to improve the turbine performance using preview sensors? Are the potential performance improvements enough to justify the high cost of these sensors? How much preview time is needed? It is clear that there is a need for a fundamental research to address these questions.

## 1.1 Thesis Overview

The transition of the current state-of-the-art wind turbine control research to industry is the basic motivation of this thesis. We investigate two specific aspects of this challenge. Can the design of advanced multivariable controllers be simplified? This aims to lower the knowledge barrier required to use multivariable controllers for control engineers in industry and help improve turbine performance. The second aspect is: How much performance improvement can be obtained with the use of preview wind sensors? The answer is important to decide if the use of these expensive sensors can be justified from an economic point of view. Investigation of these questions can be addressed using various tools from optimization literature for optimal turbine control. This section gives an outline of this thesis and the path taken to answer these questions.

Chapter 2 presents the background information for our turbine control work. We briefly describe the types of turbines available both in field and literature. The basic operation of a specific type of turbine, 3-bladed horizontal-axis upwind turbine, is explained in detail. This turbine is the focus of our research and is the most common commercially available, utility-scale turbine currently available. Common turbine control approaches and a brief review of the recent advanced control literature is presented. The research is presented in the context of that in literature and the research objectives are motivated.

Chapter 3 presents dynamic models of utility-scale turbines. First, an overview of the modeling tools available for the turbine subcomponents is presented. The models are grouped into two categories: first-principles based and the numerically derived

models. We explain in detail the first-principles based low and medium-fidelity models. The low-fidelity models are important since they are used for control design and to gain physical insight into turbine control problems. The medium-fidelity models are used for controller testing and verification of the trends observed with the lower-fidelity models. These medium-fidelity models are considered sufficient for turbine control purposes in literature. Numerically derived models correspond to linear models obtained from medium to high-fidelity turbine simulation tools. These linear models are useful for capturing the flexible structural modes of the turbine from higher-fidelity nonlinear simulations. Linearization of the high-fidelity nonlinear simulations yields linear time-varying models due to the rotor rotation and periodic disturbances on the turbine. We discuss linear time-invariant (LTI) approximations of the linear, time-varying models to use well-established control methodologies. Specifically, an LTI approximation tool commonly used for rotary wing systems, the multiblade coordinate transformation (MBC), is explained in detail. The research presented in Chapter 4 relies on the MBC approach to generate linear, time-invariant models for control design.

Chapter 4 discusses our work on simplification of the design process of advanced multivariable turbine controllers. More specifically, we propose a design framework that uses gradient-based optimization tools to tune the design parameters of linear multivariable optimal controllers for nonlinear performance objectives and design constraints. This allows a simplified design procedure since the optimization lifts the burden of the tuning of abstract design parameters that are not correlated to main design goals in an intuitive, straightforward way. An example problem, a simplified turbine control problem in above-rated wind speeds, is used to test the effectiveness of the framework. This example problem is used to analyze the blade load reduction performance objective versus pitch actuator rate-limit trade-off.

Chapter 5 is dedicated to preview control. We treat the preview control problem in low and high wind speeds separately. This is because of the different control objectives and challenges in these operating conditions. In low wind speeds, we demonstrate that there is a trade-off between power capture and gearbox loads. We formulate and solve a two-objective nonlinear optimal control problem and show that simultaneous power capture improvements and gearbox load reductions can be attained with the use of preview.

In high wind speeds, blade pitch is used to regulate the rotor speed and to reduce the structural loads. There is a fundamental performance limit imposed by the blade pitch rates. The use of a wind preview sensor to improve performance under rate-constrained control is investigated. We examine three cases: short, medium and long preview times. The analytical formulas that describe the optimal control actions and the performance limits in each case are explained in detail. We show that there is a fundamental preview time beyond which no performance improvements are obtained. This fundamental preview time is proportional to the turbulence levels observed at turbine site and inversely proportional to the pitch rate limits. These explanations and analytical formulas relied on a step wind gust that approximates the frequency spectrum of the turbulent wind conditions observed during normal operation. We also provide a framework that can be used to analyze limits of performance and preview time requirements for arbitrary wind trajectories. This is useful to analyze turbine behavior during extreme operating conditions which are defined with deterministic wind trajectories.

Chapter 6 presents conclusions and recommendations for future work.

## 1.2 Thesis Contributions

This thesis provides detailed engineering insight into wind turbine design trade-offs and makes contributions in the areas of multivariable controller design and preview control. These contributions include:

1. **Multivariable Design Tools:** In Chapter 4 we propose a preliminary control design framework that tunes the design variables of  $H_\infty$  controllers based on non-linear performance objectives and design constraints. This tool is also useful for analyzing the trade-offs between performance objectives and constraints.
2. **Performance Trade-offs:** We investigate optimal performance trade-offs and provide engineering insight into turbine control problem.
  - Results in Chapter 5 show that there is a direct trade-off between power capture and gearbox structural loads in low wind speeds. The turbulence level at the turbine site has a significant impact on this trade-off.

- In high wind speeds, we find that the structural load reduction performance is heavily constrained by the blade-pitch rates and the generator overspeed limits. This analysis can be found in Chapter 4.
3. **Preview Control:** Theoretical results and practical tools are developed in the area of preview control. These are presented in Chapter 5. The key contributions are:
- We present an analysis framework based on the nonlinear optimization methods in the literature for turbine control in below-rated wind speeds. This framework can be used to analyze the preview time requirements and the potential performance improvements with preview based on the operating conditions at the turbine site. A key result is that the use of preview can simultaneously improve the power capture and reduce the gearbox loads over the standard control law used in currently fielded turbines.
  - Analytical formulas are derived for performance limits with preview information under actuator rate constraints. These results for first-order systems with step-like disturbances are applied to turbine control in above-rated wind speeds. These formulas show three important results. First, performance improves linear with small preview times. Second, there is a fundamental preview time beyond which no additional performance improvement can be obtained. Third, this fundamental preview time is proportional to the step input magnitude and inversely related to the actuator rate limit.
  - A numerical method to generalize the preview time analytical results is presented. This allows to consider multivariable systems, a larger set of performance metrics and arbitrary disturbance trajectories can be considered. This framework is useful for analyzing the preview control problem during extreme operating conditions for wind turbines.

# Chapter 2

## Background

### 2.1 Introduction

The overall objective of wind turbine control, in its simplest form, is to minimize the cost of wind energy. Because there is no fuel cost associated with wind energy, the cost is due to a large initial investment for wind farm development and a relatively smaller cost of recurring maintenance. These costs are offset by the revenue generated through energy capture over the turbine lifetime. The turbine design task involves a delicate design balance between the efficiency of power capture and the costs associated with initial installation and recurring maintenance.

This design balance is becoming more difficult to maintain for commercial wind turbines that are growing increasingly larger. The trend toward larger designs is an outgrowth of two factors. First, the captured power is proportional to the square of the blade length. Hence larger turbines capture more power. Second, mean wind speeds are greater at higher heights. These design factors have driven the wind power industry to turbines of enormous size. Unfortunately the tower and blade flexibility increase as the dimensions increase, resulting in higher structural loads. Increased structural loads lead to additional failures, longer downtimes, and increased maintenance costs.

Turbine control algorithms have an impact on the energy capture, initial installation cost and the recurring maintenance costs. Optimized wind turbine control algorithms can lower the cost of energy in two ways. First, the turbine can capture a higher percentage of the energy available in the wind. Second, the loads on turbine structures

can be lowered, prolonging the life of turbines. A longer life means more energy will be captured and sold for profit. Alternatively, less expensive materials can be used in the next generation turbines since these structures need to withstand lesser loads with optimized control algorithms. For instance, lowering the bending moments at the tower base can enable the use of cheaper materials for the tower. This also allows the use of a smaller, lower cost turbine foundations.

This chapter provides a background on wind turbine control. Section 2.2 describes common turbine designs available in field and literature. Section 2.3 explains in detail the operation of a particular type of turbine, so called 3-bladed horizontal axis turbines. This is the most commonly used utility-scale turbine type today and is the focus of our research. Turbine performance objectives, measurements and inputs available for control are also discussed in this section. Section 2.4 explains the current control approaches and the challenges for wind turbine control. This section also gives the context of our research in terms of these challenges.

## 2.2 Types of Turbine Designs

There are various wind turbine designs proposed in the literature, and implemented on today's turbines. Most of these designs fall into a few common categories. The first distinction can be made based on turbine siting. There are land-based, onshore turbines and sea or ocean based offshore turbines. Onshore turbines use simpler foundations to balance the structure. Maintenance crews and the spare parts can be transported fast and easily, leading to lower maintenance costs. The interaction of the atmosphere and land causes higher wind speed fluctuations that can stress the turbine structure. Onshore turbines are constrained in size due to the size limit on what can be transported on public highways. Offshore turbines have access to faster, less turbulent wind. They also have no major size constraints. On the other hand, offshore turbines require more sophisticated methods to balance the turbine and counter the wave motion. This is a significant challenge especially in deep water bodies. The maintenance can also be more challenging due to distance from land.

The second distinction can be made based on the axis of rotation of the turbine rotor. Rotor of a vertical axis wind turbine has its axis of rotation vertical, i.e. perpendicular

to the earth surface. Horizontal axis wind turbine (HAWT) rotors have a horizontal axis of rotation that is parallel to the wind inflow. Most utility-scale turbines today are HAWTs due to their higher efficiency.

HAWTs can further be categorized into two groups based on location of the rotor with respect to the wind inflow and tower. Upwind HAWTs have rotors that face the wind inflow. The tower is behind the rotor with respect to the wind. This is in contrast with downwind HAWTs. With downwind designs the wind inflow hits the tower first and the rotor afterward. The main advantage of the upwind HAWTs is the reduced tower shadow. Tower shadow leads to a slower wind speed around tower even in front of the tower. This corresponds to a power loss when a blade passing through the tower. The wind speed and power reduction is much smaller with upwind designs. One disadvantage of the upwind designs is the possibility of the blades striking the tower. This is because the wind inflow bends the blades toward the tower. Common ways to mitigate this problem include increasing the distance of the rotor from the tower, pointing the axis of rotation of the turbine slightly upward with respect to horizon or use of stiffer blades. Another distinguishing characteristic between upwind and downwind turbines is the yaw mechanism requirements. Upwind HAWTs require an active yaw mechanism to keep the rotor pointing into the wind. Downwind HAWTs can maintain their downwind position passively. However, large downwind turbine designs may still require an active yaw mechanism to avoid twisting of the power cables that carry large amount of currents.

A final distinction can be made based on number of blades used for the HAWT rotor. This decision involves trade-offs between many factors such as cost of structures, aerodynamic efficiency, noise and aesthetics [6]. For instance, higher number of blades correspond to better aerodynamic efficiency in steady operation albeit at a rapidly diminishing rate. The trade-off is that a higher number of blades also corresponds to a higher rotor inertia. This is undesired as it prohibits the turbine from rapidly accelerating with wind gusts. Resulting power loss combined with higher structural costs can negate the benefits of higher aerodynamic efficiency. Another design trade-off is the extra moment balancing mechanisms required at rotor hub for rotors with even numbered blades. These can be complex and expensive for large turbines. These rotors undergo a large tilting moment every time a blade is passing through the tower. The

blade passing the tower observes a slow wind due to tower shadow and lower altitude, while the opposing blade gets a faster wind at higher altitude. The extra complexity can be a case against increasing the blade number by odd numbers for higher efficiency. Over the years the turbine industry converged to 3-bladed designs for utility-scale turbines partially due to these reasons. Some fielded smaller 2-bladed turbines also exist, but they are rare for utility-scale designs.

### 2.3 Basics of Horizontal-Axis Turbine Operation

We consider the most common commercially available, utility-scale turbine type today: onshore, horizontal-axis, upwind, 3-bladed turbines. These turbines are truly multivariable systems with many actuators and sensors used to balance the competing performance objectives of power capture and load reduction. Figure 2.1 shows the key system components. The nacelle sits atop the turbine tower and houses the main components including the generator and gearbox. Lift is generated on the turbine blades as wind flows past and this causes the blades to rotate. The blades are attached to the rotor and the central shaft of the rotor is connected to a generator via a gearbox. The generator converts the mechanical rotational energy in the shaft rotation into electrical energy. A gearbox is needed to step up the slow blade rotation speeds to the higher generator shaft speed. Large turbines typically have actuators for tower yaw, blade pitch, and generator torque. The yaw motor is used to rotate the turbine so that it faces into the wind direction. Each turbine blade has an actuator to rotate (pitch) the blade and this has the effect of varying the lift force on the blades. In addition, the generator torque can be set to control the electronic power extracted from the system. The main sensors used for industrial turbine control are rotor speed and wind speed. The wind speed is measured with an anemometer located at the back of the turbine nacelle. This wind speed measurement is corrupted by the rotating blades and hence it is of limited use for control. Several other sensors have been investigated for turbine control including tower top acceleration, blade root bending loads, and LIDAR wind speed measurements.

The trade-off between power capture and load reduction is currently achieved on today's turbines using a mode-dependent controller with objectives that depend on the wind speed [7–10]. There are essentially four operating regions as shown in the power

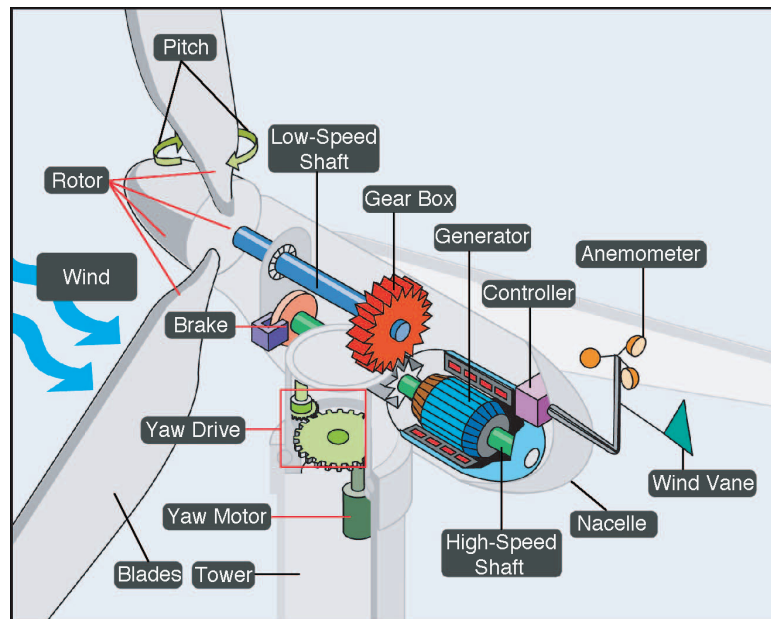


Figure 2.1: Turbine System Components [1]

versus wind speed curve in Figure 2.2. Below the cut-in speed (Region 1), there is insufficient wind and the turbine is kept in a parked, non-rotating state. Between the cut-in and rated wind speeds (Region 2), the objective is to maximize the captured power. Between the rated and cut-out wind speeds (Region 3), the objective is to maintain the rated power while minimizing the structural loads on the turbine. Blending of Region 2 and Region 3 control algorithms is used as the wind speed approaches the rated wind speed to ensure smooth transition between the Region 2 and Region 3 control objectives. The transition between Regions 2 and 3 is sometimes referred to as Region 2.5. The turbine is shut down above the cut-out speed (Region 4) to prevent structural damage. This is done by turning the leading edge of the blades into the wind to decrease the lift and the aerodynamic torque. The blades can also be turned in the other direction to increase their angle of attack into stall to reduce the aerodynamic torque [8]. As a specific example, the Clipper Liberty C100 is a typical  $2.5\text{MW}$  on-shore utility-scale turbine with a rotor diameter of  $100\text{m}$  and a tower size (hub height) of  $80\text{m}$  [11]. This particular turbine, shown in Figure 2.2, has cut-in and cut-out velocities of  $4\text{m/s}$  and  $25\text{m/s}$ . The power curve shown in Figure 2.2 is based on the operating modes for this

2.5MW turbine.

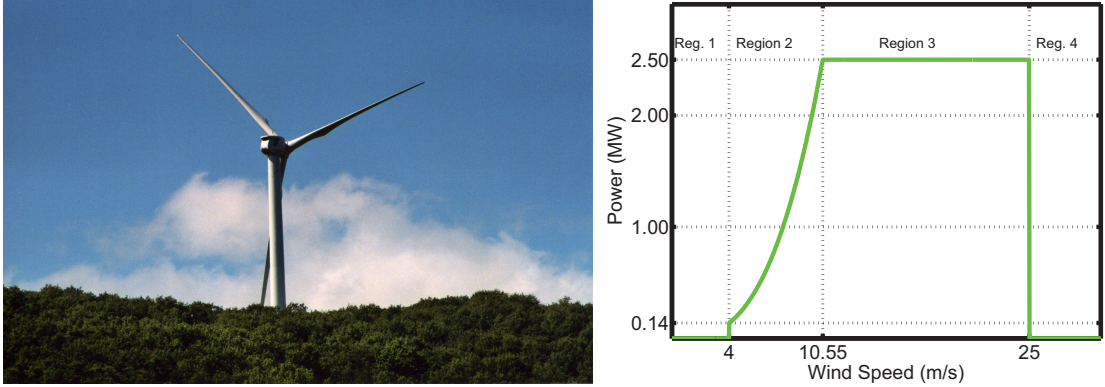


Figure 2.2: Clipper Liberty turbine [2] (left) and power curve (right)

## 2.4 Current Approaches and Challenges

Industrial turbines typically use classical control strategies for Region 2 and Region 3 control [7–10, 12]. In Region 2, the objective is to maximize power capture. This is achieved by holding blade pitch constant and commanding the generator torque. The standard Region 2 controller sets the generator torque to be proportional to the rotor speed [12]. The generator torque command can also include an additional term to add damping to the drive train vibrations [7, 13, 14]. Mathematically, this Region 2 controller takes the form:

$$\tau_g = K\omega_r^2 + B(s)\omega_r \quad (2.1)$$

$$\beta_i = \bar{\beta} \text{ for } i = 1, 2, 3 \quad (2.2)$$

where  $\tau_g$  is the generator torque command,  $\omega_r$  is the rotor speed, and  $\beta_i$  is the pitch command for the  $i^{\text{th}}$  blade. The overbars, as in  $\bar{\beta}$ , refer to constant quantities in this section. If the turbine power characteristics are known perfectly then the proportional gain  $K$  and constant blade pitch  $\bar{\beta}$  can be chosen to achieve maximum power capture in steady wind conditions [15].  $\bar{\beta}$  is called the fine pitch angle. The  $B(s)\omega_r$  term provides the additional drivetrain damping where  $B(s)$  is a filter designed to have high gain at the drivetrain resonant frequency. Note that the standard Region 2 controller does not depend on wind speed due to the poor quality of the anemometer measurement.

In Region 3, the blade pitch angles are actively controlled to maintain rotor speed at its rated value,  $\bar{\omega}_r$ . The use of blade pitch to reduce variations in rotor speed also has the effect of reducing bending loads on the blades and tower. In Region 3 the generator torque command is equal to its rated value  $\bar{\tau}_g$  plus the drivetrain damping term. Thus a typical Region 3 controller has the form:

$$\tau_g = \bar{\tau}_g + B(s)\omega_r \quad (2.3)$$

$$\beta_i = \bar{\beta} + C(s)(\bar{\omega}_r - \omega_r) \text{ for } i = 1, 2, 3 \quad (2.4)$$

In this case  $\bar{\beta}$  denotes a constant, trim blade pitch command and  $C(s)$  is a classical controller, e.g. a PID controller. The same pitch command is used for all three blades. This is commonly called "collective" pitch control.

There have been many research papers on advanced turbine control strategies [3, 13–43]. These research papers include a variety of methods to increase power capture, reduce tower/blade bending loads, and increase the drivetrain damping. For example, control methods have been developed to increase power capture by adaptively updating the Region 2 gain  $K$  in real-time [15,21,22]. Blade load reduction in Region 3 has mainly focused on advanced multivariable controllers that use individual pitch control, i.e. different pitch commands are used for each of the three blades [17–20,24–26,28]. Finally, drivetrain dampers have been designed that account for the cross-coupling between blade pitch and the drivetrain natural frequency [14]. The advanced control designs have demonstrated significant performance benefits both in simulation as well as on fielded research turbines [3, 35, 40–43]. Figure 2.3 shows a comparison of results from two different controllers tested on the 2-bladed Controls Advanced Research turbine at NREL [3]. This figure compares damage equivalent loads in each component from two different controllers: 1) a simple classical PID controller, and 2) a modern state-space controller. The state-space controller achieves significant load reduction because it is using all of the available turbine actuators optimally. This controller adds significant damping to various turbine components, with a dramatic decrease in fatigue loads.

Unfortunately it has proven difficult to successfully transition advanced, multivariable control design techniques to industrial turbines. As a result the industry control designs are still, for the most part, mainly based on the single-input, single-output

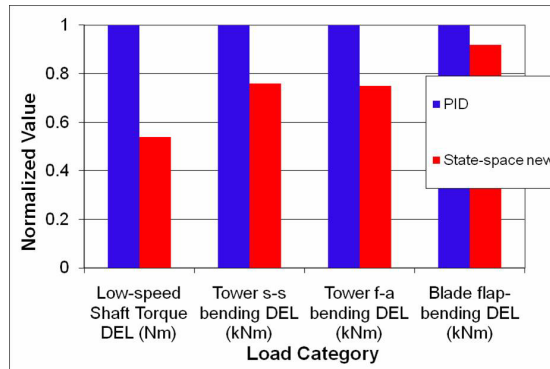


Figure 2.3: Performance: PID and state-space controller [3]

(SISO) framework with designs based on decoupled performance objectives. The advanced multi-input, multi-output (MIMO) design methodologies can deliver superior performance but they tend to have significantly more tunable design parameters. In addition, optimal control techniques use cost functions ( $H_\infty$  norm, integral quadratic costs) that can be difficult to relate to the actual turbine performance objectives of power capture and load reduction. As a result, tuning of advanced controllers can be significantly more time consuming as well as requiring specific domain expertise in the particular design methodology. This increases both the design time and costs both of which are critical in an industrial setting. We tackle this problem in Chapter 4. Our research investigates the suitability of the use of mathematical optimization tools available in literature for automated tuning of advanced multivariable turbine controllers. These tools take certain basic turbine design goals of interest and tune turbine controllers using detailed turbine models. These automated tuning tools lower the technical knowledge requirements on the control engineers for the use of advanced control methods. We present a sample problem of tuning of so called  $H_\infty$ -optimal multivariable controllers for a Region 3 control problem. These tuning methods can also be used for Region 2 control problems.

A second challenge regarding the turbine controller design is the lack of tools that quantify the ultimate performance limits for a given turbine design. Chapter 5 discusses the development of these analysis tools for Region 2 and 3 control with a focus on preview measurements. Current work in the literature use preview wind measurements with laser sensors in turbine control laws. However, the performance limits with the

use of these extra sensors is not well established. We aim to develop these tools for three main reasons. First, these tools can capture the optimal trade-off between various turbine performance metrics of interest. Second, they can show how far from optimal a controller on hand is. A designer can use this information to decide if more time should be spent on tuning or if a more advanced method should be used. The third benefit is that the impact of new sensors or actuators on turbine performance can be studied before a prototype is built. This is important since the performance benefits of using an extra sensor or actuator given an optimal controller design should be able to justify their cost.

## Chapter 3

# Wind Turbine Modeling

### 3.1 Introduction

This chapter describes dynamic models of utility-scale turbines. The models we utilize range from low-fidelity to medium-fidelity models. The lower order linear and nonlinear models are used for control design and to gain insight into turbine control problems investigated in Chapters 4 and 5. The medium-fidelity models are used for simulation testing and the verification of the trends observed with the lower order models. The medium-fidelity models are considered to be sufficiently accurate for turbine certification and controller testing by turbine certification authorities and in literature.

Accurate wind turbine modeling is important for three reasons. First, turbines are safety critical systems. Stability and performance of controllers must be tested with detailed simulation models before implementation. Second, a commercial size wind turbine is not available for testing to most researchers. Scaled-down wind turbines may be available but these are only suitable for certain research purposes. For instance, the effect of strong spatial wind variations across the blades cannot be observed with small turbines. Third, field testing of controllers is time-consuming and expensive. Waiting for the right wind conditions can take a long time or even be impractical. For example, turbines need to be certified for safe operation under extreme situations. One such example is a 50-year gust that is expected to happen once in every fifty years. It is not possible to field test every commercial turbine model for such extreme cases. International wind turbine certification standards such as IEC [44] and Germanischer

Lloyd [45] allow manufacturers to use certain medium and high-fidelity simulation tools for certification for these cases.

The remainder of the chapter is structured as follows. Section 3.2 explains the fundamental turbine modeling concepts. Low-fidelity, 1-state nonlinear models that capture rigid-body rotor dynamics are explained in Section 3.3. Section 3.4.1 discusses the medium-fidelity FAST code for aeroelastic turbine modeling. Turbine actuator models are explained in Section 3.4.2. The model of a preview wind sensor, a continuous-wave LIDAR, is described in Section 3.4.3. We use the National Renewable Energy Laboratory’s FAST code with these sensor and actuator models later in Chapters 4 and 5 for realistic controller testing. Section 3.5 describes the linear system approximations for turbine dynamics. These numerically derived linear models are presented separately from the physics based low and medium-fidelity models.

## 3.2 Overview of Turbine Modeling

Figure 3.1 summarizes the various sub-components of the turbine modeling problem. There are three high level components: atmospheric conditions, fluid-structure interaction and the turbine structure. This section describes the fundamental modeling of these components and how they interact.

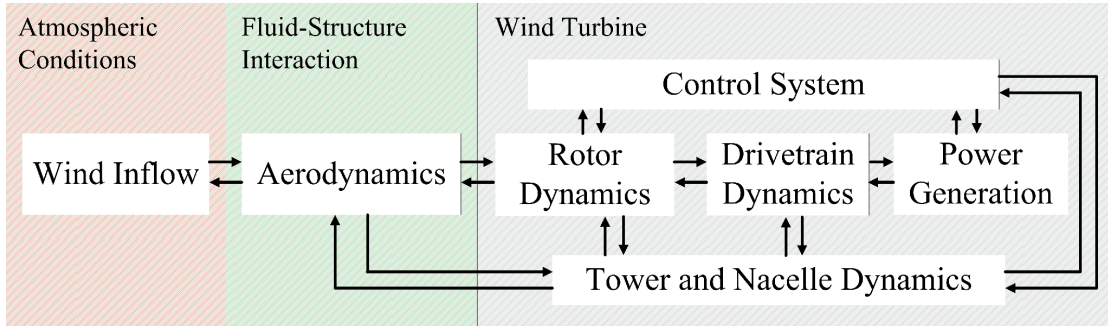


Figure 3.1: Sub-components of a turbine modeling problem

The most common methods of modeling atmospheric conditions involve a computational fluid dynamics (CFD) code or use of stochastic wind simulators. CFD codes numerically solve partial differential equations that describe fluid motion in a three dimensional space. This is done at simulation time since the turbine dynamics and fluid

motion interact. CFD codes allow modeling of wind wake behind the rotor, which is required for turbine interaction and wind farm studies. CFD codes provide high-fidelity atmospheric modeling at the cost of slow execution speed. A simpler method is to use stochastic wind simulators. These simulators use spectral models that describe the frequency distribution of the wind speed. Spectral models are used with spatial coherence models that describe how the wind speed is related between different points in space. The output is a random wind speed trajectory observed on the turbine rotor. The distinction between these models and CFD codes is that they are not based on physics of the fluid dynamics. The impact of the turbine on wind flow is ignored. Therefore these wind simulators can be run independently from turbine dynamics. This approach leads to faster turbine simulations at the expense of accuracy.

Fluid-structure interaction models capture the interaction between air, blades, tower and the nacelle. High-fidelity interaction models rely on various computational methods based on the assumptions on fluid motion such as the Reynolds number. An overview of these models can be found in Reference [46]. An example of application of such methods for wind turbines can be found in References [47, 48]. These fluid-structure interaction models provide good accuracy but are computationally intensive. A more common and faster approach is to obtain detailed airfoil characteristics of the turbine blades before simulation time. This simplifies the three-dimensional geometry and physics of the problem and allows use of two-dimensional aerodynamic models. Typically the combination of the blade element and momentum theories are used for this approach. Blade element theory involves breaking the blade down into various elements with different airfoil characteristics. Two dimensional airfoil properties are used to calculate the forces and moments on each element. Induced flow velocities, required for this calculation, are obtained from the momentum theory. Momentum theory gives equations for the tangential and axial forces given an annular element of fluid on an ideal rotor disk. Certain corrections, such as losses at blade tip, are also applied to improve accuracy. Many turbine modeling tools rely on blade element momentum theory for turbine aerodynamics.

The blades, tower and the nacelle are the components of the turbine that directly interact with the surrounding airflow. Modeling of the flexible motion of the tower and blades is important for a utility scale turbine due to the large structural loads and the large size of these components. This modeling can be done for different levels of fidelity.

Two common approaches exist in the literature. Finite element methods (FEM) can be used for high-fidelity modeling of the flexible structures. This approach divides the tower and the blades into a high number of smaller elements and calculates their motion with respect to each other. The resulting high number of degrees of freedom system is computationally expensive to simulate. A lower degrees of freedom system can be obtained with the assumed modes method [49, 50] at the expense of some accuracy. With this method the tower and the blades are treated as one-dimensional cantilever beams with tip mass and mass distribution along their length. The tower is attached to the foundation and supports the nacelle and the rotor at top. The blades are attached to the hub on the nacelle. These blades can have tip-brakes, but this is less common for current utility scale turbines. The material deformation is approximated with a number of basis functions known as mode shapes. Each mode shape corresponds to a particular deformation shape and is described by one degree of freedom. Superposition of multiple mode shapes converge to the actual deformation. These mode shapes are calculated from material properties. The mode shapes are typically computed independently for blades and tower assuming that the specific structure is at rest. In reality, there is coupling between all structural modes. It is assumed that the effect of this coupling is small and does not affect the model response.

The nacelle houses the drivetrain and the electrical generator. Most turbines use a drivetrain to connect the rotor to the generator. The drivetrain typically includes a gearbox to step up the slow rotor speed to speeds suitable for the generator. However, gearless turbine designs also exist. The aerodynamic torque is applied on the rotor side of the drivetrain. The generator places an opposing torque on the other end of the drivetrain. This system is most commonly modeled as two inertias, rotor and generator, connected with a lossy gear. The flexibility in the system is lumped into a linear torsional spring and damper placed on one side of the shafts. The generator is responsible for conversion of mechanical energy into electrical energy. The input to the generator is the generator torque demand from the turbine controller. The output is the actual generator torque. Generator torque times the drivetrain speed corresponds to the electrical power capture. The high-level input-output behavior of the generator is typically approximated by a first order linear system. More detailed models of power electronics contained in the generator are also available. These detailed models are most

commonly used to study the interaction of turbines with the power grid.

In summary, the highest-fidelity turbine modeling option is to use a combination of a CFD code, a detailed fluid-structure interaction model and a finite element code. This level of fidelity comes with the cost of heavy computational requirements. These models are typically run on supercomputers and not very suitable for Monte Carlo simulations. Monte Carlo simulations rely on many realizations of stochastic processes to generate statistically meaningful numerical results. Wind turbine industry uses Monte Carlo simulations by simulating turbine models in many wind conditions with different statistical properties. This is a requirement from wind turbine safety certification authorities [44, 45]. The high computational cost of the highest fidelity models make the use of these models in Monte Carlo simulations time- and cost-ineffective. Simpler methods are commonly used for some turbine sub-systems when they are seen sufficient. For instance, simpler, pre-calculated wind trajectories can be used instead of CFD codes when the goal is to model a single turbine's behavior. A second example is that if the airfoil properties are well known, simplified aerodynamic models can be utilized over detailed fluid-structure interaction models. These type of simplifications are also necessary for models used for control design and analysis. The execution times for the highest-fidelity models are prohibitive for the iterative controller design and testing process. Medium-fidelity models are preferred for controller testing purposes. Low-fidelity models are used for design of controllers.

There are various widely used turbine modeling tools in literature. A large set of open source tools are available from the National Renewable Energy Laboratory (NREL). These freely available tools include FAST [51], AeroDyn [52], SOWFA [53] and TurbSim [54]. FAST is a nonlinear aeroelastic simulation package for onshore and offshore turbine dynamics. It is commonly coupled with AeroDyn for the calculation of aerodynamics loads on the structure. AeroDyn uses the blade-element momentum theory with modifications. SOWFA is a combination of various CFD codes and FAST. It offers high-fidelity atmospheric modeling and simulation of multiple turbines via multiple instances of FAST. The aerodynamic loads on the turbine are calculated via blade element theory in SOWFA and the momentum theory is replaced by a CFD code. TurbSim is a stochastic, turbulent wind simulator. Its inputs are various turbulence properties. The output of TurbSim is a description of the turbulent wind field as a

function of time on turbine rotor. These pre-calculated wind trajectories can be used with AeroDyn-based tools. These sets of tools from NREL are considered to be sufficient fidelity for control purposes. FAST, AeroDyn and TurbSim tools are used extensively in this thesis. These tools are explained in more detail in Section 3.4.1.

### 3.3 Lower Fidelity Models

This section describes a one-state, nonlinear, rigid body model of the turbine rotor. This model neglects the flexibility in turbine structures. Therefore it is most useful when blade and tower loads are not being considered. Figure 3.2 shows a simple diagram of this model. The wind inflow on the rotating blades creates a torque on the rotor. This is the aerodynamic torque  $\tau_{aero}$  ( $N \cdot m$ ). The power captured by the rotor is  $P_r = \tau_{aero}\omega_r$  ( $W$ ) where  $\omega_r$  ( $rad/s$ ) is the rotor speed. The generator torque  $\tau_g$  ( $N \cdot m$ ) corresponds to the torque extracted from the shaft by the electrical generator.  $\tau_g$ , and in turn the electrical power, can be set by the turbine controller. However, there is an upper bound on  $\tau_g$  set by the generator design. Note that converting all of the available mechanical energy to electrical energy would make the rotor come to a stop. This corresponds to zero wind power capture since  $\omega_r$  is zero. In order to sustain a continued power production  $\tau_g$  should be set appropriately considering turbine dynamics.

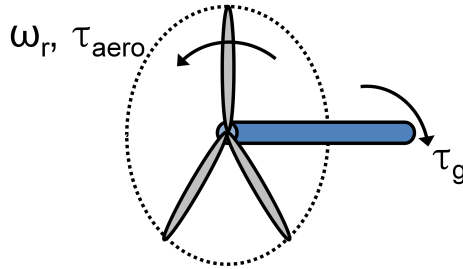


Figure 3.2: Diagram of a rigid body turbine rotor model

The power captured by the turbine rotor is approximately given by: [7]:

$$P_r = \frac{1}{2}\rho\pi R^2 v^3 C_p(\lambda, \beta) \quad (3.1)$$

where  $\rho$  is the air density ( $kg/m^3$ ),  $R$  is the rotor radius ( $m$ ) and  $v$  is the average wind speed over rotor area ( $m/s$ ).  $C_p(\lambda, \beta)$  is the nondimensional power coefficient that

represents how much of the power available in wind is captured. It is a function of the blade pitch angle  $\beta$  (*deg*) and the tip speed ratio  $\lambda := \frac{R\omega_r}{v}$  (*unitless*).

A one-state nonlinear model of the rigid-body rotor dynamics can be obtained using Newton's law for the system shown in Figure 3.2:

$$\dot{\omega}_r = \frac{1}{J}(\tau_{aero} - \tau_g) \quad (3.2)$$

where  $J$  ( $kg \cdot m^2$ ) is the combined rotor, generator and drivetrain inertia. The turbine gearbox is ignored here. The quantities  $J$ ,  $\tau_{aero}$  and  $\tau_g$  are expressed as their low-speed shaft equivalents. Using the rotor power  $P_r$  expression from Eq. (3.1) and substituting  $\tau_{aero}$  for  $\frac{P_r}{\omega_r}$  in Eq. (3.2) gives:

$$\dot{\omega}_r = \frac{\rho\pi R^2 v^3 C_p(\lambda, \beta)}{2J\omega_r} - \frac{\tau_g}{J} \quad (3.3)$$

Here the  $C_p(\lambda, \beta)$  data is usually available in lookup tables.

The accuracy of the one-state nonlinear rotor model depends on the size and the flexibility of the turbine. However, for most current turbines this model can capture the rotor dynamics accurately enough for closed-loop control purposes. We use this model in Section 5.3 for optimal Region 2 control. A linearized version of this model is used in Section 5.4 for optimal Region 3 control for rotor speed tracking.

## 3.4 Medium Fidelity Models

### 3.4.1 Turbine Dynamics

The Fatigue, Aerodynamics, Structures and Turbulence (FAST) turbine simulation package [51, 55] is used to model turbine dynamics in this thesis. FAST is a publicly available nonlinear aeroelastic turbine simulation code developed by the National Renewable Energy Laboratory (NREL). FAST captures the effects of structural flexibility that was ignored by the 1-state nonlinear rigid-body rotor model. FAST has been validated against ADAMS and Germanischer Lloyd turbine simulation codes [56]. It has been certified by Germanischer Lloyd that it is acceptable for turbine manufacturers to use FAST for onshore turbine certification.

The tower, blades and the drivetrain are treated as flexible structures in FAST. The drivetrain torsional flexibility is modeled as a linear inertia-spring-damper system. The

deflection of the tower and the blades are approximated via assumed modes method. The properties of the tower and the blades can vary along their length. These properties are specified at desired points on the structures. Linear interpolation is used between these points. For instance this allows specification of different airfoil properties along the blade length.

FAST is integrated with the AeroDyn [52] code of NREL for the calculation of aerodynamic loads. AeroDyn uses blade element momentum theory to calculate aerodynamic forces and moments. Modifications and corrections are implemented for blade tip losses and yawed wind inflow. If desired the FAST code can be coupled with other aerodynamics tools or CFD codes instead of AeroDyn.

The FAST code can model the onshore wind turbines with a total 18 degrees of freedom (DOF). An extra 6 DOF are available for modeling of platform motion for offshore wind turbines. The full list of 18 DOF in FAST for 3-bladed onshore wind turbines is as follows. 4 DOF include first and second tower bending modes in fore-aft as well as side-to-side directions. Three degrees of freedom for each blade model the first edgewise bending mode in addition to the first and second bending modes in flapwise direction. These account for 9 DOF in total. Drivetrain torsion and generator speed correspond to 2 DOF. 1 DOF accounts for the nacelle yaw motion. 2 more DOF correspond to rotor and tail furl.

The wind field used in FAST simulations can be described in two levels of fidelity. One option is to describe the spatial and temporal variations in the field by a combination of various time-varying parameters. These parameters are the average horizontal wind speed over the rotor area, vertical wind speed, wind direction, vertical and horizontal wind shears. The second option is the use of so-called full-field wind data. Wind speed in three directions on a raster grid over the rotor surface is specified as a function of time. This second option allows a more realistic modeling of the wind field by better capturing the spatial variations in the wind field. This is important for larger commercial wind turbines where wind can vary significantly over the rotor surface. This higher-fidelity option is used in our simulations. Wind files in both formats can be generated with the TurbSim [54] code of NREL. TurbSim has the capability of generating wind trajectories with various spatial and temporal correlation models. These models include common turbulence models that are used for wind turbine testing as defined in

the IEC-61400-1 [44] standards.



Figure 3.3: The Controls Advanced Research Turbine (CART3) at the NWTC site at Golden, CO. Photo courtesy of Benjamin Sanderse from Energy Research Centre of the Netherlands.

The turbine models we use are the  $600kW$  3-bladed Control Advanced Research Turbine (CART3) and the  $1.5MW$  WindPACT [57, 58] turbine. The CART3, shown in Figure 3.3, is located at Boulder, Colorado at the National Wind Technology Center (NWTC) site. The  $1.5MW$  WindPACT is a hypothetical turbine designed by the NWTC and Windward Engineering. The rotor diameters are  $40m$  and  $70m$  respectively. The size of these turbines are representative of the currently fielded commercial turbines. The FAST model data for the CART3 turbine was obtained from A. Wright [59]. The model of the WindPACT turbine is distributed with the original FAST code. These models are chosen because they are heavily used in turbine control literature.

Our medium-fidelity simulations use 15 of the 18 available DOF in FAST for onshore

turbines. 2 DOF for rotor and tail furl are not used since the CART3 and the WindPACT turbine are designed to use active pitch control to protect turbine structures in Region 3 operation. We also ignore the slow yaw dynamics of the turbine. The basic FAST code does not include actuator and sensor models. In other words, the actuator inputs affect the system immediately and the measurements are noise free. Realistic simulations require complementing the FAST code with appropriate actuator and sensor models. The following two sub-sections 3.4.2 and 3.4.3 discuss these actuator and sensor dynamics respectively. The 15 DOF FAST model implemented in Simulink with these actuator and sensor models is used as the basis of our medium-fidelity simulations.

### 3.4.2 Actuator Dynamics

The control inputs available for closed-loop control are the generator torque demand, blade pitch angle demand and the turbine yaw angle demand. A model for the pitch actuators are implemented, but the generator and yaw dynamics are ignored. This is because the blade pitch actuators play an important role on control performance. Blade pitch actuators have restrictive bandwidths for our turbine control problems of interest, namely power capture optimization and structural load reduction. In addition, there are hard bounds on pitch rates that put fundamental constraints on the achievable performance. The dynamics of these pitch actuators can be approximated by first or second order linear systems. In the case of the CART3 and the WindPACT turbine, first order models are sufficient. These pitch actuator models have bandwidths of  $30rad/s$ ,  $10rad/s$  and the pitch rate limits of  $18deg/s$ ,  $10deg/s$  respectively. The hard bounds on rate limits are implemented with our simulation models.

No yaw actuator models are implemented and the turbine yaw angle is held fixed during simulations. This is because the yaw motion and the actuator dynamics have time constants considerable larger than the other dynamics of the system. An electrical generator model is also omitted since these dynamics are significantly faster than the turbine dynamics of interest. Therefore it is assumed that the generator torque demand can be achieved almost immediately for the desired control bandwidth.

### 3.4.3 LIDAR Sensor Dynamics

A detailed model of the ZephIR LIDAR [60], a commercially available continuous wave LIDAR, is implemented with FAST for medium-fidelity simulations. A detailed LIDAR model is important for realistic evaluation of preview controllers' performance that we investigate in Chapter 5. This model captures various sources wind measurement errors inherent to the nature of the continuous wave LIDARs. The core of this model is based on the work in Reference [61]. It is assumed that the LIDAR is mounted at the turbine hub in a forward looking fashion and spinning with the rotor. The LIDAR itself also contains an internal spinning mechanism that allows its laser beam to be directed in any direction during operation independent of the rotor angle. It is assumed that the LIDAR is supplying the average of the wind measurements at three points in space to the controller. In other words, the spinning mechanism in the LIDAR is used to direct the laser beam in three directions during one sample time of the controller. The location of these three points depend on the preview time and the desired measurement point on the blade span. We use the CART3 turbine for our preview control research. The measurement point on each place is chosen at the 75% blade span or 15m from the rotor hub. The future position of the blades is estimated by a constant rotor speed assumption during the preview time. This measurement point is moved horizontally in space for the desired preview amount. The outer section of the blades is chosen since most of the turbine power capture is obtained around this section.

The LIDAR sensor measures a weighted average of the wind speed along its beam in three dimensional space. The use of this model incorporates two error sources for wind measurements. The first source of error stems from the fact that LIDAR cannot measure wind measurements at a fixed point in space. The measurements from continuous wave LIDARs involve a spatial weighting across the laser beam. This weighting is given by a Lorentzian function [61]. This function depends on the focus distance. Longer focus distances correspond to more averaging. This introduces higher errors with increasing focus distance or preview time. The second type of error arises from the orientation of the laser beam. The wind speed measurement of interest is the wind in the horizontal direction at the desired blade span. A large angle between the horizon and the laser beam means that the projection of the horizontal wind on the laser beam will be limited. Instead, the vertical and side-wise wind speeds will corrupt the measurement. The error

increases with smaller preview times and measurements that are farther away in the transverse (perpendicular to earth surface) direction from the rotor hub.

There are two more error sources that need to be considered for preview wind measurements. The first source of error arises from the fact that it is not possible to know the future rotor position. A simple predictor that assumes a constant rotor speed for the duration of preview is used to predict the future position of the blades. This prediction error increases with increasing preview times. The second error source is the assumption of the Taylor’s frozen turbulence hypothesis, but this effect is not captured in our medium-fidelity simulations. In other words, the evolution of the wind field from the measurement point to the turbine is ignored. The impact of this assumption depends on the preview time. This effect can be studied with use of an advanced computational fluid dynamics code. However, this is beyond the scope of this study. Note that the two error sources described in this paragraph are not directly tied to the LIDAR sensor model.

This LIDAR model is implemented with the FAST Simulink model by reading the full-field turbulent wind files generated by TurbSim before the simulation. These files describe the wind speed across the rotor plane at zero yaw angle as a function of time. This wind information is unfolded in space with the assumption of Taylor’s frozen turbulence hypothesis [62]. It is assumed that the wind is traveling at a constant speed which is the mean horizontal wind speed at the hub-height throughout the wind file. FAST time-shifts the data in the full-field wind files before the simulation start time. This is in order to contain the turbine rotor in the wind field for any initial yaw angle. The exact time-shift in seconds is 0.5 times the ratio of the total width of the wind data grid and the mean horizontal wind speed at hub-height [54]. This width is defined as the size of the grid in the perpendicular direction to the vertical in the rotor plane.

### 3.5 Linear System Approximations

The FAST tool and many other turbine simulation tools can output linear system approximations through numerical perturbation of dynamical equations. These lower-fidelity models allow use of well established linear control techniques. Turbine linear models differ from the 1-state nonlinear rigid-body model and the turbine models on

the FAST simulation package by the fact that they are obtained numerically and not through first principles. These linear models lose the nonlinearities captured by the 1-state nonlinear rotor model, but can capture the flexible blade and tower structural modes. Linear models that capture the structural modes are preferred in Region 3 control since structural load attenuation is one of the main control objectives in this region.

### 3.5.1 Linear Time Varying via Linearization

The nonlinear wind turbine model in FAST is represented by Equation (3.4):

$$\begin{aligned}\ddot{q} &= f(\dot{q}, q, u, F, t) \\ y &= g(\dot{q}, q, u, F, t)\end{aligned}\tag{3.4}$$

where  $q \in \mathbb{R}^{n_q}$  and  $\dot{q} \in \mathbb{R}^{n_q}$  are the turbine states. In the most general case for offshore wind turbines the value of  $n_q$  is 24. For the utility scale onshore turbines we typically use 15 of these 24 degrees of freedom as explained in Section 3.4.1.

It is possible to disable individual degrees of freedom in FAST to obtain a lower order nonlinear or linear model.  $u \in \mathbb{R}^5$  is the control input. These inputs are the generator torque, yaw angle and individual pitch angles for three blades.  $y \in \mathbb{R}$  is the measurement vector and its dimension depends on chosen outputs.  $F \in \mathbb{R}^7$  is the wind disturbance. This is the simplified wind field description option in the FAST simulation package. These 7 disturbances consist of hub-height average wind speed, horizontal wind direction, vertical wind speed, horizontal wind shear, vertical power law wind shear, linear vertical wind shear, horizontal hub-height wind gust. This simplified description is in contrast with the more complex full-field wind description that can be used in the FAST tool. This complex approach is not suitable for controls oriented linearization due to high number of inputs required to the model the wind input on a raster grid on rotor.

The linearization in FAST is obtained as follows. The nonlinear system is first simulated under steady wind conditions until the turbine reaches a trim operating condition. The trim operating condition is a periodic trajectory  $\bar{q}(t)$  that satisfies Equation (3.5)

$$\begin{aligned}\ddot{\bar{q}} &= f(\dot{\bar{q}}, \bar{q}, \bar{u}, \bar{F}, t) \\ \bar{y} &= g(\dot{\bar{q}}, \bar{q}, \bar{u}, \bar{F}, t)\end{aligned}\tag{3.5}$$

$\bar{q}(t)$  is periodic in the rotor rotation period  $T$ , i.e.  $\bar{q}(t + T) = \bar{q}(t)$ . The nonlinear system (Equation (3.4)) is linearized around  $\bar{q}(t)$  through numerical perturbation. The resulting linear time-varying model have the form of Equation (3.6).

$$\begin{aligned}\dot{\delta}_x &= A(\bar{\psi}_r(t))\delta_x + B(\bar{\psi}_r(t))\delta_u + B_d(\bar{\psi}_r(t))\delta_F \\ \delta_y &= C(\bar{\psi}_r(t))\delta_x + D(\bar{\psi}_r(t))\delta_u + D_d(\bar{\psi}_r(t))\delta_F\end{aligned}\tag{3.6}$$

where

$$\begin{aligned}\delta_x(t) &:= \begin{bmatrix} \delta_q(t) \\ \dot{\delta}_q(t) \end{bmatrix} = \begin{bmatrix} q(t) - \bar{q}(t) \\ \dot{q}(t) - \dot{\bar{q}}(t) \end{bmatrix} \\ \delta_u(t) &:= u(t) - \bar{u}(t) \\ \delta_F(t) &:= F(t) - \bar{F}(t) \\ \delta_y(t) &:= y(t) - \bar{y}(t)\end{aligned}\tag{3.7}$$

The dimensions of the  $\delta_x(t)$ ,  $\delta_u(t)$ ,  $\delta_F(t)$ ,  $\delta_y(t)$  directly follow from the state, input and output signal dimensions from Equation (3.4) used for linearization. Since the trim trajectories are periodic,  $\bar{\psi}_r(t) = \bar{\psi}_r(t+T)$ , the system equations given by Equation (3.6) are also periodic.

It is common in turbine control literature to approximate the periodic time varying system (PLTV) in Equation (3.6) by a time-invariant one. This is typically done to make use of well established linear time invariant (LTI) control techniques. LPV models built by a combination of LTI models obtained at different operating conditions are also used in the literature. These models capture the model variations due to the change in operating condition as defined by the mean wind speed over the rotor surface. There are various methods to perform the LTI approximation for PLTV systems. The simplest approaches are to evaluate the PLTV system at one rotor position or to average the state matrices over one rotor period. These approaches ignore the periodic modal characteristics of the turbine and typically do not provide an LTI model of sufficient accuracy. Floquet theory [63, 64] gives a time-varying coordinate transformation that transforms a PLTV system into one with a constant state ‘‘A’’ matrix. The Floquet transformation retains the periodic modal characteristics but physical intuition about the system states is lost in the transformed system. The most common approach for wind turbine models is to use the multi-blade coordinate (MBC) transformation [65–71]

followed by averaging. We employ this approach in our multivariable controller design work in Chapter 4. Section 3.5.2 discusses the details of the MBC transformation in detail.

### 3.5.2 LTI Approximation and Multiblade Coordinate Transformation

The linear and nonlinear wind turbine equations of motion presented in Sections 3.4.1 and 3.5.1 are derived using a variety of coordinate frames. The FAST manual [51] contains detailed figures of the coordinate frames used to derive the nonlinear turbine equations of motion (Equation (3.4)). Specifically, the tower and rotor degrees of freedom are expressed in an earth fixed coordinate frame while quantities associated with individual blades are defined in a frame that rotates with the rotor. For example, the tip displacements of the blade flapwise bending mode are defined with respect to a rotating coordinate frame attached to the blade. The MBC transformation takes the system states, inputs and outputs defined in a mixed coordinate system (both rotating and non-rotating) and expresses them in a purely non-rotating coordinate frame.

The MBC transformation was originally developed in the helicopter literature [63, 72]. It transforms quantities from rotating blade coordinates into a non-rotating, inertial coordinate frame. The MBC transformation ideally converts the PLTV system into an LTI system. In practice, applying the MBC to the PLTV models generated by FAST yields a system that is still “weakly” periodic, i.e. the transformed system is periodic but with significantly less time variation compared to the original PLTV system. An LTI approximation is obtained by averaging the state matrices of the “weakly” periodic system over one rotor period. This LTI approximation is of sufficient fidelity in many cases [67]. However, the averaging step is ad-hoc and does not rely on a quantifiable error criterion.

The MBC transformation is used to convert blade quantities back and forth between rotating and non-rotating (inertial) coordinate frames. Define the transformation matrix  $M : \mathbb{R} \rightarrow \mathbb{R}^{3 \times 3}$  as a function of rotor position:

$$M(\psi) := \begin{bmatrix} 1 & \sin(\psi) & \cos(\psi) \\ 1 & \sin(\psi + \frac{2\pi}{3}) & \cos(\psi + \frac{2\pi}{3}) \\ 1 & \sin(\psi + \frac{4\pi}{3}) & \cos(\psi + \frac{4\pi}{3}) \end{bmatrix} \quad (3.8)$$

For a given rotor position  $\psi$ ,  $M(\psi)$  transforms quantities in the inertial (non-rotating) frame to the rotating frame attached to the rotor. Conversely, the inverse of  $M(\psi)$  transforms quantities from a rotating to non-rotating frame. This inverse is explicitly given by

$$M(\psi)^{-1} = \frac{2}{3} \begin{bmatrix} \frac{1}{2} & \frac{1}{2} & \frac{1}{2} \\ \sin(\psi) & \sin(\psi + \frac{2\pi}{3}) & \sin(\psi + \frac{4\pi}{3}) \\ \cos(\psi) & \cos(\psi + \frac{2\pi}{3}) & \cos(\psi + \frac{4\pi}{3}) \end{bmatrix} \quad (3.9)$$

As a simplified example, consider a five DOF (on-shore) turbine model that includes rotor position, first tower fore-aft bending mode, and first flapwise bending mode for each blade. For constant wind conditions, this five DOF model can be specified by a nonlinear dynamical equation of the form:

$$\begin{aligned} \ddot{q} &= f(\dot{q}, q, u) \\ y &= g(\dot{q}, q, u) \end{aligned} \quad (3.10)$$

where  $q \in \mathbb{R}^5$  is defined as:

$$q := \begin{bmatrix} \text{Tower 1}^{st} \text{ Fore-Aft Tip Displacement (m)} \\ \text{Rotor position, } \psi \text{ (rad)} \\ \text{Blade 1 1}^{st} \text{ Flapwise Tip Displacement (m)} \\ \text{Blade 2 1}^{st} \text{ Flapwise Tip Displacement (m)} \\ \text{Blade 3 1}^{st} \text{ Flapwise Tip Displacement (m)} \end{bmatrix} \quad (3.11)$$

The rotor position, denoted as  $\psi$ , is defined to be zero when blade 1 is in the upward position. The input and output vectors,  $u \in \mathbb{R}^4$  and  $y \in \mathbb{R}^4$ , are defined as:

$$u := \begin{bmatrix} \text{Blade 1 Pitch Angle (rad)} \\ \text{Blade 2 Pitch Angle (rad)} \\ \text{Blade 3 Pitch Angle (rad)} \\ \text{Generator Torque (N m)} \end{bmatrix} \quad (3.12)$$

$$y := \begin{bmatrix} \text{Rotor Speed (rpm)} \\ \text{Blade 1 Root Bending Moment (kN m)} \\ \text{Blade 2 Root Bending Moment (kN m)} \\ \text{Blade 3 Root Bending Moment (kN m)} \end{bmatrix} \quad (3.13)$$

A linearization of this nonlinear FAST model yields the periodic LTV model in Equation (3.6). In this example the last three entries of the output vector are the root bending moments for the three blades measured in the rotating frame. For a given rotor position  $\psi$  these quantities are transformed to the non-rotating frame by:

$$\begin{bmatrix} y_{avg}^{nr} \\ y_{yaw}^{nr} \\ y_{tilt}^{nr} \end{bmatrix} = M(\psi)^{-1} \begin{bmatrix} y_2 \\ y_3 \\ y_4 \end{bmatrix} \quad (3.14)$$

The superscript *nr* denotes quantities expressed in an inertial non-rotating frame. After the transformation, these quantities have meanings in terms of rotor motion instead of individual blades.  $y_{avg}^{nr}$  represents average value of blade root bending moments. The average moment causes the rotor to bend as a cone.  $y_{tilt}^{nr}$  and  $y_{yaw}^{nr}$  are the blade moments resulting in rotor tilt and yaw, respectively [17]. Similarly, the blade pitch angle inputs and blade flapwise tip displacements can be mapped from rotating to non-rotating coordinates:

$$\begin{bmatrix} u_1^{nr} \\ u_2^{nr} \\ u_3^{nr} \end{bmatrix} = M(\psi)^{-1} \begin{bmatrix} u_1 \\ u_2 \\ u_3 \end{bmatrix} \quad (3.15)$$

$$\begin{bmatrix} q_3^{nr} \\ q_4^{nr} \\ q_5^{nr} \end{bmatrix} = M(\psi)^{-1} \begin{bmatrix} q_3 \\ q_4 \\ q_5 \end{bmatrix}, \quad (3.16)$$

$q_3^{nr}$ ,  $q_4^{nr}$ , and  $q_5^{nr}$  are the rotor coning, rotor tip-path-plane fore-aft tilt and rotor tip-path-plane side-side tilt, respectively [69]. Moreover,  $u_1^{nr}$  is the collective pitch command while  $u_2^{nr}$  and  $u_3^{nr}$  are cyclic individual blade pitch commands.

The system states, inputs, and outputs are defined in a mixed coordinate system, i.e. they have entries expressed in both rotating and non-rotating (inertial) coordinate frames. The MBC transformation is used to convert all quantities to a non-rotating coordinate frame. Specifically, the transformation  $M$  introduced in Equation 3.8 is used to define a transformation  $M_q$  acting on the linearized DOF:

$$M_q(\bar{\psi}(t)) := \begin{bmatrix} I_2 & 0_2 \\ 0_2 & M(\bar{\psi}(t)) \end{bmatrix} \quad (3.17)$$

The linearized DOFs are transformed as:

$$\delta_q(t) = M_q(\bar{\psi}(t)) \delta_q^{nr}(t) \quad (3.18)$$

$M_q$  transforms only those quantities that are specified in the rotating frame. Quantities specified in the inertial frame are left unchanged. Similarly, the state, input, and output transformations for the linearized system are:

$$\delta_x(t) = M_x(\bar{\psi}(t)) \delta_x^{nr}(t) \quad (3.19)$$

$$\delta_u(t) = M_u(\bar{\psi}(t)) \delta_u^{nr}(t) \quad (3.20)$$

$$\delta_y(t) = M_y(\bar{\psi}(t)) \delta_y^{nr}(t) \quad (3.21)$$

where the transformation matrices are given by

$$M_x(\bar{\psi}(t)) = \begin{bmatrix} M_q(\bar{\psi}(t)) & \mathbf{0}_5 \\ \frac{d}{dt}M_q(\bar{\psi}(t)) & M_q(\bar{\psi}(t)) \end{bmatrix} \quad (3.22)$$

$$M_u(\bar{\psi}(t)) := \begin{bmatrix} M(\bar{\psi}(t)) & 0 \\ 0 & 1 \end{bmatrix} \quad (3.23)$$

$$M_y(\bar{\psi}(t)) := \begin{bmatrix} 1 & 0 \\ 0 & M(\bar{\psi}(t)) \end{bmatrix} \quad (3.24)$$

The transformation  $M_x$  is derived by applying the chain rule to Equation 3.18 and using the definition of  $\delta_x$  in terms of  $\delta_q$  and  $\dot{\delta}_q$ . The complete MBC transformation for the linearized system is given by the collection of state, input, and output transformations ( $M_x, M_u, M_y$ ). Applying these transformations to the PLTV model in Equation 3.6 reduces the variation due to rotor position but it typically does not lead to an LTI system. Averaging the remaining variations over one rotor period often gives an LTI model of sufficient fidelity [67]. The basic approach reviewed in this section can easily be generalized to turbine models with additional DOFs specified in the inertial and/or rotating frames. Additional details of MBC can be found in [69] and in the manual for the NREL MATLAB utilities that implement the MBC transformations [70].

## Chapter 4

# Multivariable Control Design

### 4.1 Introduction

Modern wind turbines are multivariable systems with multiple actuators and sensors used to balance the competing performance objectives of power capture and load reduction. This challenging controller design problem is also complicated by the changes in the nonlinear turbine dynamics and the performance objectives with the wind speed. Controllers need to adapt to these changes based on wind speed, but an accurate wind speed measurement is typically not available. Despite these challenges, industrial turbine control is still, for the most part, based on classical, single-input single-output (SISO) designs. Classical SISO designs have a small number of easily tunable parameters engineers can manipulate. Each tunable parameter has a well-understood impact on the turbine performance. Thus industrial control designers can quickly tune the controller to obtain acceptable, although sub-optimal, performance. The advanced multiple-input multiple output (MIMO) design methodologies can deliver superior performance and reduced structural loads but they tend to have significantly more tunable design parameters. Multivariable control techniques also optimize performance with respect to mathematical costs ( $H_\infty$  norm, integral quadratic costs) that can be difficult to relate to the actual turbine performance objectives. Hence tuning of advanced multivariable controllers can be significantly more time consuming as well as requiring specific expertise in the particular design methodology. Advanced methodologies can increase performance and reduce failures but at the price of increased design time and

cost, both of which are critical in an industrial setting.

There have been many research papers on advanced strategies for Region 3 control [3, 14, 17, 20, 25, 28, 43]. These research papers include a variety of methods to reduce tower/blade bending loads and increase the drivetrain damping. Studies whose aim is to reduce blade loads in Region 3 have mainly focused on advanced multivariable controllers that use individual pitch control, i.e. different pitch commands are used for each of the three blades [17, 20, 24, 25, 28]. Drivetrain dampers have been designed that account for the cross-coupling between blade pitch and the drivetrain natural frequency [14]. The advanced control designs have demonstrated significant performance benefits both in simulation as well as on fielded research turbines [3, 43]. However, these methods have not transitioned well to industry due to design time and development cost constraints.

This chapter focuses on a framework for efficient design of multivariable controllers for industrial systems described by nonlinear dynamics. A two-layered architecture is proposed. The lower layer uses signal-based  $H_\infty$  control design, with weighted tuning parameters, to construct multivariable controllers based on linear model approximations. The upper layer is used to specify the performance constraints and objectives such as power capture, structural load reduction and blade pitch-rate limits. A gradient optimization is used to tune the parametrized controller weighting functions in the lower layer based on user specified performance criteria in the upper layer. This approach combines the mathematical tractability and computational efficiency of  $H_\infty$  multivariable control with the ease of design tuning for specific performance metrics on the nonlinear plant. The proposed framework aims for fast and easy design of advanced multivariable controllers thus speeding their transition to the industry. We use a largely simplified Region 3 turbine control design problem to test the efficiency of the proposed framework. For this problem the upper design layer considers important turbine design limitations such as blade pitch rates, generator overspeed and damping of flexible modes of the system. The lower layer tracks rotor speed and rejects wind disturbances. This example is based on a medium-fidelity nonlinear aeroelastic simulation model. It should be noted that this is a preliminary example that ignores the variations in the nonlinear model and the operating-condition based control objectives. However, it still serves to investigate the applicability of this framework on a simpler class of control problems.

The remainder of the chapter is structured as follows. Section 4.2 gives an overview

of the proposed design framework. The example Region 3 turbine control problem is presented in Section 4.3. Results obtained for this example problem are discussed in Section 4.4. Our conclusions are summarized in Section 4.5.

## 4.2 Multivariable Control Design Framework

This section explains the proposed design framework for tuning advanced multivariable controllers. We propose this framework with two main objectives. The first goal is to automate the tuning of advanced multivariable controllers. This simplifies the tuning of the abstract design parameters and lowers the knowledge requirement for the application of the advanced methods. The second goal is to directly incorporate the nonlinear plant and the real performance metrics of interest to the design and tuning process. The aim is to eliminate the iterations between linear control design and the nonlinear Monte Carlo testing. The proposed framework can be generically applied to any nonlinear time-varying plant, i.e. this design framework is not specific to wind turbines.

### 4.2.1 Problem Formulation

Figure 4.1 presents a classical feedback diagram for an industrial system.  $K$  represents the controller to be designed and  $P$  is the plant to be controlled. The plant  $P$  can be a nonlinear, time-varying system. Assume  $P$  is described by the following ordinary differential equations:

$$\begin{aligned} \dot{x} &= f(x, d, u, t) \\ w &= h_1(x, d, u, t) \\ y &= h_2(x, d, u, t) \\ x(0) &= x_0 \end{aligned} \tag{4.1}$$

where  $t \in \mathbb{R}$  is time.  $x(t) \in \mathbb{R}^{n_x}$ ,  $d(t) \in \mathbb{R}^{n_d}$ ,  $u(t) \in \mathbb{R}^{n_u}$  and  $y(t) \in \mathbb{R}^{n_y}$  are the state, disturbance, control input and measurement at time  $t$ , respectively.  $x(0)$  is the initial condition at time  $t = 0$ .  $w(t) \in \mathbb{R}^{n_w}$  is a signal which is used to specify the performance objectives and constraints.  $f : \mathbb{R}^{n_x} \times \mathbb{R}^{n_d} \times \mathbb{R}^{n_u} \times \mathbb{R} \rightarrow \mathbb{R}^{n_x}$  is the vector field,  $h_1 : \mathbb{R}^{n_x} \times \mathbb{R}^{n_d} \times \mathbb{R}^{n_u} \times \mathbb{R} \rightarrow \mathbb{R}^{n_w}$  is the performance equation and  $h_2 : \mathbb{R}^{n_x} \times \mathbb{R}^{n_d} \times \mathbb{R}^{n_u} \times \mathbb{R} \rightarrow \mathbb{R}^{n_y}$  is the measurement equation. There is a rich body of mathematical results providing

technical conditions which ensure the existence and uniqueness of solutions over a time interval  $[0, t_f]$ . We assume that the vector field, measurement equation, performance equation and initial condition are such that there exists a unique solution  $x \in L_2^{n_x}[0, t_f]$ , measurement  $y \in L_2^{n_y}[0, t_f]$  and performance  $w \in L_2^{n_w}[0, t_f]$ .

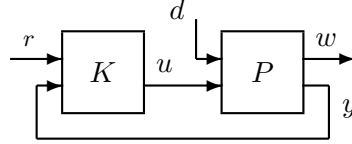


Figure 4.1: Nonlinear, classical feedback diagram

Eq. (4.1) assumes that  $w(t)$  contains all the signals that might be used to specify some performance constraints without loss in generality. Mathematically oriented objectives, e.g. signal  $L_2$ -norm, or more complicated objectives such as damage-equivalent loads in a turbine structure can be used. In the most general case, a performance constraint can be specified as a functional on  $w(t)$  that maps it to a scalar number. Let  $C_i : L_2^{n_w}[0, t_f] \rightarrow \mathbb{R}$  denote the functional that describes the  $i^{\text{th}}$  performance constraint by  $C_i(w) \leq 0$ . In other words,  $C_i$  maps the trajectory  $w(t)$  to a scalar non-positive number if the  $i^{\text{th}}$  performance constraint is satisfied. Assume there are  $m$  such constraints and let  $C : L_2^{n_w}[0, t_f] \rightarrow \mathbb{R}^m$  denote the vector stacking of all such constraints. In other words, the performance constraints are denoted by  $C(w) \leq 0$ . Similarly, let  $G : L_2^{n_w}[0, t_f] \rightarrow \mathbb{R}$  denote an objective function that quantifies the performance of the output by  $G(w)$ . For example, if  $w(t)$  is the bending load on the turbine tower then the  $L_\infty$  norm,  $G(w) := \max_t |w(t)|$ , represents the peak bending load over time on the turbine tower.

Denote a trim initial condition and time-varying operating trajectory with  $\bar{x}_0, \bar{d}(t), \bar{u}(t), \bar{y}(t)$  for  $t \in [0, t_f]$ . The control problem considered is as follows: Design a controller  $\bar{K}$  such that the feedback connection of the nonlinear, time-varying plant  $P$  and the controller  $\bar{K}$  in Figure 4.2 satisfies the performance constraints  $C(w) \leq 0$  when operating close to  $\bar{x}_0, \bar{d}(t), \bar{u}(t), \bar{y}(t)$ . The controller  $\bar{K}$  has the inputs  $\delta r = \xi_r(r, u, y, \bar{d}, \bar{u}, \bar{y})$  and  $\delta y = \xi_y(r, u, y, \bar{d}, \bar{u}, \bar{y})$  where  $\xi_r : \mathbb{R}^{n_r} \times \mathbb{R}^{n_u} \times \mathbb{R}^{n_y} \times \mathbb{R}^{n_d} \times \mathbb{R}^{n_u} \times \mathbb{R}^{n_y} \rightarrow \mathbb{R}^{n_r}$  and  $\xi_y : \mathbb{R}^{n_r} \times \mathbb{R}^{n_u} \times \mathbb{R}^{n_y} \times \mathbb{R}^{n_d} \times \mathbb{R}^{n_u} \times \mathbb{R}^{n_y} \rightarrow \mathbb{R}^{n_y}$ . The plant input  $u(t)$  is related to the controller output  $\delta u$  through  $u = \xi_u(r, u, y, \bar{d}, \bar{u}, \bar{y})$  where  $\xi_u : \mathbb{R}^{n_r} \times \mathbb{R}^{n_u} \times \mathbb{R}^{n_y} \times$

$\mathbb{R}^{n_d} \times \mathbb{R}^{n_u} \times \mathbb{R}^{n_y} \rightarrow \mathbb{R}^{n_u}$ . The functions  $\xi_u$ ,  $\xi_y$  and  $\xi_r$  represent input, measurement and reference transformations that relate the signals in the interconnection to the control objectives. In the standard case, these transformations simply subtract off and add back trim conditions as would be used in most linear control designs implemented for a nonlinear plant. The more general notation used here is to allow for other types of transformations, e.g. the multiblade coordinate transformation in turbine control. These transformations and objectives are selected by the designer before the design task of  $\bar{K}$ . For instance, let  $y(t)$  represent the turbine tower structural load. The objective is to keep  $y(t)$  constant at the average of its trim trajectory over time to minimize structural fatigue. Then the transformation  $\xi_y = y - \frac{1}{T} \int_0^T \bar{y}(t) dt$  is chosen to represent this objective where  $T$  is the trim oscillation period. The combination of the  $\bar{K}$ ,  $\xi_u$ ,  $\xi_y$ ,  $\xi_r$  corresponds to the  $K$  in Figure 4.1 where the dependency of  $K$  on  $\bar{d}(t), \bar{y}(t), \bar{u}(t)$  was omitted for simplicity.

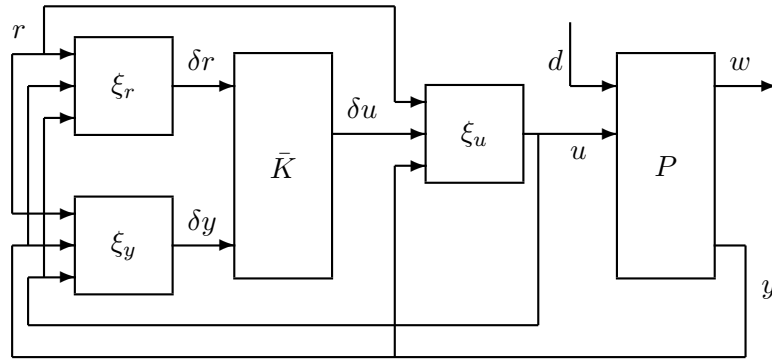


Figure 4.2: Controller implementation on the nonlinear plant

Many potential issues are glossed over in this formulation. First, the controller  $K$  may fail to satisfy the performance constraints at an initial condition far from the  $\bar{x}_0$ . Second,  $d(t)$  can be a stochastic signal. The plant behavior around the deterministic  $\bar{d}(t)$  may not sufficiently capture the system dynamics for other potential trajectories. Third, the control objectives can be a function of the disturbance  $d$  when a reliable measurement of  $d$  is not available. This raises issues with the choice of  $\xi_r$ ,  $\xi_u$  and  $\xi_y$  for the implementation of the controller. Consider the turbine tower structural load example with  $\xi_y = y - \frac{1}{T} \int_0^T \bar{y}(t) dt$  mentioned in the previous paragraph. In reality, the control objective the average tower load depends on  $d$ . In other words, we rely on

the assumption that the dependence of  $\xi_y$ ,  $\xi_r$  and  $\xi_u$  on  $d$  is sufficiently small. This corresponds to an assumption of small wind variations such that the aimed load level of  $\int_0^T \bar{y}(t)dt$  is not changing significantly for the example tower structural load problem.

#### 4.2.2 Design Process

We choose a linear controller architecture for  $\bar{K}$  to make use of the well-established control design methods available in the literature. Figure 4.3 shows a classical linear feedback interconnection. The plant  $P_{lin}$  in Figure 4.3 is a linear time-invariant approximation to the nonlinear time-varying plant  $P$  around the trim operating conditions  $\bar{x}_0, \bar{d}(t), \bar{u}(t), \bar{y}(t)$ . The inputs and the outputs of  $P_{lin}$  are  $[\delta d; \delta u]$  and  $[\delta w; \delta y]$ , respectively. It is assumed that  $\delta d$  includes sensor noise inputs and  $\delta y$  is the noisy measurement. The inputs of the linear controller  $\bar{K}$  are  $[\delta r, \delta y]$  and its output is  $\delta u$ .  $W_{perf} : \mathbb{R}^{n_r} \times \mathbb{R}^{n_w} \rightarrow \mathbb{R}^{n_{w_s}}$  is the performance weight that emphasizes the important dynamics in the  $\delta w$ , where  $n_{w_s}$  is the number of performance outputs in  $\delta w_s$ . For example,  $W_{perf}$  can be a low-pass filter on  $\delta r - \delta w$  that emphasizes the importance of the low-frequency tracking errors.

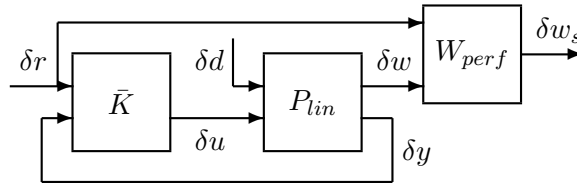


Figure 4.3: Linear, classical feedback interconnection

We use signal-based  $H_\infty$  control design [73, 74] as the core of the proposed multivariable design framework. In signal-based  $H_\infty$  control design, all the performance objectives are encapsulated in a single metric using frequency domain weights. The objective is to minimize the gain, measured as an induced  $L_2$  norm (also known as the  $H_\infty$  norm), from the weighted (uncertainty, wind, noise) inputs to the weighted (actuator, tracking performance) outputs. Actuator and performance weights specify the relative importance for each objective. There are several other important objectives that are typically implicit in classical control designs. Specifically, the controller should reject sensor noise and wind disturbances, minimize actuator usage, and the

performance should be robust to model uncertainties.

Figure 4.4 presents a typical  $H_\infty$  design interconnection. This interconnection is used to specify the relative importance of the signals encountered in the linear system approximation in Figure 4.3 for optimal control design. The signals in this interconnection can be categorized into four groups. The exogenous inputs are  $[\delta\hat{d}_u, \delta\hat{d}, \delta\hat{r}]$  where the hat notation  $\hat{\cdot}$  denotes the normalized,  $L_2$  norm bounded signals. The outputs are  $[\delta u_s, \delta w_s]$  where the subscript  $s$  denotes the weighted signals. The controller takes the measurements  $[\delta y, \delta r]$  and outputs  $\delta u$ . The weights  $W_{d_u}$ ,  $W_d$  and  $W_r$  represent the expected frequency content of the typical  $\delta d_u$ ,  $\delta d$  and  $\delta r$  signals, respectively. Similarly, the weights  $W_u$ ,  $W_{perf}$  represent the relative importance of the  $\delta u$  and  $\delta w$  respectively. These weights can be either constant or dynamic. In the latter case they must be stable and proper systems.

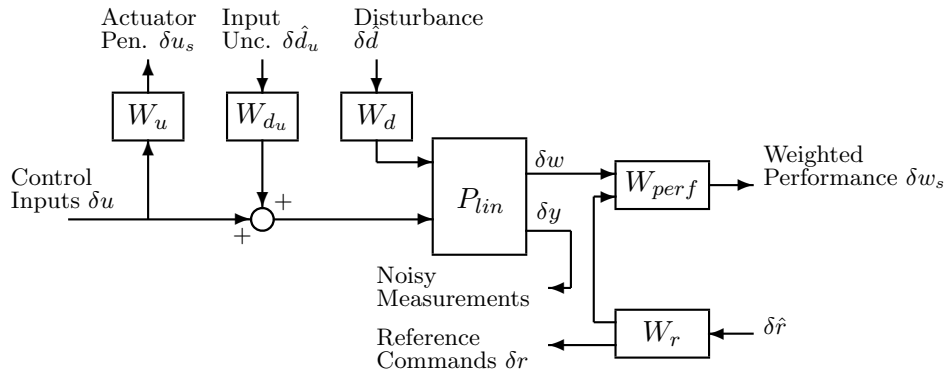


Figure 4.4:  $H_\infty$ -optimal controller design interconnection

$W_d$  represents the expected frequency content of the exogenous disturbances and measurement noise. Disturbance data can typically be obtained from open-loop or offline data from the plant  $P$ . Noise information is derived from laboratory experiments or is based on manufacturer measurements. An example is the wind disturbance experienced by a turbine. Typically this data is available from the met towers installed for wind farm feasibility studies at the site. Fast Fourier Transformation and power spectral density estimation techniques can be used to extract the frequency content of this time-domain data.

$W_r$  is used in problems requiring tracking a reference command. It shapes the frequency content of the expected reference signals. For example  $\delta r$  can be the desired

pitch rate command for a plane. Fighter pilots typically generate control stick inputs up to  $12\text{rad/s}$ . In this case  $W_r$  can have a low-pass filter characteristic with a bandwidth of  $12\text{rad/s}$ .

$W_{d_u}$  is the input uncertainty that lumps the uncertainties in the plant  $P_{lin}$  into a single weight. This uncertainty modeling method was chosen due to its simplicity. Since the output of the  $W_{d_u}$  is added to the actual control signal  $\delta u$ , a choice can be made considering the expected  $\|\delta u(t)\|_\infty = \max_t |\delta u(t)|$  and the frequencies where the model uncertainties are large, i.e. where the dynamics of  $P$  and  $P_{lin}$  differ largely.  $W_{d_u}$  can be set as dynamic weight such that its gain is a small percentage of the  $\|\delta u(t)\|_\infty$  in the frequency range where the model uncertainties are small. A higher gain should be used at frequencies where the model deviations in  $P$  from  $P_{lin}$  is large. This weight limits the frequencies where the controller will be active. Specifically, there is no control authority when the magnitude of the uncertain input  $\delta d_{u_s}$  is as large as the control signal  $\delta u$ . This is because the uncertain, weighted signal  $\delta d_{u_s}$  with arbitrary phase can cancel the command from the controller.

The performance penalty  $W_{perf}$  can contain two types of weights. For the tracking objectives, it can contain a desired ideal model for the closed-loop system and weigh the difference between the ideal and the actual response. Often it is desired to have a good match at low-frequencies within the actuator bandwidth.  $W_{perf}$  can also penalize the other variables internal to the  $P_{lin}$  that are not a part of the tracking objectives.

$W_u$  is used to penalize the control signal usage. This is necessary to limit the actuator use to keep them within their deflection and rate limits in the face of the tracking and disturbance rejection objectives already defined. One choice is a high pass filter that penalizes high-frequency control signal beyond the bandwidth of the actuators.

Denote the  $H_\infty$  design interconnection with inputs  $[\delta \hat{d}_u, \delta \hat{d}, \delta \hat{r}, \delta u]$  and outputs  $[\delta w_s, \delta u_s, \delta y, \delta r]$  as  $\tilde{P}_{lin}$ . In the most general case, all such interconnections can be represented in the linear fractional transformation form shown in Figure 4.5. The  $H_\infty$ -norm of this closed-loop system is defined as [74]:

$$\|F_l(\tilde{P}_{lin}, \bar{K})\|_\infty = \max_\omega \bar{\sigma}(F_l(\tilde{P}_{lin}, \bar{K})(j\omega)) \quad (4.2)$$

where  $F_l$  is the lower linear fractional transformation,  $\omega$  is the frequency-domain variable,  $\bar{\sigma}$  is the peak singular value across all input-output channels as a function of the

frequency. The aim is to synthesize a controller  $\bar{K}$  that minimizes  $\|F_l(\tilde{P}_{lin}, \bar{K})\|_\infty$ , i. e.  $\bar{K} \triangleq \min_{\bar{K}} \max_{\omega} \bar{\sigma}(F_l(\tilde{P}_{lin}, \bar{K})(j\omega))$ . Notice that the only argument of this optimization problem is  $\tilde{P}_{lin}$ . In other words, a corresponding  $H_\infty$  controller  $\bar{K}$  can be synthesized once the design weights are set in the design interconnection to form  $\tilde{P}_{lin}$ .

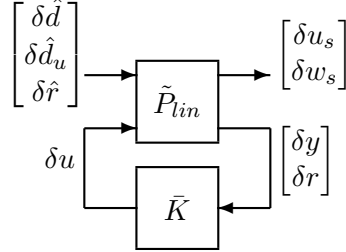


Figure 4.5: LFT representation for controller design

This linear control design formulation requires consideration of the issues explained in Section 4.2.1 as well as several new ones. First, the linear time-invariant plant  $P_{lin}$  only captures the dynamics of  $P$  when operating near  $\bar{x}_0, \bar{u}, \bar{d}$ . Also the time-invariant formulation assumes that the variations in  $P$  over time are small. The robustness of the controller for these small variations are set by the input uncertainty weight  $W_{d_u}$ . Second, the inputs and outputs of  $P_{lin}$  are the variations around the trim trajectories, i.e.  $\delta u = u - \bar{u}$ ,  $\delta y = y - \bar{y}$ . This can pose a challenge when it is desired for  $\bar{K}$  to act on other functions of the trim trajectory. For instance, the trim trajectory for a turbine blade structural load consists of fluctuations around an average value. The design interest is to attenuate these fluctuations. These fluctuations are not observed in the outputs of the LTI plant  $P_{lin}$ . This is because  $P_{lin}$  only captures the deviations from the trim trajectory whereas these fluctuations are in the trim trajectory. Lastly, the  $H_\infty$  controller is optimal in terms of the induced  $L_2$ -norm on  $\delta w_s$  signal as opposed to the  $G(w)$  functional that captures the main design objective. Therefore a typical design procedure involves a three step approach:

- Linear controller design
- Time-intensive nonlinear testing
- Design revision and iteration

The design revision step relies on designer's knowledge about the plant and the chosen control method. This iteration continues until satisfactory performance is achieved in the nonlinear testing step. This iterative approach increases design time and cost.

### 4.2.3 Auto-Tuning Framework

There is a correspondence between the generalized plant  $\tilde{P}_{lin}$  and  $\bar{K}$ , i.e. given a  $\tilde{P}_{lin}$  an  $H_\infty$  optimal  $\bar{K}$  can be synthesized. This correspondence can be used to formulate a finite-dimensional nonlinear control problem that optimizes  $\bar{K}$  based on performance requirements  $C(w) \leq 0$  and objectives  $G(w)$  specified in the time and frequency domains. The weights used to construct the generalized plant  $\tilde{P}_{lin}$  can be parametrized for tuning. As an example, block diagonal weights are used to penalize each actuator and performance penalty signal independently. Each weight is parametrized as:

$$W(s) = F_0(1 + \gamma_1) \frac{s + z_0(1 + \gamma_2)}{s + p_0(1 + \gamma_3)} \quad (4.3)$$

where  $F_0, z_0, p_0$  are the initial gain, location of the zero and the pole of this 1<sup>st</sup> order weight.  $\gamma_1, \gamma_2, \gamma_3$  represent percentage-wise adjustments made by the optimization. Let  $\gamma \in \mathbb{R}^{n_\gamma}$  be the vector of the parameters of  $W_u$  and  $W_{perf}$  that appear in the  $H_\infty$  architecture. For each set of weight parameters  $\gamma$ , a controller, denoted  $\bar{K}_\gamma(s)$ , can be easily computed using standard robust control software tools [75]. This formulation requires a strict lower-bound of  $-1$  on each element of  $\gamma$ . This ensures the stability of the weights assuming that the initial parametrized weight is stable and minimum-phase. The nonlinear optimization problem is formulated as follows:

$$\begin{aligned} & \underset{\gamma}{\text{minimize:}} \quad G(w_\gamma) \\ & \text{subject to:} \quad C(w_\gamma) \leq 0 \\ & \quad \quad \quad lb \leq \gamma \leq ub \\ & \quad \quad \quad \text{Equation (4.1)} \\ & \quad \quad \quad \bar{K}_\gamma \triangleq \min_{\bar{K}} \max_{\omega} \bar{\sigma}(F_l(\tilde{P}_{lin}(\gamma), \bar{K})(j\omega)) \\ & \quad \quad \quad u = \xi_u(r, \bar{K}_\gamma[\delta r; \delta y], y, \bar{d}, \bar{u}, \bar{y}) \\ & \quad \quad \quad \delta y = \xi_y(r, u, y, \bar{d}, \bar{u}, \bar{y}), \quad \delta r = \xi_r(r, u, y, \bar{d}, \bar{u}, \bar{y}) \\ & \quad \quad \quad \text{Given } x(0), r[0, t_f] \text{ and } d[0, t_f] \end{aligned} \quad (4.4)$$

where  $\gamma \in \Gamma \subseteq \mathbb{R}^{n_\gamma}$  is the allowable set of decision variables that are used to construct an advanced, multivariable controller  $\bar{K}_\gamma$ . Maximization problem is without loss of generality since  $\min_\gamma G(w_\gamma) = -\max_\gamma [-G(w_\gamma)]$ . The subscript  $\gamma$  in  $\bar{K}_\gamma$  and  $w_\gamma$  denotes their dependence on  $\gamma$ . The design task is to synthesize a  $\bar{K}_\gamma$  that satisfies the performance constraints specified in  $C(w_\gamma) \in \mathbb{R}^m$ . The  $\bar{K}_\gamma$  is optimized with respect to the performance objective functional  $G(w_\gamma) \in \mathbb{R}$ . The  $G(w_\gamma)$  and  $C(w_\gamma)$  depend on  $w_\gamma(t)$ , which depends on  $\bar{K}_\gamma$ ,  $P$ ,  $r$ ,  $d$  and the initial conditions  $x(0)$ . In other words, given a set of decision variables  $\gamma$  an  $H_\infty$ -optimal controller  $\bar{K}_\gamma$  is designed using the generalized plant  $\tilde{P}_{lin}(\gamma)$ . The nonlinear plant  $P$  is simulated with the  $\bar{K}_\gamma$  with the transformations  $\xi_u$ ,  $\xi_y$ ,  $\xi_r$  for the initial condition  $x(0)$  and the disturbance trajectory  $d(y)$ . The resulting  $w(t)$  trajectory is used to evaluate the performance objective  $G(w_\gamma)$  and constraints  $C(w_\gamma)$ . The gradient based algorithm tunes the design parameter  $\gamma$  based on  $G(w_\gamma)$  and  $C(w_\gamma)$  iteratively.

An initial feasible set of decision variables  $\gamma$  that satisfy constraints  $C(w_\gamma) \leq 0$  and bounds  $lb \leq \gamma \leq ub$ , is required. This is a common requirement of the constrained nonlinear optimization solvers. The following iterative Phase I optimization procedure can be followed to obtain an initial feasible point:

1. Choose a random parameter set or some intelligent heuristic based set of parameters on a few performance specifications such as controller bandwidth. This set of parameters will yield an  $H_\infty$  controller that stabilizes the LTI plant  $\tilde{P}_{lin}$  under some certain mild conditions [74].
2. Simulate the closed-loop nonlinear simulation with the  $H_\infty$  controller obtained in Step 1. In case the nonlinear closed-loop system is unstable skip to Step 3. If the nonlinear closed-loop system is stable and the simulations achieve a finite cost, continue with the Phase I optimization given in Eq. (4.5). The optimization in Eq. (4.5) minimizes the slack variable  $\zeta$  to obtain a set of design parameters  $\gamma$  that easily satisfies design constraints in  $C(w_\gamma)$ .

$$\begin{aligned}
 & \underset{\gamma, \zeta}{\text{minimize:}} \quad \zeta \\
 & \text{subject to:} \quad C(w_\gamma) \leq \zeta \\
 & \quad \quad \quad \text{Other constraints in Eq. (4.4)}
 \end{aligned} \tag{4.5}$$

3. Scale down the disturbances (wind gusts and measurement noise) to a sufficiently small level that the nonlinear closed-loop system is stable and the simulations achieve a finite cost. Specifically, the scaled disturbance signal is  $\check{d} = \Lambda(d - \bar{d}) + \bar{d}$  where  $\Lambda \in (0, 1]$  is the scale factor. At this point the  $H_\infty$  controller stabilizes the nonlinear closed-loop system for smaller amplitude perturbations from the trim. Solve the optimization in Eq. (4.6) until  $\Lambda = 1$ . This yields an  $H_\infty$  controller that stabilizes the nonlinear system on the desired disturbance signals. The Phase I optimization in Eq. (4.5) can be used at this point to find a feasible design.

$$\begin{aligned} & \underset{\gamma, \Lambda}{\text{maximize:}} \quad \Lambda \\ & \text{subject to:} \quad C(w_\gamma) \leq \infty \end{aligned} \tag{4.6}$$

Other constraints in Eq. (4.4) where  $d$  is replaced with  $\check{d}$

This problem formulation makes no assumptions about the objective functional  $G(w_\gamma)$ , constraint functional  $C(w_\gamma)$ , or how the parameter vector  $\gamma$  enters into the system dynamics and measurement equation. Consequently, this minimization is a computationally difficult problem to solve. In general, it is not a convex optimization and it may have many local optima that are not global optima. Our goal will be to use gradient-based optimization to find a parameter vector that achieves a local maxima. This will generally not find a global maxima. However, it does provide a means to improve upon a ‘bad’ initial control design. The gradient based solver approximately requires  $n_\gamma + 1$  nonlinear simulations at each iteration. The total number of simulations can be approximated by  $n_{it}(n_\gamma + 1)$  where  $n_{it}$  is the number of iterations. If the computation time for one simulation is  $t_{sim}$  then the expected time for the optimization can be approximated with  $t_{sim}n_{it}(n_\gamma + 1)$ . Assuming that the  $t_{sim}$  is approximately independent of the decision variables, it can be calculated with a simulation before the optimization. Therefore the total design time or the desired number of iterations can be chosen beforehand.

### 4.3 Example Problem: Turbine Region 3 Controllers

This section presents an example of the proposed control design framework. A turbine control problem in above-rated wind speeds (Region 3) is considered. We present a

simplified problem. Design of a controller that will be implemented on an actual turbine requires many extra design considerations. However, this example still serves to demonstrate the applicability of the proposed framework.

Typical Region 3 control design objectives consist of rotor speed regulation as well as blade, tower and gearbox structural load minimization goals. These are disturbance rejection goals and there are no reference tracking objectives. A major performance constraint is to keep the generator speed under its over-speed limit. Structural load specifications include peak load and damage equivalent loads (DELs). These performance objectives must be satisfied under model uncertainties and limitations of the pitch actuators. Specifically, pitch actuators have a limited bandwidth and they are subject to pitch-rate constraints.

The nonlinear plant considered is the WindPACT 1.5MW turbine. A model of this plant,  $P$ , is distributed with the FAST [51] aeroelastic turbine simulation package.  $P$  includes first-order linear models of the pitch actuators that have a  $10rad/s$  bandwidth. The disturbance,  $d(t) \in \mathbb{R}^4$ , is the turbulent wind conditions that are generated by NREL's TurbSim [54]. A single 450s wind trajectory with  $18m/s$  average hub-height wind speed and 5% turbulence was chosen for Region 3 operation. This corresponds to a typical, mild turbulence level. We use the simplified wind field description in FAST that consists of variations in average horizontal wind speed over the rotor area ( $m/s$ ), vertical wind speed ( $m/s$ ), wind direction ( $deg$ ) and a constant vertical power-law wind shear of 0.2 (*unitless*). The control input  $u(t) \in \mathbb{R}^3$  is the pitch angle command for each blade in ( $rad/s$ ). The generator torque is held constant at its rated value of  $8376.58Nm$  and is not included in  $u(t)$ . The plant measurements  $y(t) \in \mathbb{R}^6$  consist of rotor position ( $rad$ ), rotor speed ( $rpm$ ), flapwise root bending moment for each blade ( $kNm$ ) and the tower bending moment at root in the fore-aft direction ( $kNm$ ). The variables used for the performance constraints and objectives,  $w(t) \in \mathbb{R}^6$ , are chosen to be the same with the vector  $y(t)$ . Ideal measurements with no noise are used in simulations of  $P$ . The following section, Section 4.3.3, explains the linearization process to obtain an LTI turbine model  $P_{lin}$  as well as the  $\xi_u, \xi_y$  input-measurement transformations used to select the controller inputs and outputs.

### 4.3.1 Linear Model and Input-Measurement Transformations

Assume a constant wind speed trim operating condition  $\bar{d} \in \mathbb{R}^4$  where the only nonzero elements of the disturbance vector are the average horizontal wind speed over the rotor area  $18m/s$  and the constant vertical power-law wind shear of 0.2 (*unitless*). Let  $\bar{u}$  be the corresponding constant pitch angle for trim. The turbine is subjected to time-varying loads even in constant wind conditions because persistent disturbances such as tower shadow, gravity and aerodynamic forces depend on the rotor position and structural flexibility. As a result, the wind turbine trim values are time-varying and periodic even in constant wind conditions. In other words,  $\bar{y}(t) \in \mathbb{R}^6$  is a periodic trim trajectory with period  $T = \frac{2\pi}{2.15} = 2.92s$  where  $2.15rad/s$  is the rated rotor speed. The value of  $\bar{u} = 0.335rad$  is calculated through FAST through an iterative method. Linearizations computed around  $\bar{d}$ ,  $\bar{u}$ ,  $\bar{y}$  at various rotor positions result in a periodic, linear time-varying (LTV) system with period equal to the rotor rotation period. The inputs  $[\delta d; \delta u]$  and the outputs  $[\delta w; \delta y]$  of this periodic LTV are the deviations from their respective trim trajectories. For design simplicity we eliminate 3 elements of  $\delta d$  and only leave the variations in average horizontal wind speed over the rotor area ( $m/s$ ) in the linear model. This is the input channel with the largest variations and it has the most impact on the outputs.

The multiblade coordinate transformation (MBC) followed by averaging is used to obtain an LTI approximation from the periodic LTV model. The details of this approach can be found in Section 3.5. The MBC transformation expresses the turbine variables that are defined in rotating coordinate frames in a non-rotating coordinate frame. This LTI approximation of the periodic LTV system is shown in Figure 4.6 and denoted as  $P_{lin}$ .  $\bar{\psi}_r(t)$  denotes the trim trajectory of the rotor position that is contained in  $\bar{y}(t)$ .  $M_u(\bar{\psi}_r) : \mathbb{R}^3 \rightarrow \mathbb{R}^3$  and  $T_y^{-1}(\bar{\psi}_r) : \mathbb{R}^6 \rightarrow \mathbb{R}^6$  are the MBC transformation functions. The input transformation  $M_u(\bar{\psi}_r)$  is given in Eq. (4.7):

$$M_u(\bar{\psi}_r(t)) = \begin{bmatrix} 1 & \cos(\bar{\psi}_r(t)) & \sin(\bar{\psi}_r(t)) \\ 1 & \cos(\bar{\psi}_r(t) + 2\pi/3) & \sin(\bar{\psi}_r(t) + 2\pi/3) \\ 1 & \cos(\bar{\psi}_r(t) + 4\pi/3) & \sin(\bar{\psi}_r(t) + 4\pi/3) \end{bmatrix} \quad (4.7)$$

The measurement transformation  $T_y^{-1}(\bar{\psi}_r)$  can be written with the help of the inverse

of the  $M_u$ :

$$M_u^{-1}(\bar{\psi}_r(t)) = \frac{1}{3} \begin{bmatrix} 1 & 1 & 1 \\ 2 \cos(\bar{\psi}_r(t)) & 2 \cos(\bar{\psi}_r(t) + 2\pi/3) & 2 \cos(\bar{\psi}_r(t) + 4\pi/3) \\ 2 \sin(\bar{\psi}_r(t)) & 2 \sin(\bar{\psi}_r(t) + 2\pi/3) & 2 \sin(\bar{\psi}_r(t) + 4\pi/3) \end{bmatrix} \quad (4.8)$$

$$T_y^{-1}(\bar{\psi}_r(t)) = \begin{bmatrix} 1 & 0 & \mathbf{0}_{1 \times 3} & 0 \\ 0 & 1 & \mathbf{0}_{1 \times 3} & 0 \\ \mathbf{0}_{3 \times 1} & \mathbf{0}_{3 \times 1} & M_u^{-1}(\bar{\psi}_r(t)) & \mathbf{0}_{3 \times 1} \\ 0 & 0 & \mathbf{0}_{1 \times 3} & 1 \end{bmatrix} \quad (4.9)$$

The superscript  $nr$  notation for  $\delta u^{nr}$ ,  $\delta y^{nr}$ ,  $\delta w^{nr}$  denotes the quantities expressed in non-rotating frame. More specifically, the transformed control input is  $\delta u^{nr} = [\delta\beta_{coll}; \delta\beta_{tilt}; \delta\beta_{yaw}]$ . The  $\delta\beta_{coll}$  ( $rad$ ) is the collective pitch angle. It is the average pitch angle from the three blades. The  $\delta\beta_{tilt}$  and  $\delta\beta_{yaw}$  ( $rad$ ) correspond to cyclic blade pitch motions that control the tilting and yawing motion of the turbine rotor, respectively. The only elements of the  $\delta y$  that are transformed to the non-rotating coordinate frame are the 3<sup>rd</sup> through 5<sup>th</sup> elements. These transformed variables are  $\delta M_{avg}$ ,  $\delta M_{tilt}$ ,  $\delta M_{yaw}$ .  $\delta M_{avg}$  is the average bending loads on the three blades ( $kNm$ ) that cause the rotor to assume a cone shape. The  $\delta M_{tilt}$  and  $\delta M_{yaw}$  ( $kNm$ ) are bending moments at the root that cause the rotor to tilt and yaw.

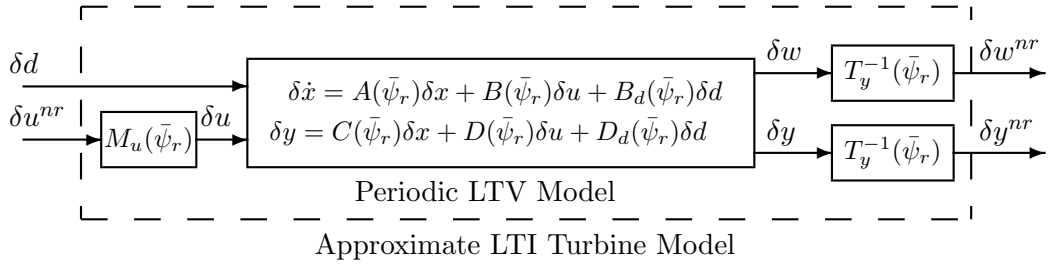


Figure 4.6: MBC application and Approximate LTI Turbine Model

In summary, the input and measurements of the nonlinear plant  $P$  and the linear turbine model  $P_{lin}$  are related through the transformations  $u = M_u^{-1}(\bar{\psi}_r(t))\delta u^{nr} + \bar{u}$  and  $\delta y^{nr} = T_y^{-1}(\bar{\psi}_r(t))(y(t) - \bar{y}(y))$ . However, there are two implementation challenges with

this approach. First, the MBC transformation is a function of the trim trajectory of rotor position. When implemented, the rotor position of the actual turbine will diverge from its trim trajectory due to varying wind conditions. Hence it is desired to use the actual rotor position, i.e.  $T_y^{-1}(\psi_r)$  rather than  $T_y^{-1}(\bar{\psi}_r)$ , for the MBC transformation. Second, it is desired from the controller to attenuate the variations around the average of the  $\bar{y}(t)$  over time in each channel. This is especially important for the bending load measurements. Therefore the actual implementation of the transformations are  $u = \xi_u(\delta u^{nr}, y, \bar{u}) = M_u^{-1}(\psi_r(t))\delta u^{nr} + \bar{u}$  and  $\delta y^{nr} = \xi_y(y, \bar{y}) = T_y^{-1}(\psi_r)(y(t) - \frac{1}{T} \int_0^T \bar{y}(t) dt)$ .

### 4.3.2 $H_\infty$ Design Interconnection and the Initial Design

Figure 4.7 shows the system interconnection used for the disturbance rejecting controller design. The design task is to select weights in the  $H_\infty$  design interconnection in Figure 4.7 to satisfy performance specifications on the nonlinear turbine model. These weights can be separated into two categories. The weights  $W_d$ ,  $W_{noise}$  and  $W_{d_u}$  are selected to describe the frequency content of the wind disturbances, sensor noise and model uncertainties. These quantities are set by the turbine design and the environmental conditions. These weights are set a-priori and left as constants in the nonlinear optimization. The second class of weights consist of  $W_u$  and  $W_{perf}$ . These weights describe the actuator limitations and the performance trade-off between multiple objectives. Tuning of these weights to achieve the desired performance and robustness can be time consuming and it requires specific domain expertise in the  $H_\infty$  design methodology. This increases both the design time and costs. Therefore this task is left to the proposed automated tuning framework.

We aim to obtain an initial design that satisfies design constraints  $C(w_\gamma) \leq 0$  in a relatively small amount of time. Optimality with respect to cost function is not considered. The resulting controller is likely sub-optimal but will be tuned by the gradient-based optimization based on design specifications in the objective and constraint functions  $G(w_\gamma)$  and  $C(w_\gamma)$ .

$W_d$  represents the frequency-content of the worst-case wind conditions for the turbine operation. This can be obtained either from wind turbulence models appropriate for the turbine location or from time-domain data that is gathered at the wind farm. Available time domain data can be mapped to the frequency domain via the Discrete Fourier

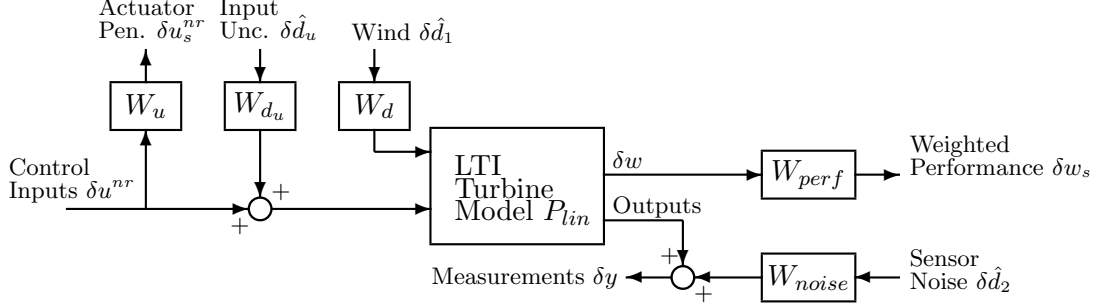


Figure 4.7: System Interconnection for  $H_\infty$  Region 3 Controller Design

Transform. The frequency domain magnitude data can then be over-bounded by a transfer function to obtain  $W_d$ . For this study, operation under a mild turbulence level (5%) is considered. Wind data with 5% turbulence with an average wind speed of  $18m/s$  is generated using TurbSim [54] developed by NREL. A transfer function is obtained as described from the hub-height wind data. The resulting weight is given by:

$$W_d = 0.25 \frac{s/60 + 1}{s/4 + 1} \quad (4.10)$$

$W_n$  represents the noise on the sensors. We choose  $W_n$  as constant block diagonal weights that correspond to the 1% of the  $\bar{y}$ . This approximately models noise with amplitude equal to 1% of each signal.

The input uncertainty  $W_{d_u}$  is chosen based on the expected peak pitch angle input of  $0.5rad$ . For the sake of simplicity in the example problem a constant and low level of uncertainty, a block diagonal weight with the 2% of the trim pitch inputs, is chosen. A more detailed uncertainty modeling approach can involve modifying the parameters of the nonlinear model and obtaining many linearizations. An uncertainty set that covers all these linearizations can be used.

The actuator and performance penalty weights,  $W_u$  and  $W_{perf}$ , are tuned by the optimization algorithm. The initial values of these weights are chosen to obtain a conservative controller with limited bandwidth. The block diagonal actuator penalty weight  $W_u = diag(W_{coll}, W_{tilt}, W_{yaw})$  consists of penalties on the collective and cyclic pitch action. These penalties are chosen as 1<sup>st</sup> order high-pass filters to penalize high-frequency control action. Specifically, the zero locations of these filters are chosen

at the bandwidth of the actuator models to penalize actuation beyond the actuator bandwidth. The gain of  $W_{coll}$  is selected to be lower than the cyclic pitch penalties. Hence the resulting controllers focus on collective pitch control. Collective pitch action has a dominant role in rotor speed tracking and tower fore-aft bending. In addition, this prevents controllers from using excess pitch-rates with individual pitch control. Therefore this selection is helpful for satisfying the constraints in  $C(w_\gamma)$  even though it may be sub-optimal for blade load reduction. All three weights have zeros at  $s = 10$  and poles at  $s = 80$ . Their DC (low-frequency) gains are 0.25, 1 and 1 respectively.

The block diagonal performance weight  $W_{perf}$  consists of weights on rotor speed error ( $W_{p\omega_r}$ ), collective blade bending moments ( $W_{pMavg}$ ), blade bending moment in tilt and yaw directions ( $W_{pMtilt}$  and  $W_{pMyaw}$ ) and the tower fore-aft bending moment at the tower root ( $W_{pTFA}$ ). All these weights are parametrized as 1<sup>st</sup> order transfer functions except the penalty on the tower fore-aft bending moments. This weight was chosen as a constant since it is sufficient to penalize its sharp peak without imposing significant penalty at other frequencies. All 1<sup>st</sup> order weights are initially set to have the same pole/zero location. The pole is set to be at very low frequencies ( $s = 0.05$ ) to obtain a low bandwidth controller. The location of this pole was set such that the performance penalties roll-off before all of the turbine flexible modes. The location of the zero  $s = 80$  is set more than 1 decade away to keep the penalties at high-frequencies small enough. The gains of each penalty were adjusted quickly after a few iterations on nonlinear simulation to ensure that the controller is focused on rotor speed tracking and tower load reduction. The gains used for the initial design for each performance weight are 0.25,  $10^{-4}$ ,  $10^{-4}$ ,  $10^{-4}$ ,  $2 \times 10^{-6}$  respectively.

For fixed operating conditions, the  $H_\infty$  weight parameters can be tuned by solving the optimization in Equation 4.4 using gradient-based optimization methods [76, 77]. The cost and constraint functions in this optimization that depend on the weight parameters and can be evaluated as follows. The controller  $\bar{K}_\gamma$  is constructed for a given parameter vector  $\gamma$ . The turbine performance is simulated on medium-fidelity nonlinear models for a fixed set of conditions (noise, wind, and model errors) to obtain the captured power and bending loads as a function of time. Performance constraints, e.g. actuator position and rate limits, can similarly be formulated and evaluated in the constraint  $C(w_\gamma) \leq 0$ . This optimization will return local but not necessarily globally

optimal parameters. The operating conditions include the wind and sensor noise profiles as well as modeling errors. These are stochastic quantities and hence the cost and constraint functions are actually random values depending on the wind/noise realizations. Stochastic optimization techniques are applicable but, for simplicity, the cost and constraint functions are evaluated by sufficiently long simulations that capture a sufficiently rich set of wind variations. More realistic design tasks can contain many different realizations of the turbulent wind trajectories as well as the extreme operating conditions that the turbine need to withstand. This more realistic approach is important to obtain statistically meaningful results and to reach conclusions about safe turbine operation.

The following control problem is studied: blade damage equivalent load minimization subject to limits on generator speed, blade pitch-rate and the damping of the tower fore-aft motion. This problem is studied for various blade pitch-rate limitations to test the applicability of the proposed framework. This problem also allows gaining insight into actuator limitations and performance trade-offs. Details of the performance objective and constraint cost and constraint functions are explained in Section 4.3.3.

### 4.3.3 Cost and Constraint Functions

The performance objective  $G(w_\gamma)$  captures blade load reduction performance in terms of damage equivalent loads. Given a controller  $\bar{K}_\gamma$  that is a function of decision variables  $\gamma$ , a medium-fidelity model of the turbine is simulated in the FAST simulation package. Time traces of the blade bending moments are processed with MCrunch [78] developed by NREL to obtain damage equivalent loads (DELs).  $G(w_\gamma)$  is computed by averaging the DELs from the three blades. Damage equivalent loads are a complex, nonlinear cost function. DELs are non-integrable and need to be calculated after the simulation is completed.

The performance constraint  $C(w_\gamma) \leq 0$  is based on the turbine component specifications and operating conditions. The vector valued constraint functional  $C(w_\gamma)$  has the following structure:

$$C(w_\gamma) := \begin{bmatrix} \|\omega_\gamma\|_\infty - D_1 \\ \|\dot{\beta}_\gamma\|_\infty - D_2 \\ \|T_\gamma\|_\infty - D_3 \end{bmatrix} \quad (4.11)$$

where  $T$  is the transfer function from wind speed input to tower fore-aft motion.  $D_1$  is the overspeed limit,  $D_2$  is the pitch rate limit, and  $D_3$  is the open-loop peak magnitude of  $T$ . The first two entries are functions of time and for these signals  $\|\cdot\|_\infty$  denotes the peak value in time. The third entry is a transfer function and  $\|\cdot\|_\infty$  denotes the peak magnitude of the frequency response. The numerical values of the  $D_1$  and  $D_3$  are  $2.252rad/s$  and  $83.3dB$  respectively. This problem is solved for  $D_2 = 6, 8$  and  $10deg/s$  to gain insight into blade pitch rate versus performance trade-offs.

The first constraint,  $\|\omega_\gamma\|_\infty - D_1 \leq 0$ , is keeping the generator speed under its overspeed limit. An overspeed event should be avoided at all times since it can lead to physical damage in the generator components. This requires the controller to successfully attenuate large gusts observed in Region 3 operation. The equivalent rotor speed to this generator overspeed limit is  $D_1 = 2.252rad/s$  for the WindPACT turbine. This corresponds to a  $0.105rad/s$  deviation from the trim rotor speed.

The second constraint,  $\|\dot{\beta}_\gamma\|_\infty - D_2 \leq 0$ , is the pitch rate bounds of the pitch actuators. This limitation is due to the large inertia of the turbine blades and the forces acting on them. Pitch rate limits are enforced in the nonlinear optimization through  $C(w_\gamma)$ , but these hard bounds are not implemented in the FAST simulation model of the WindPACT. This was done to avoid introducing a non-smooth constraint for the generic gradient based optimization algorithm.

The third constraint of interest,  $\|T_\gamma\|_\infty - D_3 \leq 0$ , is the damping of the tower fore-aft motion. Tall, slender turbine towers lead to a very lightly damped flexible mode. This design choice is made for reducing the material and transportation costs. The frequency of this flexible mode is adjusted at design time such that it is above the rated rotor speed, but below three times of this value for 3-bladed turbines. This is done for avoiding the rotor rotation and the blades passing in front of the tower exciting this flexible mode. This mode can most easily be observed in open-loop Bode plots from wind disturbances to tower fore-aft motion as a sharp peak at the tower natural frequency. The peak gain (infinity-norm) of this transfer function is related the damping of the tower fore-aft bending mode. It is assumed that the turbine is operating under mild turbulent conditions (5%) and no extra damping is demanded from the controller for this study. However, the infinity-norm of this transfer function is constrained to be less than or equal to the infinity-norm of open-loop response,  $D_3 = 83.3dB$ . This constraint

prevents the control design from reducing blade loads at the expense of excessive tower loads.

#### 4.3.4 Gradient-based Optimization

This nonlinear optimization problem is solved with the commercially available software MATLAB Optimization Toolbox [79] via active-set methods. This optimization is repeated for three different pitch rate limits. The inputs of the gradient-based algorithm are the design constraints and a set of initial weights. A total of  $n_\gamma = 19$  decision variables are used in the optimization. The actuator penalty weight consists of collective and cyclic pitch input penalties. The two cyclic pitch inputs use the same weight. The resulting two first-order weights require 6 decision variables. Four first-order weights and a static gain weight in the performance penalty weight require 13 decision variables. Controllers are evaluated on a 450s wind trajectory on the FAST simulator to calculate the cost and constraint functions. The resulting controllers are not necessarily globally optimal. However, these results can give rough guidelines on the trade-offs between pitch-rate limits and performance objectives. This is because all optimization problems start from the same initial design and the only difference is the relaxation of the pitch rate constraints.

### 4.4 Example Problem Results

This section presents the analysis of the resulting  $H_\infty$  controllers and simulations. The gradient-based solver took 12 iterations and 250 function evaluations, i.e. simulations, on average before converging to an optimal point. The number of function evaluations are approximately in agreement with the  $n_{it}(n_\gamma + 1)$  prediction with  $n_\gamma = 19$ . The final values of the cost function and the constraint functions are listed in Table 4.1. The first column of this table lists the pitch-rate limits specified in the gradient-search algorithm. The second column lists the final value of the cost function, i.e. average of the DELs from three blades. The third, fourth and fifth column present the values of the vector valued constraint function. The entries of this function are described in the previous section. Being close to 0 from below means that the final solution is close to the limits of the constraint. These columns are given in the units of *rad/s*, *deg/s*, *dB*

respectively. The fifth column represents the infinity norm of the wind to tower fore-aft motion. For example a value of  $-6dB$  means the peak gain of the closed loop with the resulting controller is  $6dB$  less than the open loop response. The main observation from this table is that all solutions are similarly constrained by the rotor over-speed and blade pitch rate limits. Increasing the allowed pitch rate has a significant impact on the achieved blade load reduction levels.

Table 4.1: Optimization Results

$D_2$ (deg/s)	$G(w_\gamma)$	$C(w_\gamma)$		
	Blade DEL (kNm)	$\ \omega_x\ _\infty - D_1$ (rad/s)	$\ \dot{\beta}_x\ _\infty - D_2$ (deg/s)	$\ T_x\ _\infty - D_3$ (dB)
6	326	-0.0186	-0.112	-6.792
8	288	-0.0230	-0.014	-5.147
10	255	-0.0131	-0.098	-6.629

Closed loop Bode plots from wind perturbations to rotor speed errors are given in Figure 4.8. The blue solid line is the open loop response and the green solid line is the closed loop with the initial controller. The red dotted line, cyan dash-dotted line and black dotted line represent the response with the final controllers obtained from gradient-based tuning with 6, 8 and 10deg/s pitch rate limits respectively. At frequencies lower than 0.2rad/s the initial controller and the 6deg/s pitch-rate controller have higher attenuation. In the range of 0.2 to 10rad/s, the 8deg/s and 10deg/s controllers have higher attenuation. The worst case amplification in this plot is much smaller for these controllers. However, note that in Table 4.1 all controllers have a peak tracking error ( $\|\omega_x\|_\infty - D_1$ ) that is very close to the overspeed limit. This behavior can most likely be explained by the fact that all controllers show similar behavior beyond 10rad/s. This is the bandwidth of the pitch actuators of the WindPACT 1.5MW turbine. Moreover, the low-pass performance weight on rotor speed tracking errors rolls-off before this frequency for all controllers. Therefore the increased pitch rate limits have a limited impact on the peak tracking error caused by the wind gusts.

Three plots can be used to analyze the controller behavior and the impact of the extra pitch rates on blade load reduction. Figures 4.9 and 4.10 present the Bode plots from wind perturbations to collective blade bending moments and the rotor-tilt moment. Power spectral densities (PSD) of the collective and tilt bending moment signals from

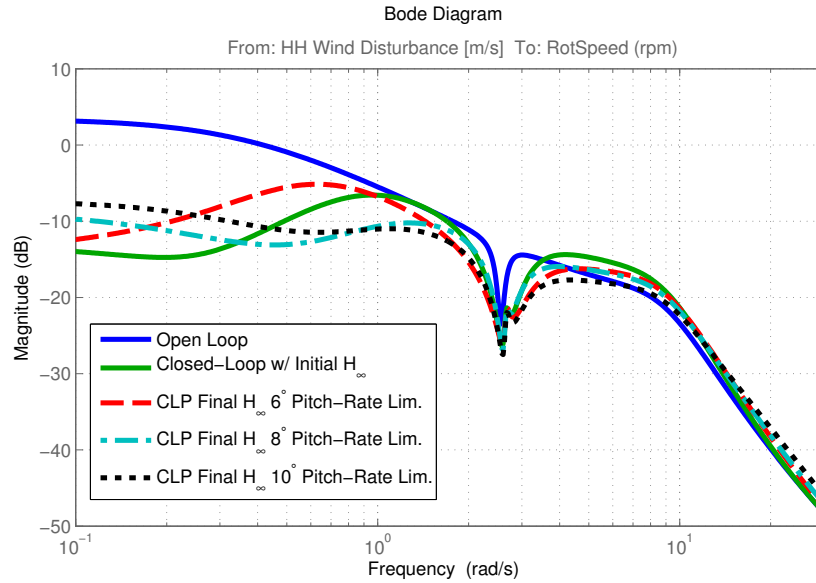


Figure 4.8: Bode plot from wind perturbations to rotor speed error.

the FAST simulations are presented in Figure 4.11. These signals are obtained by applying the MBC transformation to the root bending moments from three blades. The PSD plot is important to investigate the behavior of the proposed framework by connecting the nonlinear performance metrics with the linear system analysis via Bode plots. The plots for the moments in the yaw direction are not presented since they had similar trends to the moments in the tilt direction. Figure 4.11 shows that the largest portion of the collective loads occur below  $1\text{rad/s}$ . The controller with  $8\text{deg/s}$  pitch rate improves attenuation over the  $6\text{deg/s}$  controller up to  $1.5\text{rad/s}$  in the collective moment Bode plot in Figures 4.9. The  $10\text{deg/s}$  controller improves this attenuation further. These are consistent with the PSDs in Figure 4.11. Figure 4.11 also shows that the largest portion of the tilt loads are seen below  $2\text{rad/s}$  with an additional peak around  $6.45\text{rad/s}$ . This is three times the rated rotor speed. In this channel there is a large difference between the  $6\text{deg/s}$  and  $8\text{deg/s}$  controller. The  $10\text{deg/s}$  controller is slightly worse than the  $8\text{deg/s}$  controller. This is also seen in the tilt channel Bode plot in Figure 4.10. However, the peaks in the collective loads' PSD is much higher than the peaks in the tilt channel. Therefore this worse performance in this channel is less important. The extra  $2\text{deg/s}$  pitch rate limit over the  $8\text{deg/s}$  is used in the collective

bending channel. As seen in the Table 4.1 the  $10deg/s$  controller is able to achieve a 10% smaller blade DEL over the  $8deg/s$  controller by focusing on these collective loads. These loads are caused by the wind fluctuations that cover a large enough area to impact the three blades simultaneously. The optimization algorithm is seen to optimize the controller in accordance to the nonlinear simulation outputs and the performance metrics.

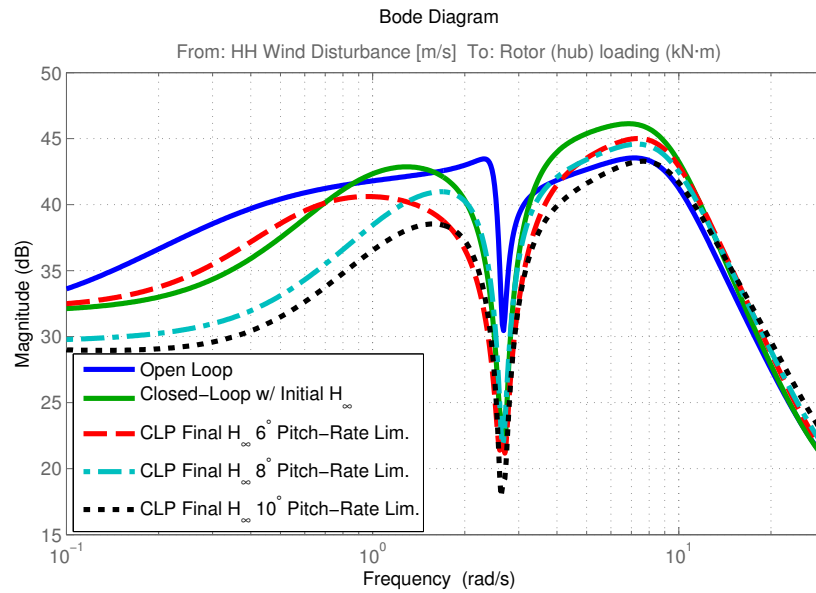


Figure 4.9: Bode plot from wind perturbations to collective blade bending moments.

The Bode plot for the tower fore-aft bending mode is shown in Figure 4.12. There is a good correlation between pitch-rate limits and tower load attenuation even though tower loads were not explicitly penalized. This is also intuitive because collective root bending moments  $M_{avg}$  have an interpretation in terms of rotor hub loading, which in turn affects forces at the tower top. Therefore improvements at  $M_{avg}$  attenuation are correlated with attenuation of the tower fore-aft bending moments. This can be seen by comparing the Bode plots in Figure 4.12 and 4.9. In both figures the  $8deg/s$  controller improves attenuation over the  $6deg/s$  controller up to  $1.5rad/s$  frequency range. The  $8deg/s$  controller is slightly worse up to  $5rad/s$ . At higher frequencies both controllers perform similarly. The  $10deg/s$  controller is better than both controllers up to  $10rad/s$  and perform similarly beyond this frequency. The similar control behavior beyond

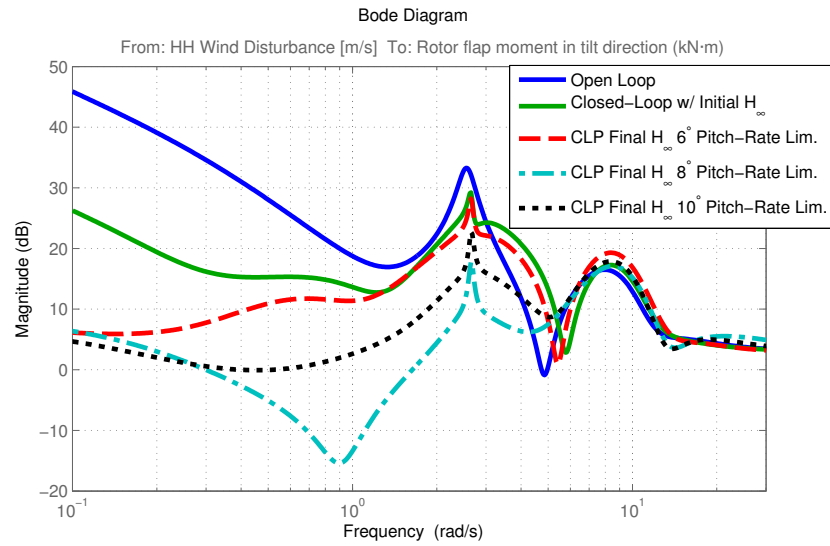


Figure 4.10: Bode plot from wind perturbations to blade bending moments in tilt direction.

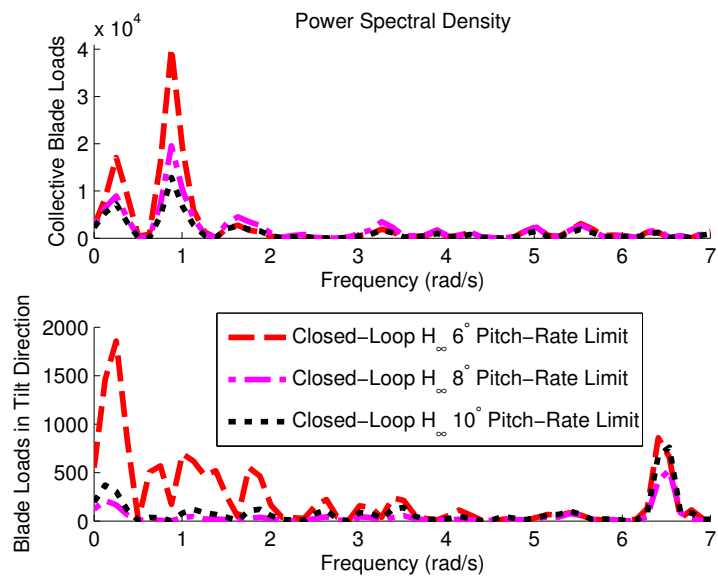


Figure 4.11: Power spectral densities of the blade bending moments in non-rotating coordinates.

$10\text{rad/s}$  is shared in all channels and is likely due to the pitch actuator bandwidth.

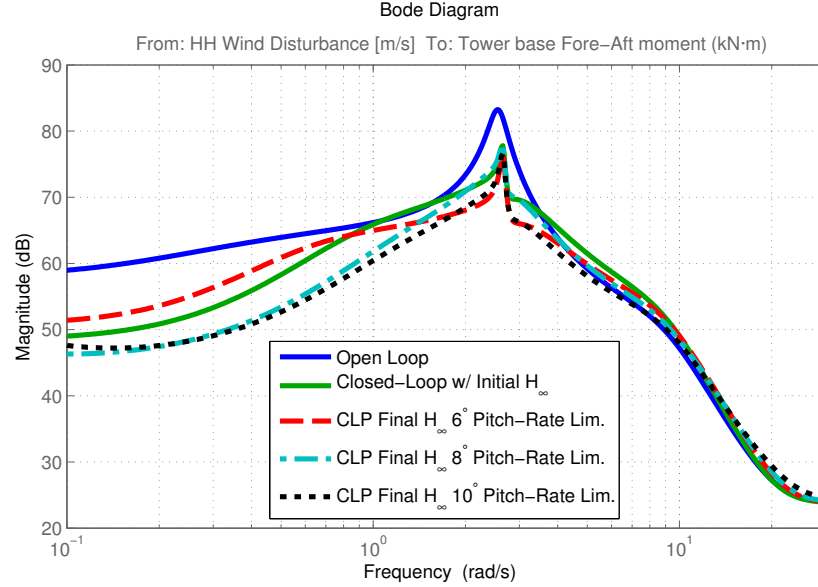


Figure 4.12: Bode plot from wind perturbations to tower fore-aft bending.

## 4.5 Conclusions and Recommendations

The simple example problem used to test the basic effectiveness of the proposed framework showed some preliminary promising results. Particularly, it was seen that the framework was able to tune the advanced multivariable  $H_\infty$  controllers to improve the performance of a nonlinear plant in terms of a non-integrable and non-smooth performance metric.

The proposed framework can help transition MIMO tools to industry, but reaching a more concrete conclusion requires further research. Some of the basic goals of a more realistic controller design problem such as robustness and sensitivity to measurement noise was not studied in detail here. Moreover, the test case presented here considered operation around a single operating condition. This framework further needs to be generalized if the nonlinear plant cannot be sufficiently approximated by a linear model obtained at a single operating condition. Wind turbines fall into this category. Turbines also have condition-dependent performance goals that are based on wind speed. This

requires further consideration and generalization of the proposed method.

# Chapter 5

## Preview Control

### 5.1 Introduction

Performance of the turbine controllers can be improved in two ways. First, a new controller that better utilizes the available sensors and actuators can be designed. Second, current sensors and actuators can either be modified or complemented with new ones. This chapter investigates the second approach. In particular, our interest is to understand the impact of the addition of a preview wind sensor on limits of turbine performance and controller design trade-offs.

Wind speed fluctuations play a key role in turbine performance. In Region 2 operation, maintaining the optimal tip speed for maximum power capture corresponds to a wind speed tracking problem. Having the large rotor inertia to respond to these fluctuations is a challenging control problem. In Region 3 operation, the turbine control system tries to reject wind disturbances to attenuate structural loads on the blades and the tower. Restrictive blade pitch rate limits impose a fundamental limit on the turbine performance for responding to rapid gusts. Pitch-rate limits also impact turbine control during extreme operating conditions. These are extreme weather events observed once a year or once in fifty years on average.

Current turbines use anemometers mounted on the rear of the nacelle for wind speed measurements. However, these anemometers measure a disturbed wind field since they are located behind the turbine rotor. The low quality anemometer measurements are typically not used for closed-loop control. Alternatively, an advanced preview wind

sensor, e.g. LIDARs, can be used to measure the incoming wind field. These sensors can be mounted on the rotor hub in a forward looking fashion. This setup offers three key benefits. First, a higher accuracy measurement of the undisturbed wind field can be obtained. Second, spatial variations in the wind field can be detected. Lastly, wind fluctuations are detected before their impact on the turbine. Turbine control systems can be designed to utilize this information and minimize the impact of wind speed variations.

Turbine controller design with preview wind information involves some new design variables. The first question is how much preview time is required for optimal performance. The second question is what kind of wind information should be used by the controller. This question arises because the controller can only take in a finite number of variables that represent the spatial and temporal variations in the wind field. We investigate the first question, how much preview, in this chapter. For the second question we assume a realistic wind measurement set up with current commercially available sensors.

Aside from the question of how much preview, it is also of interest to know how much the turbine performance can be improved. We investigate the ultimate performance bounds that can be achieved by any controller for Region 2 and 3 operation. Vastly different control objectives for these regions necessitate a separate analysis for them. We also consider turbine performance in extreme events. The impact of the physical limitations and the error characteristics of continuous wave LIDARs on turbine performance and preview time requirements are also investigated. Knowing these performance bounds are of great interest for two reasons. First, these bounds can serve as a certificate of optimality for a given controller design. Control engineers can decide if a particular design is worthwhile of detailed simulation and field testing. These are time-intensive tasks, which is crucial in industrial setting. The second reason is that an additional sensor comes with an economic cost. The performance improvements obtained from this additional sensor should justify its cost.

The remainder of the chapter is structured in five main sections. Section 5.2 gives an overview of the recent research for the preview control of wind turbines. Section 5.3 considers the use of preview for Region 2 control. We analyze the design trade-offs between power capture and gearbox structural loads. Preview control in Region 3 is

investigated in Section 5.4. We consider the impact of the blade pitch-rate limits on turbine performance. Section 5.5 presents a framework that can be used to investigate the limits of turbine performance during extreme operating conditions. We present an example use of this framework and analyze a 50-year gust. The conclusions are presented in Section 5.6.

## 5.2 Related Work

Various methodologies have been studied for turbine preview control in recent years. Reference [81] considers Region 2 control, References [31, 33, 81, 82] focus on Region 3 control whereas references [82, 83] uses preview information for extreme operating events.  $H_\infty$ -optimal [31], linear parameter varying [83] and model predictive controllers [33, 81–83] are some of the main methods used in the literature. Ideal preview measurements [31, 33, 81, 82], a normally distributed noise [83] and detailed preview sensor models [31, 33] are considered. Reference [31] is of particular interest to us since it also uses  $H_\infty$  controllers for turbine control in above-rated wind speeds. This reference investigates pitch rate constrained  $H_\infty$  preview controllers designed via linear matrix inequality methods. The maximum singular value of these full-information  $H_\infty$  controllers are presented for various preview times and pitch rate limitations. These preview controllers are simulated on a medium-fidelity turbine model with ideal and noisy preview measurements. The load reduction performance is deteriorated with noisy measurements while ideal measurements yielded improved results compared to a baseline non-preview controller.

In summary, all these control design methods rely on numerical studies to investigate the impact of different sensor models and additional preview time. The resulting controllers are tested with Monte Carlo simulations on medium to high-fidelity, nonlinear turbine models to understand the impact of preview time. These studies provide useful insight about the effects of additional preview information. However, all the approaches depend on specific design choices, e.g. the control methodology and design weights. We focus on finding the ultimate performance bounds achievable by any controller and the trade-off between turbine control objectives.

### 5.3 Region 2 Preview Control

The  $K\omega_r^2$  standard control law [7] is the most common method to control the turbine generator torque in below-rated (Region 2) wind conditions. The popularity of this law is mainly due to its simple design and relatively good power capture performance. In addition, this control law only requires a measurement of the rotor speed. However, it is not without its shortcomings. First, the standard law only yields the optimal power capture under steady wind conditions. Second, there is a fundamental trade-off between the gearbox loads and power capture. It is not clear if the standard control law is Pareto optimal in terms of this trade-off. In other words, it is unknown if there exists a different controller that can improve the power capture and lower the gearbox loads simultaneously. Finally, the standard law does not utilize preview wind measurements that can be obtained from advanced sensors such as LIDARs. These preview wind measurements can be used to alleviate the effects of wind fluctuations to improve the power capture and reduce gearbox loads.

The trade-off between gearbox loads and the power capture can be seen in various results in the literature. For instance reference [7] describes a method that relies on a measurement of rotor acceleration. The authors report approximately 1% improvement in power capture, but with elevated swings in the generator torque that can be harmful for the gearbox. On the other hand, reference [15] uses a smaller gain in the standard law. Results show higher energy capture with lower generator torque in turbulent wind conditions. This result suggests that the standard law is not Pareto optimal since the lower generator torque is also likely to correspond to a lower gearbox load. The optimality of various Region 2 controllers in the literature is not quantified. Therefore it is not clear how far these controllers from the optimal in terms of the trade-off between the power capture and the gearbox loads.

We formulate a two-objective nonlinear optimal control problem that yields the Pareto optimal trade-off between the power capture and the gearbox loads in presence of preview wind information. The effect of the preview time and turbulence intensity on this trade-off is studied. The optimization problem is formulated in continuous-time based on a one-state rigid-body model of the National Wind Technology Center's

(NWTC) Control Advanced Research Turbine 3 (CART3) [59]. This optimization problem is solved numerically. Our main result is that the use of preview wind information can improve the power capture and reduce the drivetrain loads simultaneously. It is also seen that the standard  $K\omega_r^2$  control law is not Pareto optimal in turbulent wind conditions.

The remainder of this section is structured as follows: Section 5.3.1 details the formulation of the turbine optimal control problem. Section 5.3.2 analyzes the effect of the preview time and turbulence intensity on the optimal performance.

### 5.3.1 Problem Formulation

The nonlinear optimal control problem studied in this section relies on the one-state rigid body turbine model described in Section 3.3. This model has the following form:

$$\dot{\omega}_r = \frac{\rho\pi R^2 v^3 C_p(\beta, \lambda)}{2J\omega_r} - \frac{\tau_g}{J} \quad (5.1)$$

where the first term corresponds to the aerodynamic torque divided by the effective drivetrain inertia denoted as  $J$ .  $\tau_g$ , generator torque, is the control input used for Region 2 control. We obtain  $C_p(\lambda, \beta)$  data from the medium-fidelity models on the FAST simulation package. This was done by simulating the turbines in steady Region 2 level winds with a simple PI controller for  $\lambda$  tracking. The blade pitch  $\beta$  is held constant at a given value and the PI controller adjusts the generator torque  $\tau_g$  to achieve the desired  $\lambda$ . The  $C_p$  is obtained from the simulation after the turbine reaches a steady operation with small fluctuations in the power coefficient.

Flexible turbine gearboxes are often modeled as a mass-damper-spring system that connects the rotor and generator inertia. The damage in the gearbox is measured by the torque transmitted from the low-speed shaft to the high-speed shaft through the spring and the damper. The one-state model in Eq. (5.1) does not capture the flexible gearbox dynamics. However the variations in the generator torque  $\tau_g$  closely represent the oscillations in the transmitted torque. Variations in  $\tau_g$  are used as a measure of the gearbox damage in place of the more realistic damage-equivalent loads calculations based on the rotor shaft torque. This simpler model will be used in the formulation of our optimal control problem.

The fundamental trade-off between the gearbox loads and power capture can be motivated as follows. We assume a fixed blade pitch angle  $\beta^*$  that is optimal for power capture in steady wind. Therefore the power coefficient  $C_p$  is only a function of the tip-speed ratio  $\lambda$ . Define  $C_p^*$  as the maximum power coefficient.  $\lambda^*$  is defined to be the turbine operating condition that achieves this maximum. Note that the operating condition that achieves the  $C_p^*$  is unique. The rotor speed corresponding to this operating condition is  $\omega_r^* = \frac{v\lambda^*}{R}$ . Assume there exists a generator torque input  $\tau_g^*$  that maintains the turbine operating at constant  $\lambda^*$  and  $C_p^*$ . Substituting  $C_p(\lambda)$ ,  $\omega_r$ ,  $\dot{\omega}_r$  in Eq. (5.1) with  $C_p^*$ ,  $\frac{\lambda^*v}{R}$  and  $\frac{\lambda^*\dot{v}}{R}$  respectively yields an analytical expression for  $\tau_g^*$ :

$$\tau_g^* = \frac{\rho\pi R^3 C_p^*}{2\lambda^*} v^2 - \frac{J\lambda^*}{R} \dot{v} \quad (5.2)$$

The  $\tau_g^*$  that yields the maximum power capture is proportional to the square of the wind speed  $v$  and its rate of change. The variations in  $v^2$  and  $\dot{v}$  can be substantial in turbulent wind conditions. Figure 5.1 shows a simulation of the one-state CART3 model with  $\tau_g^*$  and the standard control law  $K\omega_r^2$  for a 600s wind trajectory. The wind trajectory used in this simulation is obtained from NWTTC's TurbSim [54] application. This wind trajectory closely represents the wind conditions at the CART3's site. It contained an average wind speed of 6m/s and a turbulence intensity of 35%. The values of the  $\lambda^*$  and  $C_p^*$  for CART3 are approximately 6 and 0.46. The top plot in Figure 5.1 shows the power coefficient  $C_p$  as a function of time and the bottom plot shows the generator torque demand during a gust. Over this 600s period the  $\tau_g^*$  yields 7.7e7J energy capture whereas the standard law yields 6.9e7J. This is approximately an 11% improvement. However, the maximum torque that the generator of the CART3 can sustain is 3524Nm. The peak-to-peak torque swings of 1e5Nm seen with the  $\tau_g^*$  cannot be realized. These type of large oscillations in  $\tau_g$  create a large strain on the drivetrain. Moreover, the generator torque has large negative values that correspond to a large amount of electrical power drawn from the grid. It is of interest to understand this trade-off between the power capture and the drivetrain loads.

A nonlinear model predictive controller is used to study the trade-off between the power capture and the drivetrain loads. The optimal generator torque input  $\tau_g$  is

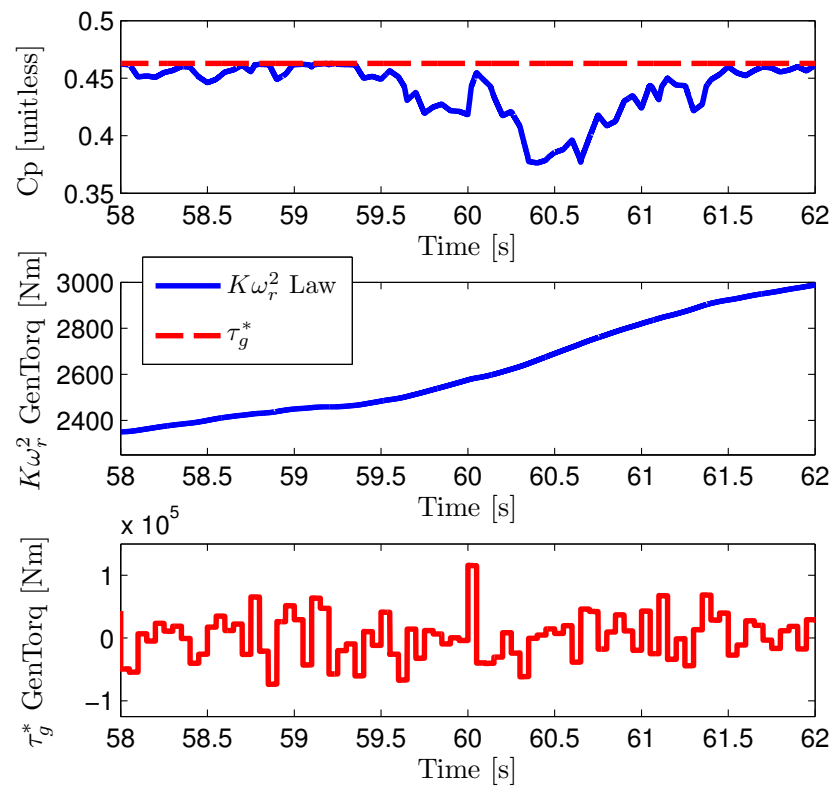


Figure 5.1: Control of the CART3 for the maximum power capture

calculated at each time step by solving the following optimal control problem:

$$\begin{aligned} & \underset{\tau_g(t) \in [0, T]}{\text{minimize}} \int_0^T \tau_g^2(t) - \alpha v^3(t) C_p(\lambda(t)) dt & (5.3) \\ & \text{subject to: Equation (5.1)} \\ & \omega_r(0) = \omega_{r0} \end{aligned}$$

The  $\tau_g^2$  term in the cost function corresponds to minimizing the actuator usage. This leads to a smaller gearbox damage. The  $-v^3 C_p(\lambda)$  term represents maximizing the power capture on rotor. The coefficient  $\alpha$  is the weight on the power capture. It is assumed that  $v(t)$  in  $t \in [0, T]$  is supplied by an advanced wind preview sensor such as a LIDAR. In other words, studying this optimization problem for a terminal time  $T$  corresponds to the use of  $T$  seconds of wind preview information for control. The current rotor speed  $\omega_{r0}$  is also available to the controller. The  $\tau_g(t)$  that yields the optimal trade-off between these weighted objectives is being calculated. The control input  $\tau_g(0)$  is implemented. The optimization problem is solved again at the next time step with the new wind and rotor speed measurements. The system is started at the  $\omega_{r0}$  that yields the optimal power coefficient  $C_p^*$  for  $v(0)$ . We analyze this problem for a single, long (600s) realization of the random process  $v(t)$ . This long realization helps capture the statistical properties of the  $v(t)$ . However, more realistic and statistically meaningful results require solving this problem with many realizations of  $v(t)$ .

The optimization problem in Eq. (5.3) is a nonlinear optimal control problem with a fixed terminal time. Denote  $L(\omega_r(t), \tau_g(t), t) = \tau_g^2(t) - \alpha v^3(t) C_p(\lambda(t))$ . The turbine dynamics in Eq. (5.1) are denoted as  $\dot{\omega}_r = f(\omega_r(t), \tau_g(t), v(t))$ . The three necessary optimality conditions for the optimal  $\tau_g$  in Eq. (5.3) are given by [84]:

$$\begin{aligned} \dot{\omega}_r &= f(\omega_r(t), \tau_g(t), v(t)) \\ \dot{\xi} &= - \left( \frac{\partial f}{\partial \omega_r} \right)^T \xi - \left( \frac{\partial L}{\partial \omega_r} \right)^T \\ 0 &= \left( \frac{\partial f}{\partial \tau_g} \right)^T \xi + \left( \frac{\partial L}{\partial \tau_g} \right)^T \end{aligned} \quad (5.4)$$

with boundary conditions  $\omega_r(0) = \lambda^* v(0)/R$  and  $\xi(T) = 0$ .  $\xi(t)$  is the Lagrange multiplier function. These equations are known as the Euler-Lagrange equations in the calculus of variations [84]. This is a two-point boundary-value problem. The partial

derivatives in Eq. (5.4) correspond to the following expressions for the turbine control problem defined in Eq. (5.3):

$$\begin{aligned}
\frac{\partial f}{\partial \omega_r} &= -\frac{\rho\pi R^2 v^3 C_p(\lambda)}{2J\omega_r^2} + \frac{\rho\pi R^3 v^2}{2J\omega_r} \frac{dC_p(\lambda)}{d\lambda} \\
\frac{\partial L}{\partial \omega_r} &= -\alpha R v^2 \frac{dC_p(\lambda)}{d\lambda} \\
\frac{\partial f}{\partial \tau_g} &= \frac{1}{J} \\
\frac{\partial L}{\partial \tau_g} &= 2\tau_g
\end{aligned} \tag{5.5}$$

This problem is solved numerically to obtain the optimal control input  $\tau_g$  over the time horizon of  $t \in [0, T)$ . This solution is obtained as follows. The variables in Eq. (5.4) ( $\omega_r$ ,  $\tau_g$ ,  $\xi$ ) are discretized in time with sample time of  $T_s$ . The derivative terms on the left-hand side of the Eq. (5.4) are approximated via forward-differences, i.e.  $\dot{\omega}_r(0) \approx (\omega_r(T_s) - \omega_r(0))/T_s$ . The three equations in Eq. (5.4) are converted to the following nonlinear equations:

$$M_1 \begin{bmatrix} \omega_r(0) \\ \omega_r(T_s) \\ \omega_r(2T_s) \\ \omega_r(3T_s) \\ \vdots \\ \omega_r(T) \end{bmatrix} = \begin{bmatrix} f(\omega_r(0), \tau_g(0), v(0)) \\ f(\omega_r(T_s), \tau_g(T_s), v(T_s)) \\ \vdots \\ \vdots \\ f(\omega_r(T - T_s), \tau_g(T - T_s), v(T - T_s)) \end{bmatrix} \tag{5.6}$$

$$M_1 \begin{bmatrix} \xi(0) \\ \xi(T_s) \\ \xi(2T_s) \\ \vdots \\ \xi(T - T_s) \\ \xi(T) \end{bmatrix} = - \begin{bmatrix} \frac{\partial f}{\partial \omega_r} \Big|_{t=0} \xi(0) \\ \frac{\partial f}{\partial \omega_r} \Big|_{t=T_s} \xi(T_s) \\ \vdots \\ \vdots \\ \frac{\partial f}{\partial \omega_r} \Big|_{t=T-T_s} \xi(T - T_s) \end{bmatrix} - \begin{bmatrix} \frac{\partial L}{\partial \omega_r} \Big|_{t=0} \\ \frac{\partial L}{\partial \omega_r} \Big|_{t=T_s} \\ \vdots \\ \vdots \\ \frac{\partial L}{\partial \omega_r} \Big|_{t=T-T_s} \end{bmatrix} \tag{5.7}$$

$$\begin{bmatrix} \xi(0) \\ \xi(T_s) \\ \xi(2T_s) \\ \vdots \\ \xi(T) \end{bmatrix} = 2J \begin{bmatrix} \tau_g(0) \\ \tau_g(T_s) \\ \tau_g(2T_s) \\ \vdots \\ \tau_g(T) \end{bmatrix} \quad (5.8)$$

with the boundary conditions of  $\omega_r(0) = \omega_{r0}$  and  $\xi(T) = \xi_T$ . The  $M_1$  is the  $\frac{T}{T_s}$  by  $\frac{T}{T_s} + 1$  forward difference matrix:

$$M_1 = \frac{1}{T_s} \begin{bmatrix} -1 & 1 & 0 & \dots & \dots & 0 \\ 0 & -1 & 1 & 0 & \ddots & \vdots \\ \vdots & \ddots & \ddots & \ddots & \ddots & \vdots \\ \vdots & \ddots & \ddots & \ddots & 1 & 0 \\ 0 & \dots & 0 & 0 & -1 & 1 \end{bmatrix}$$

Let  $\bar{\omega}_r$  denote the  $\mathbb{R}^{\frac{T}{T_s}+1}$  stacked vector of  $\omega_r(0), \omega_r(dt), \dots, \omega_r(T)$  that appears in Eq. (5.6). Similarly let  $\bar{\xi}$  and  $\bar{\tau}_g$  denote the  $\mathbb{R}^{\frac{T}{T_s}+1}$  stacked vectors of  $\xi(k)$  and  $\tau_g(k)$  for  $k \in \{0, T_s, 2T_s, \dots, T - T_s, T\}$  that appear in Eqs. (5.7) and (5.8). The optimality conditions are nonlinear equations in  $\bar{\omega}_r, \bar{\xi}$  and  $\bar{\tau}_g$ . Each one of these unknown vectors has  $\frac{T}{T_s} + 1$  variables. Therefore there is a total  $\frac{3T}{T_s} + 3$  equations and unknowns. The boundary conditions set 2 of these unknowns. The  $\bar{\xi}$  is eliminated from these equations by plugging Eq. (5.8) in Eq. (5.7). This eliminates  $\frac{T}{T_s} + 1$  equations and unknowns. Hence the final problem has  $\frac{2T}{T_s}$  unknowns. We numerically solve the resulting equations in MATLAB via trust-region methods. The analytical Jacobian of these equations are supplied to the numerical solver in MATLAB. At the beginning of the solution, the initial guess for the optimal  $\bar{\omega}_r$  and  $\bar{\tau}_g$  is obtained from simulation of the one-state model with the  $K\omega_r^2$  law for the given wind trajectory. At the following time steps the  $\bar{\omega}_r$  and  $\bar{\tau}_g$  solution from the previous time step is used to come up with a new initial guess. More specifically, elements of the  $(\bar{\omega}_r, \bar{\tau}_g)$  are shifted by one element to discard the data for the previous time step. The new guess for the last elements of  $\bar{\tau}_g$ , is calculated using a linear interpolation from the preceding two elements. The new last element of the  $\bar{\omega}_r$  is calculated using Euler integration based on the previous  $\bar{\omega}_r$  and the last element of  $\bar{\tau}_g$ . At a preview time of  $T = 15s$  and a sampling time of  $T_s = 0.02s$  this

problem contains  $2T/T_s = 1500$  variables. Solution of one such optimization step takes less than  $0.1s$  on a typical desktop computer.

### 5.3.2 Power Capture versus Drivetrain Loads Trade-off

First we study the impact of the preview time on the optimal performance. A wind trajectory that represent the turbulence conditions at the CART3 site is generated with NWTC's TurbSim code. This trajectory is generated at an average wind speed of  $6m/s$  and has a turbulence intensity of 35%.  $T = 15, 30$  and  $600s$  of preview times are investigated. Current preview wind sensors can typically supply wind information up to  $200m$  distance from turbines. The rated wind-speed of CART3 is  $12.5m/s$ . Therefore  $200m$  preview corresponds to  $16s$  and is sufficient for Region 2 control. The  $30s$  case investigates the benefits of extra preview. The  $600s$  preview case represents the limiting case where the full wind trajectory is available to the controller.

The optimization problem in Eq. (5.3) is solved in model predictive control style over a simulation window of  $600s$ . These simulations are run with different weights on energy capture ( $\alpha$  in Eq. (5.3)) to capture the optimal trade-off between the power capture and gearbox load reduction objectives. These performance metrics are normalized with respect to their respective values obtained with the  $K\omega_r^2$  law for the same wind trajectory. Figure 5.2 presents the optimal performance trade-off with different preview times. It is seen that the  $15s$  preview is mostly sufficient for the optimal control action. However, it should be noted that larger turbines than the CART3 may require longer preview times. This is because it is harder to make the larger rotor inertia respond to large wind gusts. In the case of CART3,  $T = 30s$  preview yields a limited performance improvement over the  $15s$  preview. This performance is almost optimal and the performance difference with the limiting  $600s$  preview case is negligible. It is also seen that a large performance improvement over the standard law can be obtained with the use of preview. A notable 6% improvement in power capture can be obtained while retaining similar gearbox loads. Similarly a 30% load reduction can be obtained while achieving a similar power capture to the  $K\omega_r^2$  law. The limiting case for the maximum energy capture is an 11% improvement over the  $K\omega_r^2$ . This is calculated from the analytical formula given in Eq. (5.2). The corresponding normalized actuator usage, the ratio of  $\|\tau_g(t)\|_2$  for the maximum power capture case and the  $K\omega_r^2$  law, is approximately 25.

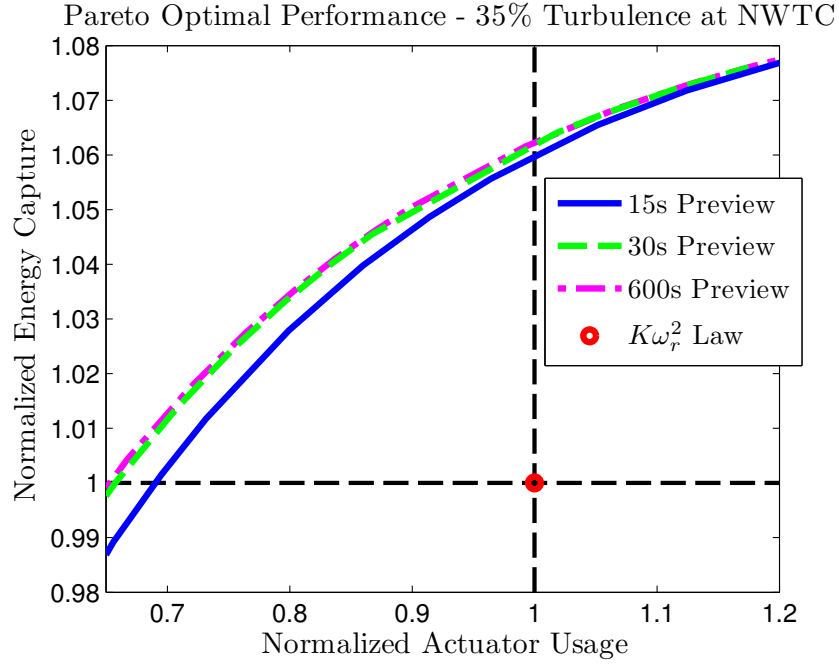


Figure 5.2: Pareto optimal performance trade-off with different preview times

Figure 5.3 shows the time-domain behavior of the standard control law  $K\omega_r^2$  and the model predictive controller with  $\alpha = 1.1e5$ . This model predictive controller yields the same gearbox loads with the  $K\omega_r^2$  law and captures 6% more energy over the 600s wind trajectory. Figure 5.3 compares the power captured by the rotor, the tip speed ratio and the generator torque. The wind trajectory used in this problem is presented in the bottom plot. The optimal tip-speed ratio  $\lambda^* = 6$  for CART3 is denoted with the red-dashed line in the tip-speed ratio plot.

It is possible to gain some simple insight into controller behavior by analyzing the time-domain results in Figure 5.3. The MPC with preview is able to improve power capture without much increase in generator torque. This relies on two factors. First, it is operating closer to  $\lambda^* = 6$  when the wind speed is highest. This is crucial for power capture. Second, the power coefficient  $C_p(\lambda)$  drops more sharply for values  $\lambda < \lambda^*$  than  $\lambda \geq \lambda^*$ . This can be seen in Figure 5.4 that presents the  $C_p - \lambda$  curve for the CART3. Wind gusts can lead to sharp drops in  $\lambda$  below  $\lambda^*$ . The preview MPC controller avoids this situation to capture more power during gusts. The mean value of the  $\lambda$  for the  $K\omega_r^2$

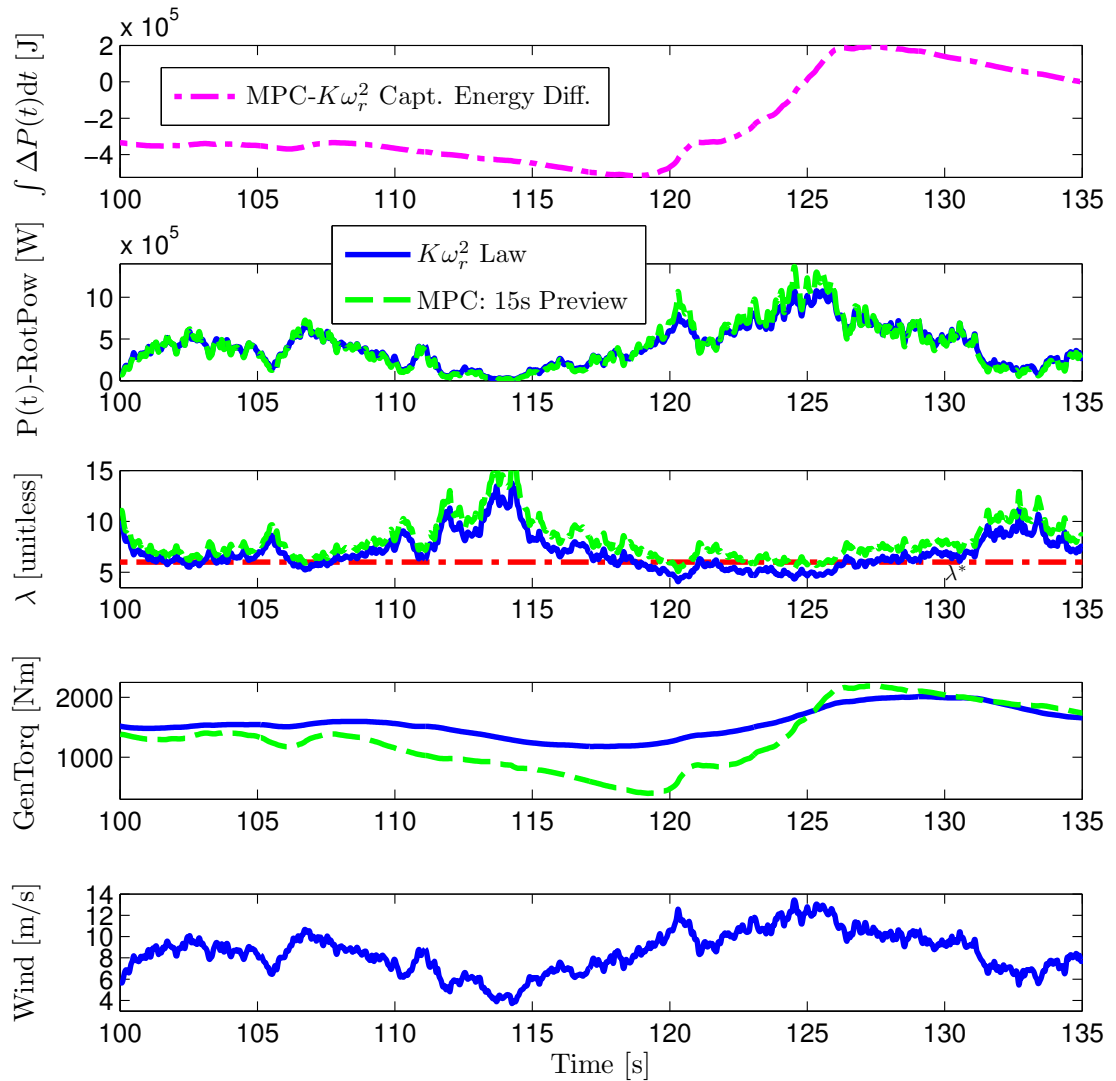


Figure 5.3: Time-domain plots of the standard control law and the model predictive controller

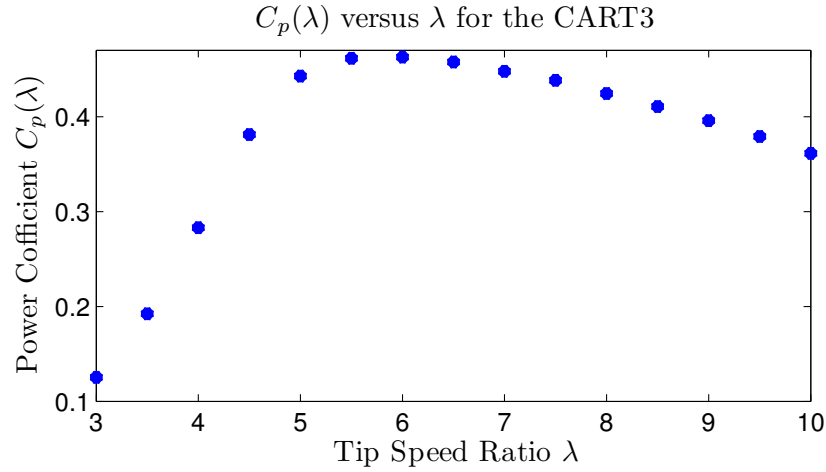


Figure 5.4:  $C_p$  versus  $\lambda$  data for the CART3

and 15s preview MPC are 7.5 and 8.3 respectively. The standard deviations are 3.5 and 2.9, respectively. The preview MPC is sacrificing a small amount of power capture by operating at larger  $\lambda > \lambda^*$ . This is especially true during lower wind speeds when the power capture is less important. The top plot in Figure 5.3 has a slight downward slope up until  $t \approx 118s$  showing that the MPC is capturing less power. The benefit of this reduced power is the reduced generator torque. Before the onset of the gusts the rotor is accelerated such that the  $\lambda$  drops to the  $\lambda^*$  when the gust hits. This behavior can be seen at  $\approx 120s$  and  $\approx 125s$  in Figure 5.3. The gain in power capture during gusts is much larger than the power sacrificed in lower wind speeds. The energy capture difference between the preview MPC and  $K\omega_r^2$  becomes positive rapidly in the top plot in Figure 5.3. This shows that the MPC is capturing significantly more power during the highest wind speeds by operating near  $\lambda^*$ . On the other hand, the  $K\omega_r^2$  law drops below the  $\lambda^*$  value at the highest wind speeds and captures less power.

The second problem investigated is the effect of the turbulence level on the optimal performance. Three wind trajectories that have an average wind speed of 6 (m/s) and turbulence intensities of 35%, 22%, and 14% are considered. The 35% turbulent wind case corresponds to the wind conditions at the CART3 site. A realistic preview time of  $T = 15s$  is considered. The model predictive controller defined in Eq. (5.3) is simulated over 600s simulation windows. The normalized performance metrics are calculated for

each wind trajectory. These results are presented in Figure 5.5. There are three key observations in Figure 5.5. First, the distance between the Pareto optimal front and the  $K\omega_r^2$  law increases with increasing turbulence intensity. Second, simultaneous large improvements in power capture and reductions in gearbox loads can be obtained with use of preview. Third, sustaining larger drivetrain damage than the  $K\omega_r^2$  law in low-turbulent wind conditions yields limited power capture improvements. However, there is an important trade-off between the extra power capture and the loads with larger wind fluctuations. Whether a control method that yields higher power with higher loads is desirable depends on the extra cost incurred by the extra drivetrain damage. Development of cost models for turbine structures that relate the sustained damage to an economic cost is an open area of research.

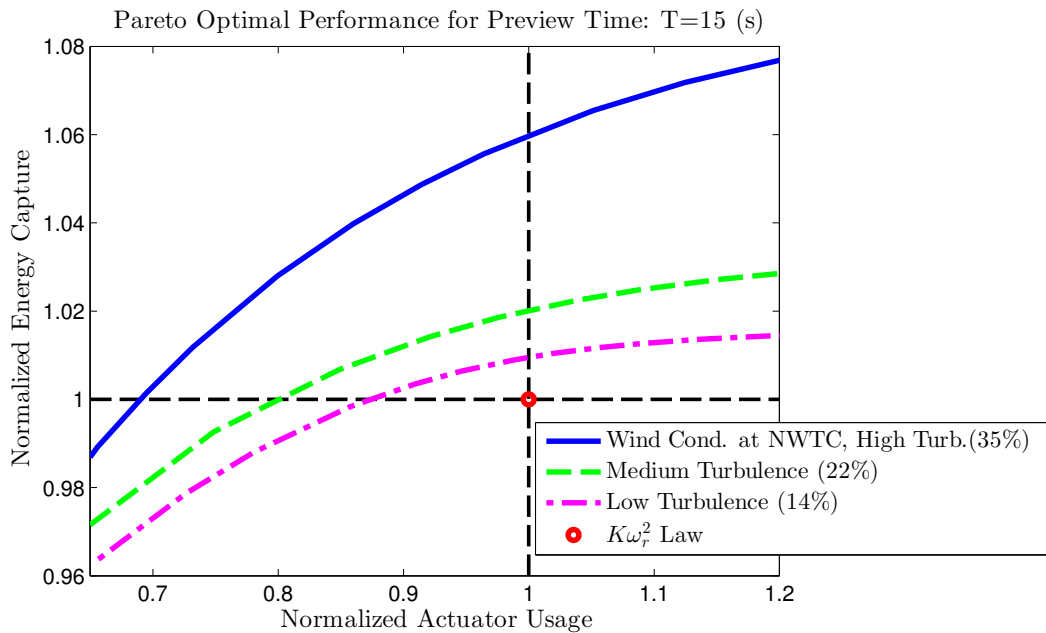


Figure 5.5: Pareto optimal performance trade-off with a fixed preview time of 15 (s)

## 5.4 Region 3 Preview Control<sup>1</sup>

Turbine Region 3 control problem has different objectives and challenges than the Region 2 control problem. Blade pitch is the main control input used in Region 3 control whereas the generator torque is held constant or set to achieve a constant power. The large turbine blades encountered in commercial turbines often have restrictive rate limits. This section aims to understand the fundamental trade-offs between performance, wind preview time, and blade pitch rate limits in Region 3 control.

The main control objective is to use preview information to reject wind disturbances subject to blade pitch rate constraints. We study Region 3 rotor speed regulation problem using two different fidelity models. First, an optimal control problem is formulated in continuous-time for a simple one-state, linear rigid-body model of a wind turbine. The exact, analytical solution of this problem provides insight into the fundamental performance limits. Second,  $H_\infty$  preview controllers are designed for a number of preview times. These controllers are simulated on a medium-fidelity, nonlinear turbine model with realistic preview sensor models. The performance versus preview time characteristics of the  $H_\infty$  controllers are in agreement with the predictions from the lower-fidelity models. Thus we believe the analytical results obtained with the low-order model can provide design guidelines for the use of preview information in turbine control.

The remainder of this section is structured as follows: Section 5.4.1 presents the problem formulation and the analytical results for the simple one-state model of the turbine. Section 5.4.2 discusses the results with the medium-fidelity nonlinear model of the turbine and compares these with the analytical results. The challenges associated with the preview wind measurements are also discussed in Section 5.4.2.

---

<sup>1</sup> In reference to IEEE copyrighted material which is used with permission in this thesis, the IEEE does not endorse any of the University of Minnesota's products or services. Internal or personal use of this material is permitted. If interested in reprinting/republishing IEEE copyrighted material for advertising or promotional purposes or for creating new collective works for resale or redistribution, please go to [http://www.ieee.org/publications\\_standards/publications/rights/rights\\_link.html](http://www.ieee.org/publications_standards/publications/rights/rights_link.html) to learn how to obtain a License from RightsLink.

### 5.4.1 Analytical Results for One-State Turbine Model

An exact analytical solution to solve the optimal control problem for a first-order system with preview information was provided in [85]. This section applies a simplified version of the results in [85] for rotor speed tracking in above-rated wind conditions (Region 3). The control objective is to minimize the peak tracking error. The  $L_\infty$  (peak) norm is used to measure the tracking error for two reasons. First, minimizing the peak rotor speed error is crucial to avoiding generator over-speed. Second, variations in rotor speed are correlated to structural loads on the turbine. Hence reducing variations in rotor speed typically leads to reduced peak blade, tower and gearbox loads. Peak loads encountered under extreme wind conditions are a driving design factor for large, commercial wind turbines that contain highly flexible structures.

The wind turbine considered for the analysis is the three-bladed Controls Advanced Research Turbine (CART3) located at the National Wind Technology Center (NWTC). The CART3 is chosen for this study because it has been used extensively in the literature. This provides the opportunity to understand performance trends observed in previous work on preview control for wind turbines [31] and [33] in the context of the analytical results provided in this paper.

#### Problem Formulation

The one-state linear turbine model used for the control problem formulation can be obtained either from FAST or the one-state nonlinear model described in Section 3.3 and 5.3.1. For the sake of a simple description we assume that this linear model is obtained from the latter option. Eq. (3.3) has one state ( $\omega_r$ ), two control inputs ( $\tau_g$  and  $\beta$ ) and one exogenous disturbance ( $v$ ). Equation (3.3) can be numerically linearized at a trim condition  $(\bar{\omega}_r, \bar{\tau}_g, \bar{\beta}, \bar{v})$  to obtain a one-state model of the form:

$$\dot{\delta}_{\omega_r}(t) = a \delta_{\omega_r}(t) + b \delta_{\beta}(t) + c \delta_v(t) \quad (5.9)$$

Here the  $\omega_r$  is the rotor speed,  $\beta$  is the pitch angle and  $v$  is the wind speed.  $\delta$  denotes the deviations from these variables' trim values. The constant coefficients  $a$ ,  $b$  and  $c$  in this linear model correspond to the damping, control gain, and disturbance gain, respectively. In Region 3 the trim condition  $\bar{\omega}_r$  is the rated rotor speed and hence

$\delta_{\omega_r}(t)$  is the rotor speed tracking error. The control objective is to regulate  $\delta_{\omega_r}(t)$  to zero. The disturbance is “matched” in Equation (5.9) and hence it can be perfectly canceled by setting  $\delta_\beta(t) = -\frac{c\delta_v(t)}{b}$ . However, perfect cancellation is not possible if the actuator is subject to rate constraints and the wind speed is rapidly changing. An advanced sensor, e.g. LIDAR, can be used to generate a preview measurement of the wind disturbance, i.e. a measurement of  $\delta_v(\tau)$  for  $\tau > t$ . This preview measurement can be used to partially overcome the disturbance rejection limitations imposed by actuator rate constraints.

Assume the controller has access to  $T$  seconds of preview wind information. The essence of the performance vs. preview trade-off is captured by the following control optimization problem:

$$\begin{aligned}
p(T) &:= \min_{\dot{\beta} \in C[-T, \infty)} \|\delta_{\omega_r}\|_\infty \\
&\text{subject to: Equation (5.9)} \\
&|\dot{\beta}(t)| \leq r \\
&\delta_{\omega_r}(-T) = 0, \delta_\beta(-T) = 0 \\
&\delta_{v_T}(t) = \begin{cases} 0 & \text{if } t < 0 \\ v^* & \text{if } t \geq 0 \end{cases}
\end{aligned} \tag{5.10}$$

where  $C[-T, \infty)$  is the vector space of continuous functions defined on the interval  $[-T, \infty)$ . The infinity-norm for the continuous signal  $\delta_{\omega_r}$  is defined as

$$\|\delta_{\omega_r}\|_\infty = \sup_{t \in [-T, \infty)} |\delta_{\omega_r}(t)|$$

In words, the turbine is initialized at the equilibrium  $\delta_{\omega_r}(-T) = 0$  and is disturbed by a wind gust of magnitude  $v^*$  at time  $t = 0$ . The objective is to design the optimal pitch input that minimizes the peak deviation in  $\delta_{\omega_r}$ . Here the pitch rate constraint is written as  $|\dot{\beta}| < r$  without the symbol  $\delta$  since the trim pitch rate  $\dot{\beta}$  is zero.  $\delta_\beta$  is rate constrained and hence the wind gust cannot be perfectly canceled. The control problem formulation allows  $\delta_\beta$  to anticipate the disturbance, i.e. the blades can begin moving at  $t = -T$  to cancel the step gust at  $t = 0$ . This models a situation in which the controller has a measurement of the disturbance with  $T$  seconds of preview.  $p(T)$  denotes the optimal performance as a function of the preview time  $T$ . The rest of the presentation assumes, without loss of generality, that  $v^* \geq 0$ .

The step wind gusts used in this formulation do not fully capture the effects of turbulent wind conditions. However, the frequency spectra of many common turbulence models [54] exhibit a roll-off characteristic similar to of a step gust. Hence step wind gusts can provide a useful approximation to the turbine performance under turbulence.

The frequency spectrum of the turbulent wind conditions generated for CART3 is shown in Figure 5.6 (blue solid line). TurbSim [54], developed at NWTC, was used to generate the turbulent wind data. The parameters for generating the turbulent wind data are taken from the work by Laks, et al. [33] and are listed in the Table 5.4.1. These wind conditions are considered to be realistic for the NWTC site where the CART3 is located. The average wind speed of  $18m/s$  was chosen to ensure constant Region 3 operation. The wind conditions generated by TurbSim include spatial and temporal variations. Only the frequency spectrum of the hub-height average wind minus the trim wind speed is shown. The green dash-dotted line in Figure 5.6 is the spectrum of a  $2.5m/s$  step wind gust. The spectrum of the step gust is a good approximation for the turbulent spectrum over a wide frequency band of  $0.01$  to  $25rad/s$ . The red dashed curve in Figure 5.6 is the  $H_\infty$  design weight used to describe the expected spectrum of the disturbances. This curve and weight will be discussed further in the next section.

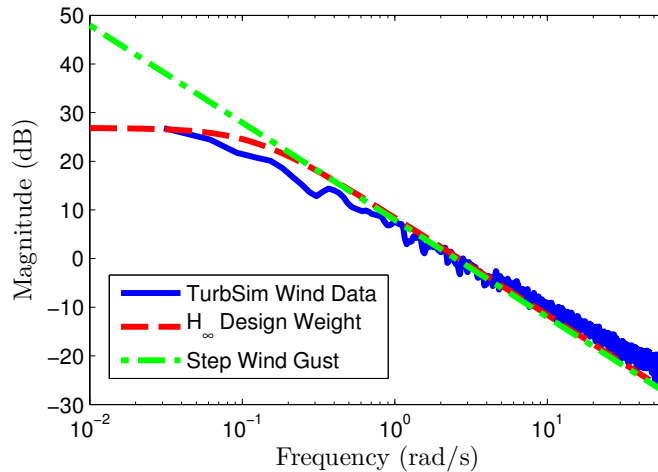


Figure 5.6: Frequency spectrum of the hub-height average speed of the turbulent wind conditions

The CART3 model [59] is trimmed at  $\bar{v} = 18m/s$  for Region 3 linearization. This

Parameter	Value
Mean Wind Speed	18 <i>m/s</i>
Vertical Wind Shear ( $\alpha_0$ )	0.110
Vertical Stability ( $Ri_{TL}$ )	-0.18
Mean Friction Velocity ( $U_{*D}$ )	0.682 <i>m/s</i>

Table 5.1: Atmospheric parameters used in TurbSim for generating turbulent wind data

is approximately the mean of the rated and cut-out wind speed specifications for this turbine. The rated rotor speed, generator torque and corresponding trim pitch angles are  $\bar{\omega} = 3.881 \text{ rad/s}$ ,  $\bar{\tau}_g = 152130 \text{ Nm}$ , and  $\bar{\beta} = 16.52 \text{ deg}$ . The resulting numerical values of  $a$ ,  $b$  and  $c$  are  $-0.2771 \frac{1}{s}$ ,  $-0.0527 \frac{1}{\text{deg}\cdot\text{s}^2}$  and  $0.0731 \frac{1}{\text{m}\cdot\text{s}}$ . A step wind gust of  $v^* = 2.5 \text{ m/s}$  on top of the  $18 \text{ m/s}$  steady wind was used for the problem formulation in Equation (5.10). This amplitude was obtained from fitting the turbulent wind spectrum used for CART3 simulations with of a step gust as shown in Figure 5.6. The only remaining parameter in the optimal control problem (Equation (5.10)) is the pitch rate limit  $r$ . The CART3 pitch actuators have rate limits of  $18 \text{ deg/s}$ . The design value of the actuator rate limit is conservatively chosen as  $r = 6 \text{ deg/s}$  for this analysis. This conservative choice is made because the controllers designed in this section are also tested in extreme wind conditions in Section 5.5. A controller designed to yield  $6 \text{ deg/s}$  peak pitch rate for step and turbulent wind conditions can use higher pitch rates in extreme wind conditions. These conservative controllers avoid pitch rate saturations that can destabilize the closed loop system.

The remainder of this section provides the optimal pitch control as a function of the preview time. Additional details, including proofs of optimality, can be found in [85]. The optimal solution consists of four cases: zero, small, medium, and large preview times. The characterizations of these four cases depends on a fundamental preview time defined as  $T^* := \frac{cv^*}{r|b|}$ . In addition, the optimal solution depends on the non-dimensional decay rate  $\alpha := aT^*$ . For the CART3 linearization data the constants are  $T^* = 0.577 \text{ s}$  and  $\alpha = -0.160$ . The results are presented for the approximation that  $\alpha = 0$  (equivalently  $a = 0$ ). This introduces less than 1% error because  $\alpha \ll 1$  for the CART3 data. More importantly, this approximation leads to simpler analytical formulas that can be used to gain insight into the preview control problem. This approximation arises because a utility-scale wind turbine has a large rotor inertia. The large inertia

translates into a small decay rate  $a$  relative to the fundamental time scale  $T^*$  that arises in the preview control problem, i.e.  $aT^* \ll 1$ . The exact amount of error introduced by this approximation can be obtained by comparing the full solution presented in [85] to the simplified results presented here.

**No Preview:**  $T = 0$

If there is no preview ( $T = 0$ ) then the optimal response is to ramp the blades at their maximum rate  $\dot{\beta} = r$  until  $\delta\beta$  cancels the wind gust. It takes  $T^* := \frac{cv^*}{r|b|}$  seconds to pitch the blades  $\delta\beta$  from 0 to  $\frac{cv^*}{|b|}$ . This optimal input can be written as:

$$\delta_{\beta_0}(t) = \begin{cases} r(t+T) & \text{if } -T \leq t < T^* - T \\ \frac{cv^*}{|b|} & \text{if } t \geq T^* - T \end{cases} \quad (5.11)$$

Integration of the system dynamics (Equation (5.9)) with  $a = 0$  yields the trajectory:

$$\delta_{\omega_0}(t) = \begin{cases} cv^*(t+T) - \frac{|b|r(t+T)^2}{2} & \text{if } -T \leq t < T^* - T \\ \frac{(cv^*)^2}{2r|b|} & \text{if } t \geq T^* - T \end{cases} \quad (5.12)$$

Therefore the minimal peak rotor speed tracking error (Equation (5.10)) with no preview is given by  $p(0) = \frac{(cv^*)^2}{2r|b|}$ .

**Small Preview:**  $T \leq (\sqrt{2} - 1)T^*$

For “small” preview times, the optimal pitch action is still given by  $\delta_{\beta_0}(t)$  in Equation (5.11). Specifically,  $\delta_{\beta_0}(t)$  is optimal for preview times that satisfy  $T \leq (\sqrt{2} - 1)T^*$ . Figure 5.7 shows the response of the turbine rotor with the optimal input  $\delta_{\beta_0}(t)$  for three different “small” preview times. The wind gust occurs at  $t = 0$  for each response. The controller starts acting when the wind gust information enters the system at  $t = -T$ . In other words, the controller has exactly  $T$  seconds to act before the gust. The solid line in this figure is the response  $\delta_{\omega_0}(t)$  for no preview (Equation (5.12)). For the CART3 data,  $T^* = 0.577s$  and the minimal peak rotor speed error with no preview is  $p(0) = 0.0527rad/s$ . The dashed and dash-dotted lines are the optimal responses for  $T = 0.1s$  and  $T = 0.23s$ . All three trajectories achieve their peak magnitude at  $t = T^* - T$  and have  $\dot{\delta}_{\omega_r}(t) = 0$  for  $t \geq T^* - T$ .

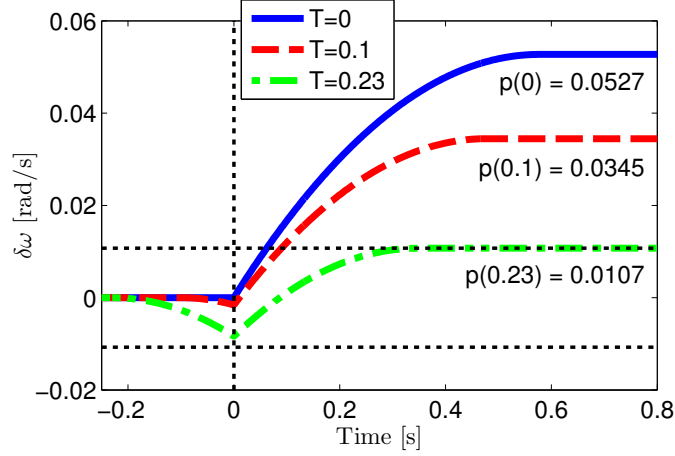


Figure 5.7: Time responses of rotor speed error ( $\delta\omega_r(t)$ ) for “small” preview times. The wind gust occurs at  $t = 0$  for all responses

For  $T = 0.1$  s, the rotor speed is  $\frac{-|b|r(t+T)^2}{2}$  at the onset of the step gust ( $t = 0$ ). At  $t = 0$ , the rotor speed reverses direction due to the step wind gust and eventually reaches a steady state at  $\delta\omega_r(T^* - T) = 0.0345\text{rad/s}$ . The preview has two benefits. First, the control input is able to partially overcome the rate limit by pitching the blades toward  $\frac{cv^*}{|b|}$  before the step wind gust occurs. Second, the initial negative motion of the rotor speed leaves the turbine in a better position to absorb the wind disturbance. In particular, the large positive peak at  $\delta\omega_r(T^* - T)$  is reduced because disturbance must first overcome the negative value of  $\delta\omega_r(0)$  at the time of the step gust. As a result the optimal cost is reduced from  $p(0) = 0.0527\text{rad/s}$  to  $p(0.1) = 0.0345\text{rad/s}$ .

The response for  $T = 0.23\text{s}$  shows a similar trend with the error further reduced to  $p(0.23) = 0.0107\text{rad/s}$ . Note that, for  $T = 0.23\text{s}$ , the negative motion of the rotor speed prior to the gust reaches  $\delta\omega_r(0) = -0.0084\text{rad/s}$ . This is very close to the magnitude at  $\delta\omega_r(T^* - T) = 0.0107\text{rad/s}$ . As the preview time is further increased, the error at the time of the gust,  $\delta\omega_r(0)$ , continues to become more negative (larger in magnitude). In addition,  $\delta\omega_r(T^* - T)$  continues to decrease in magnitude. This trend continues until  $T$  becomes large enough that  $|\delta\omega_r(0)| = |\delta\omega_r(T^* - T)|$ . The two peaks are precisely equal at  $T = (\sqrt{2} - 1)T^*$ . For  $T > (\sqrt{2} - 1)T^*$ ,  $\delta\beta_0$  in Equation (5.11) is no longer

optimal because the blade pitch before the wind gust creates a negative peak at  $\delta_{\omega_r}(0)$  that dominates the cost. In other words, the control action before the gust specified in Equation (5.11) does more harm than good.

**Moderate Preview:**  $(\sqrt{2} - 1)T^* < T \leq T^*$

For “moderate” preview times  $(\sqrt{2} - 1)T^* < T \leq T^*$ , the optimal pitch action is of the form:

$$\delta_{\beta_T}(t) = \begin{cases} -r(t+T) & \text{if } -T \leq t < t_1 - T \\ +r(t+T-2t_1) & \text{if } t_1 - T \leq t < 2t_1 + T^* - T \\ \frac{cv^*}{|b|} & \text{if } t \geq 2t_1 + T^* - T \end{cases} \quad (5.13)$$

where  $t_1 := \frac{T^2 + 2TT^* - T^{*2}}{4(T+T^*)}$ . The subscript in  $\delta_{\beta_T}$  denotes that the optimal pitch action depends on  $T$  through the parameter  $t_1$ . For  $t \leq t_1 - T$  the optimal input  $\delta_{\beta_T}$  ramps the blades at maximum rate in the wrong direction, i.e. away from the value  $\frac{cv^*}{|b|}$  required to cancel the step wind gust. Then it ramps the blades at maximum rate in the other direction until it reaches  $\frac{cv^*}{|b|}$ . As noted above, the optimal cost for preview time  $T = (\sqrt{2} - 1)T^*$  becomes constrained by the negative peak at  $\delta_{\omega_r}(0)$ . The magnitude of  $\delta_{\omega_r}(0)$  is reduced by ramping the blades initially in the wrong direction. The initial pitching in the wrong direction allows the system to be closer to the final pitch angle at the time of gust ( $t = 0$ ) without causing a larger rotor speed error.

Figure 5.8 shows the rotor speed response and optimal input  $\delta_{\beta_T}(t)$  for three different “moderate” preview times. The solid, dashed, and dash-dotted lines are the responses for  $T = 0.3s$ ,  $0.4s$ , and  $T^* = 0.577s$ . All three trajectories have  $\dot{\delta}_{\omega_r}(t) = 0$  for  $t \geq 2t_1 + T^* - T$ . For each preview time the state trajectory  $\delta_{\omega_r}(t)$  achieves the peak magnitude  $p(T)$  at both  $t = 0$  and  $t = 2t_1 + T^* - T$ . In other words, the value of  $t_1$  is chosen to balance both the negative peak at  $\delta_{\omega_r}(0)$  and the positive peak at  $\delta_{\omega_r}(2t_1 + T^* - T)$ .

For each trajectory the optimal control  $\delta_{\beta_T}$  is negative for  $t < 2t_1 - T$ . This causes  $\delta_{\omega_r}(t)$  to initially move in the positive direction and achieve a local maximum at  $\delta_{\omega_r}(2t_1 - T)$ . As the preview time  $T$  increases,  $\delta_{\omega_r}(2t_1 - T)$  becomes more positive while the magnitudes of  $\delta_{\omega_r}(0)$  and  $\delta_{\omega_r}(2t_1 + T^* - T)$  are both reduced. When  $T = T^*$  the first positive peak at  $t = 2t_1 - T$  satisfies  $|\delta_{\omega_r}(2t_1 - T)| = |\delta_{\omega_r}(0)| = |\delta_{\omega_r}(2t_1 + T^* - T)|$ . For

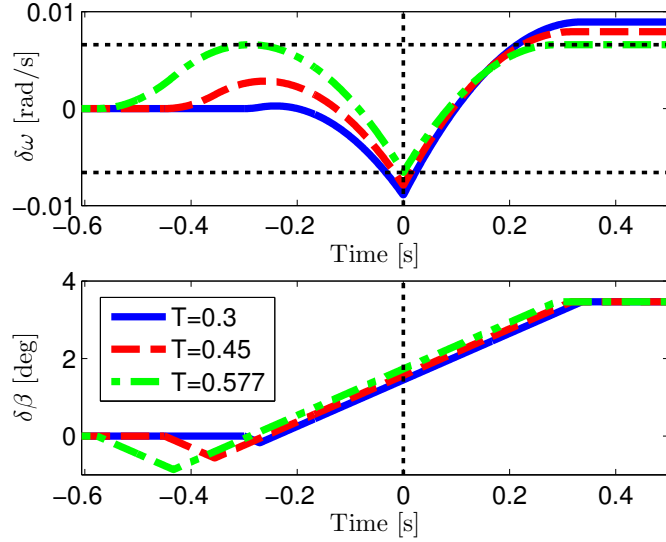


Figure 5.8: Time responses of rotor speed error ( $\delta\omega_r(t)$ ) and optimal pitch command ( $\delta\beta(t)$ ) for “moderate” preview times. The wind gust occurs at  $t = 0$  for all responses

$T > T^*$ , the input  $\delta\beta_T$  in Equation (5.13) is no longer optimal because the magnitude of  $\delta\omega_r(2t_1 - T)$  dominates the cost. For the given data,  $T^* = 0.577s$  and hence the dash-dotted curve in Figure 5.8 represents the optimal response for the limiting case of “moderate” preview ( $T = T^*$ ). The optimal input  $\delta\beta$  shown in the bottom subplot changes from  $\dot{\delta}\beta = -r$  to  $\dot{\delta}\beta = +r$  at  $t_1 - T$ . The top subplot shows that the optimal  $\delta\omega_r(t)$  for  $T = 0.577 s$  achieves its maximum magnitude at times  $2t_1 - T$ ,  $0$ , and  $2t_1 + T^* - T$ .

One issue may arise with “moderate” preview times when the wind speeds are just above the rated wind speed required for Region 3 operation. The initial blade pitch action with  $\dot{\delta}\beta = -r$  is limited in this situation since the blades may hit the  $\beta$  lower-bound of pitch-to-feather turbines. This means the blade pitch angles cannot be lowered any more to gain rotor speed before the gust. In this case the performance can be conservatively considered to be bounded by the performance given with “small” preview times. This is a limited performance loss since “moderate” preview times yield limited performance improvement as seen in Figure 5.9.

**Long Preview:**  $T > T^*$

For  $T > T^*$  one might suspect that  $p(T)$  can be further reduced by pre-pending the control action  $\delta_{\beta_{T^*}}(t)$  with an initial negative ramp of the blades. This might simultaneously reduce the magnitudes of  $\delta_{\omega_r}(2t_1 - T)$ ,  $\delta_{\omega_r}(0)$ , and  $\delta_{\omega_r}(2t_1 + T^* - T)$  which constrain the performance for  $T = T^*$ . In actuality, no further improvement can be obtained for  $T > T^*$ , i.e. there is a fundamental bound on the performance improvements achieved via preview. This fact is formalized in the following theorem:

**Theorem 1**  $p(T) = p(T^*)$  for all  $T \geq T^* = \frac{cv^*}{r|b|}$ . The minimal cost is  $p(T^*) = \frac{(cv^*)^2}{16r|b|}$

**Proof:** Follows from reference [85].

The optimal input for  $T > T^*$  is not unique but one choice is given by:

$$\delta_{\beta_T}(t) = \begin{cases} 0 & \text{if } t < -T^* \\ \delta_{\beta_{T^*}}(t) & \text{if } t \geq -T^* \end{cases} \quad (5.14)$$

where  $\delta_{\beta_{T^*}}$  is the optimal input given by Equation (5.13) for  $T = T^*$ . This choice wastes the first  $T - T^*$  seconds of preview by leaving the input at zero and then executes the control action  $\delta_{\beta_{T^*}}$  once  $T^*$  seconds of preview remains.

## Summary

The solution to the optimal control problem (Equation (5.10)) for  $a = 0$  (no damping in Eq. (5.9)) is summarized in Table 5.2. Figure 5.9 shows the minimum rotor speed error versus preview time.  $T^* = \frac{cv^*}{r|b|}$  is a fundamental preview time beyond which no additional performance improvements are obtained. The fundamental preview time and optimal tracking cost  $p(T^*)$  are both inversely related to the rate limit  $r$  and control gain  $b$  in Eq. (5.9).  $T^*$  grows linearly with increasing magnitude of the wind gust  $v^*$  and disturbance gain  $c$  while  $p(T^*)$  grows quadratically. In addition,  $p(0) = \frac{(cv^*)^2}{2r|b|}$  and  $p(T^*) = \frac{(cv^*)^2}{16r|b|}$ . Thus, preview information can, at best, reduce the peak tracking error by a factor of eight compared to the performance with no preview. Finally, the use of preview has the largest impact for  $T \leq (\sqrt{2} - 1)T^*$ . For these small preview times, the rotor speed error reduces linearly in  $T$ . Only minor improvements in the cost are obtained for preview times  $(\sqrt{2} - 1)T^* < T \leq T^*$ .

Preview Time	Optimal Cost, $p(T)$	Optimal Input, $\delta\beta(t)$
$T \leq (\sqrt{2} - 1)T^*$	$\frac{(cv^*)^2}{2r b } - cv^*T$	Equation (5.11)
$(\sqrt{2} - 1)T^* < T \leq T^*$	$\frac{ b r}{16} \frac{(-T^2 + 2TT^* + T^{*2})^2}{(T + T^*)^2}$	Equation (5.13)
$T > T^*$	$\frac{(cv^*)^2}{16r b }$	Equation (5.14)

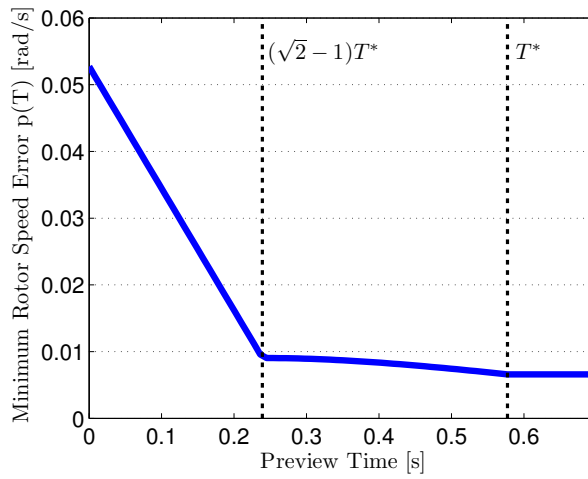
Table 5.2: Summary of results for  $a = 0$ 

Figure 5.9: Performance versus preview time predictions from analytical results

### Effect of Operating Condition

The results presented in the previous sub-sections are based on a 1-state rigid body model of the CART3 trimmed at 18  $m/s$ . The parameters  $a$ ,  $b$  and  $c$  of this model change with the mean wind speed. We have obtained linearizations from the rated wind speed of the CART3, 12.5 $m/s$ , up to 24 $m/s$  to investigate the effect of operating conditions on preview time requirements. The  $b$  and  $c$  parameters from each of these models are used to calculate the fundamental preview time  $T^*$ . Figure 5.10 shows the  $T^*$  versus the trim wind speed. The  $T^* = 83s$  calculated for 12.5 $m/s$  trim wind condition is not plotted. This is because  $T^*$  decreases rapidly with increasing trim wind speed. Trim pitch angle difference between 12.5 $m/s$  and 12.6 $m/s$  is approximately 1.5 $deg$ . Blades with the pitch rate limit 18 $deg/s$  can travel 1.5 $deg$  in a much shorter time than the difference in the fundamental preview times between these two trim wind speeds.

The preview time versus trim wind speed trend observed in Figure 5.10 agrees well with general turbine design considerations. This trend is largely driven by the variations in the control gain parameter  $b$ . Turbine power and torque capture are designed to be insensitive to pitch angle variations around the optimal pitch angle for power capture in Region 2. This corresponds to a small  $b$  value. This is in order to minimize power losses due to uncertainties related to calculation of this optimal pitch angle. As the turbine enters Region 3, the pitch angle is increased to shed some of the power in wind. To achieve this effect the turbine design favors a higher  $b$  value at increasing pitch angles. For instance,  $b = -0.0070$  and  $-0.0260$  at trim wind speeds equal to 12.6 $m/s$  and 14 $m/s$ , respectively. The fundamental preview time  $T^*$  is inversely related to  $b$ . Hence the increase in control effectiveness  $b$  from 12.6 $m/s$  to 14 $m/s$  corresponds to the decrease in fundamental preview time.

#### 5.4.2 Validation with $H_\infty$ Preview Controllers

This section presents an  $H_\infty$  preview controller using a design architecture similar to that used by Laks, et al. [31]. This is a 2-input (rotor speed and wind speed measurements) and 1-output (collective pitch) controller. The performance vs. preview time is evaluated using the NWTC's Fatigue, Aerodynamics, Structures, and Turbulence (FAST) nonlinear simulation code [51]. A detailed LIDAR sensor model is implemented

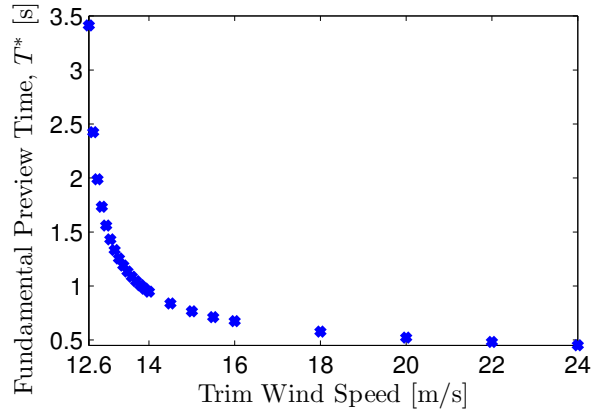


Figure 5.10: Fundamental preview time versus trim wind speed

to capture the challenges associated preview wind sensing. The performance trends for this medium-fidelity model are compared with the trends predicted by the simple, rigid-body analysis described in the previous section.

A low order linear model of the CART3 was used for the control design. The low order, 5 degrees of freedom design model contained modes for generator speed, tower first fore-aft bending and blade first flapwise bending. This model is based on a linearization of the FAST model of CART3 at  $18\text{m/s}$  hub-height wind speed. The turbine dynamics depend on rotor position and have a non-steady trim trajectory. Hence linearizations are performed on a grid of rotor positions and result in linear time-varying (LTV) models. This LTV model is converted to an LTI model using the multi-blade coordinate transformation [20,37,63,67,69] followed by averaging of the resulting matrices. Finally, the turbine model was discretized using a bilinear (Tustin) transformation with a sample time of  $T_s = 0.025\text{s}$ . The discretization step was needed for modeling of the wind preview information. Finally, the first-order pitch actuator models with  $30\text{ rad/s}$  bandwidth were added to the design model. The final design model had 11 states. The continuous time model without the actuators has the following form before the discretization step:

$$\dot{x} = Ax + Bu$$

$$y = Cx + Du$$

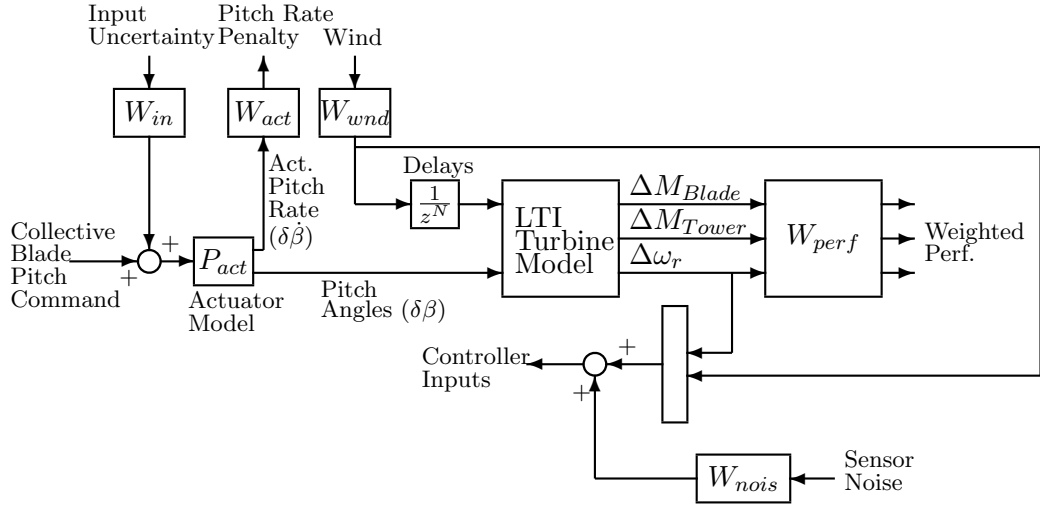


Figure 5.11: System Interconnection for  $H_\infty$  Collective Pitch Controller Design

The first two states of this linear system are the tower 1<sup>st</sup> tower fore-aft bending mode tip-displacement ( $m$ ) and rotor position ( $rad$ ). The next three states correspond to the collective and cyclic 1<sup>st</sup> blade flapwise bending mode displacements. States 6-10 are the derivatives of the first five states. The system inputs are the hub-height wind disturbance ( $m/s$ ) and collective blade pitch angles ( $rad$ ). The outputs are the collective blade flapwise root bending moment ( $kN \cdot m$ ), tower base fore-aft bending moment ( $kN \cdot m$ ) and rotor speed ( $rpm$ ). The state and output matrices have the block partitioned form:

$$A = \begin{bmatrix} 0 & I_5 \\ A_{21} & A_{22} \end{bmatrix}$$

$$C = \begin{bmatrix} C_1 & C_2 \end{bmatrix}$$

The system matrices are given by:

$$A_{21} = \begin{bmatrix} -34.76 & -0.0616 & 4.709 & 0.2444 & -1.483 \\ -0.7381 & -0.0016 & 2.431 & -0.0007 & -0.0304 \\ 72.79 & 0.0822 & -238.7 & -0.697 & 2.370 \\ 6.918 & -10.54 & -1.269 & -186.5 & -13.32 \\ -49.13 & -8.738 & 5.088 & 13.98 & -188.5 \end{bmatrix}$$

$$A_{22} = \begin{bmatrix} -0.1006 & -0.0605 & 0.0049 & 0.0023 & 0.0106 \\ -0.0125 & -0.0781 & 0.013 & -0.0001 & 0.0014 \\ -6.375 & -19.58 & -3.680 & 0.0264 & 0.0095 \\ 10.74 & 0.0979 & 0.0567 & -3.518 & -7.765 \\ 5.404 & -0.511 & 0.0997 & 7.765 & -3.501 \end{bmatrix}$$

$$B = \begin{bmatrix} 0 & 0 \\ 0 & 0 \\ 0 & 0 \\ 0 & 0 \\ 0 & 0 \\ 0.0775 & -2.1115 \\ 0.0118 & 1.1015 \\ 6.0254 & -405.343 \\ -0.0254 & 29.4093 \\ -0.7780 & 11.8315 \end{bmatrix}$$

$$C_1 = \begin{bmatrix} 192.5 & 0.389 & 900 & -1.24 & 9.04 \\ 58220 & 50.81 & -211 & -153.5 & 1173 \\ 0 & 0 & 0 & 0 & 0 \end{bmatrix}$$

$$C_2 = \begin{bmatrix} -7.58 & -9.18 & 0.383 & -0.0006 & -0.099 \\ 24.92 & -3.42 & -0.447 & -1.520 & -6.969 \\ 0 & 9.55 & 0 & 0 & 0 \end{bmatrix}$$

$$D = \begin{bmatrix} 7.8878 & -219.6507 \\ -3.7719 & 102.9489 \\ 0 & 0 \end{bmatrix}$$

A  $H_\infty$  preview controller is designed based on this reduced-order, discrete-time LTI model of the CART3. The control objective is rotor speed tracking as well as tower

and blade load reduction at higher (Region 3) wind speeds. The control input is the collective pitch angle of three blades. The measurement for control is the rotor speed. In addition, it is assumed that the controller has access to a preview wind measurement that is the average of three point measurements in space supplied by the LIDARs. The preview measurements are modeled by augmenting the wind disturbance input of the design model with  $N$  delays. The controller has access to a measurement of the wind disturbance input to the chain of  $N$  delays. As a result, the controller has a measurement of the wind disturbance with a preview of  $NT_s$  seconds prior to its impact on the turbine. The amount of preview available to the  $H_\infty$  controller is adjusted by changing the number of delays  $N$ .

Signal-weighted  $H_\infty$  control designs were performed for a variety of preview times  $N$  using the system interconnection shown in Figure 5.11. The block labeled “LTI Turbine Model” is the discrete-time LTI design model without the actuator dynamics and the  $N$  steps of delay on the wind input. The block  $P_{act}$  contains the pitch actuator model for CART3. The first output of this model is the actuator pitch rate and the second output is the pitch angle. The extra pitch rate output was created to penalize blade pitch rates to normalize control usage across all the designs. The system interconnection contains weights for performance, input uncertainty, measurement noise, actuator usage, and wind disturbance. All weights except  $W_{act}$ , which penalizes the pitch command rate, are independent of the preview time. The weights were initially specified in continuous-time and then converted to discrete-time using a bilinear (Tustin) transformation with a sample time of  $T_s = 0.025s$ .

The continuous-time transfer functions for each weight are provided in the Table 5.3. The performance weight is block diagonal  $W_{perf} = \text{diag}(W_{BladeM}, W_{TowerM}, W_{\omega_r})$  with the individual blocks penalizing flapwise collective blade bending moment, tower fore-aft bending moment, and rotor speed tracking respectively. The performance penalty  $W_{BladeM}$  emphasizes attenuation of the blade bending moment at middle to high frequencies. This choice is made because the DC and lower frequency components of the blade bending moments, due to persistent wind disturbances, cannot be attenuated. The penalty weight on the tower bending  $W_{TowerM}$  is chosen to add extra damping at the tower bending moment frequency. The performance penalty  $W_{\omega_r}$  is chosen to attenuate low-frequency tracking errors. The input disturbance  $W_{in}$  models dynamic

uncertainty across all frequencies. The weight  $W_{nois} = \text{diag}(W_{n,\omega_r}, W_{n,wnd})$  is a  $2 \times 2$  diagonal weight that models noise on the rotor speed and wind speed, respectively. The rotor speed and wind speed measurement noise weights are chosen as a high pass to avoid excitation of the high-frequency modes of the turbine. The actuator weight  $W_{act}$  is used to penalize the blade pitch rates. This penalty acts directly on the pitch rates as opposed to the pitch command rates. The gain of the constant weight  $K$  is chosen as a function of the wind preview time  $N$ . The value of  $K$  is tuned through simulations to obtain a closed-loop peak pitch rate of  $6 \text{ deg/s}$  for a  $2.5 \text{ m/s}$  uniform wind gust input for all  $H_\infty$  controllers of different preview lengths. This ensures that controllers for all preview times have roughly the same actuator usage. This normalization is carried out so that the  $H_\infty$  controllers have the same peak pitch rate with the analytical solutions presented in the previous section. Values of gain  $K$  versus preview time are provided in Table 5.4. The second column of this table, denoted as “Delay States (N)”, lists the number of delay states used in the design interconnection to model preview wind information.

One design weight of particular importance is the weight on the wind disturbance  $W_{wnd}$ . This weight represents the frequency spectrum of the operating wind conditions. This spectrum is important because the preview time required for optimal pitch action depends on the turbulent wind conditions. For instance slow wind variations with small magnitude require smaller preview times. Larger magnitude fluctuations observed in higher turbulence require longer preview times. The weight  $W_{wnd}$  used in this design is obtained from time-series turbulent wind data generated by TurbSim as described in the Section 5.4.1. The frequency spectrum of this wind profile, shown in Figure 5.6, is fit with a first-order transfer function to obtain  $W_{wnd}$ . The preview time required by the  $H_\infty$  controllers depend on this weight. This is similar to the fact that the fundamental preview time  $T^*$  is related to the step wind gust magnitude  $v^*$  used in the analytical results.

## Results with Ideal Measurements

This section presents the results with ideal preview measurements. Note that this “ideal” measurement case is still impacted by the prediction errors regarding future rotor position and the Taylor’s frozen turbulence assumption.

Weight	Transfer Function
$W_{\omega_r}$	$0.002 \frac{s + 50}{s + 0.05}$
$W_{BladeM}$	$2 \times 10^{-7} \frac{s + 50}{s + 0.2}$
$W_{TowerM}$	$5 \times 10^{-7} \frac{s + 50}{s + 5}$
$W_{in}$	0.03
$W_{n,\omega_r}$	$1.5 \frac{s + 0.1}{s + 5}$
$W_{n,wnd}$	$15 \frac{s + 0.5}{s + 75}$
$W_{wnd}$	$\frac{2.64}{s + 0.12}$
$W_{act}$	$K(N)$

Table 5.3: Weights for  $H_\infty$  Preview Control Design

Preview Time (s)	Delay States (N)	Gain K
0	0	3.850
0.10	4	3.250
0.20	8	2.700
0.30	12	2.100
0.40	16	1.500
0.50	20	1.000
0.60	24	0.500
0.70	28	0.035
0.80	32	0.041
$\geq 0.80$	$\geq 32$	0.041

Table 5.4: Values of gain K used in actuator penalty weight  $W_{act}$

The closed-loop response of the nonlinear CART3 system to a 2.5  $m/s$  uniform wind step disturbance is shown in Figure 5.12 for  $H_\infty$  controllers with three different preview lengths. The blue solid, red dashed, and green dash-dot lines are the responses for the controllers with 0.0s, 0.4s, and 0.8s of preview, respectively. The simulation results are time shifted such that the step wind gust occurs at  $t = 0$ . The controller with small 0.4s preview starts pitching the blades as soon as information about the incoming gust is received ( $t = -0.4s$ ). The control action looks similar to that of the no-preview controller but time-shifted by 0.4s. This behavior shows close agreement with the predictions from the analytical results, i.e. similar pitch action for small and no preview. As the preview time increases further 0.8s, the controller starts pitching the blades earlier at  $t = -0.8s$ . The additional preview enables the controller to achieve larger pitch angles at the time of the gust ( $t = 0$ ) than the other controllers. The  $H_\infty$  controller achieves a much smaller error by having a more negative (larger in magnitude) error before the gust. The  $H_\infty$  controllers with preview times larger than 0.8s yield very similar results to the controller with 0.8s preview and are not plotted. The long preview time (0.8s) used here is slightly longer than the  $T^* = 0.577s$  calculated with the analytical results. The initial pitching toward the fine pitch angle with long preview times observed with analytical results are not seen here. The analytical result uses the  $L_\infty$  (peak) norm to measure performance while the  $H_\infty$  norm is induced by the  $L_2$  (power) norm on signals. We believe the difference in behavior is simply due to this difference in the objective functions of the optimizations.

Figure 5.13 summarizes the rotor speed tracking performance of the  $H_\infty$  controllers on the nonlinear FAST simulations with step and turbulent wind gusts with ideal three point measurements of the wind field. The blue stars represent  $H_\infty$  controllers with step wind gusts. The red circles are the  $H_\infty$  controllers in turbulent wind conditions. The green triangles are the analytical solutions based on the one-state rigid body rotor model of the turbine. All nonlinear simulations with step gusts had peak pitch rates between 5.95 and 6.05 ( $deg/s$ ). The nonlinear simulations in turbulent wind had peak pitch rates between 4.75 and 7 ( $deg/s$ ). The vertical lines in this plot correspond to the “small” and “long” preview times predicted by analytical solutions.

There are three key observations in Figure 5.13. First, the peak rotor speed error is

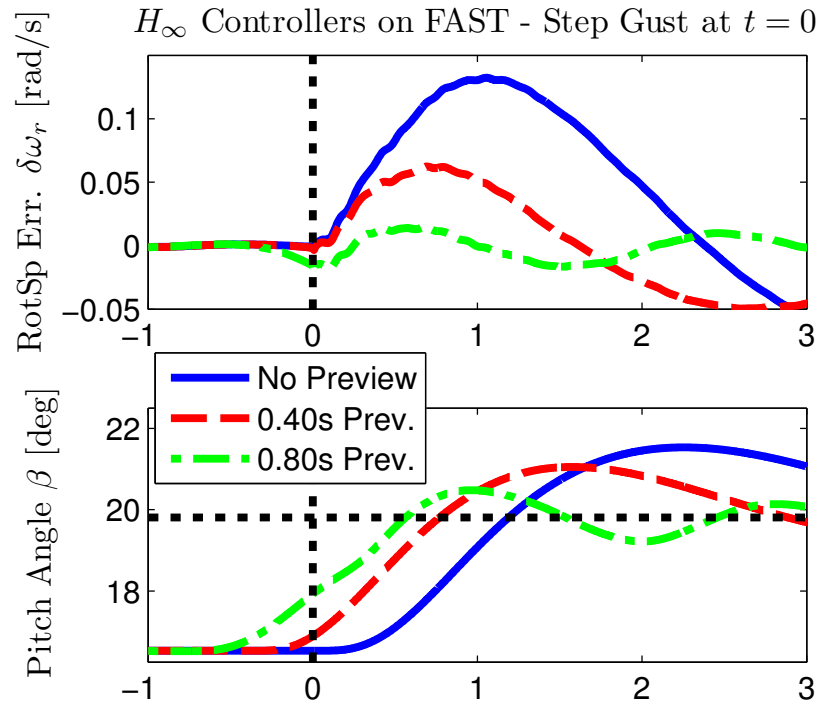


Figure 5.12: Closed-loop response of the CART3 FAST model to a 2.5 m/s step uniform wind gust. The wind gust occurs at  $t = 0$  for all responses

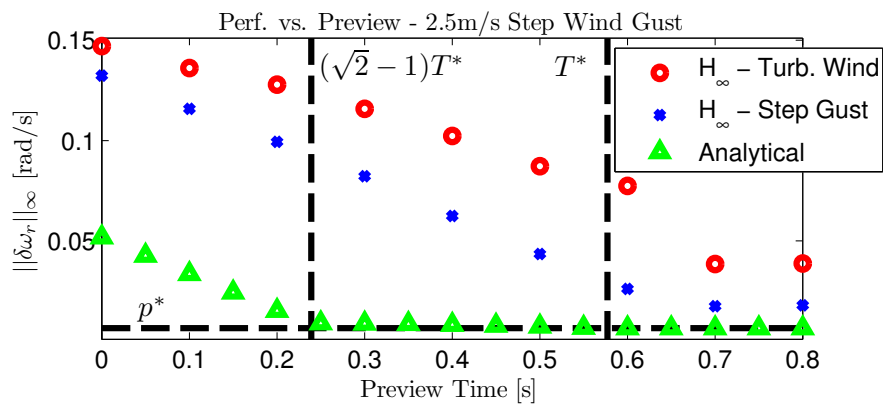


Figure 5.13: Peak rotor speed error vs. preview time for step and turbulent wind for  $H_\infty$  controllers on FAST simulations. Ideal three point measurements of the wind field is used.

reduced linearly with small preview times both for  $H_\infty$  controllers and analytical solutions. Second, there is a preview time beyond which no performance improvements are obtained. Third, the performance of the  $H_\infty$  controllers in the full nonlinear CART3 simulations with turbulent and step wind are very close in terms of rotor speed tracking. The slope of the improvement and the ultimate performance bounds are captured accurately by the analytical results. However, the optimal preview times observed with the  $H_\infty$  controllers are slightly longer than the  $T^*$ . Our design iterations have shown that the optimal preview time for the  $H_\infty$  controllers depend strongly on the weight that capture the wind measurement noise. Actuator penalty and input uncertainties also play a role on this optimal preview time. More conservative controllers tend to use longer preview times.

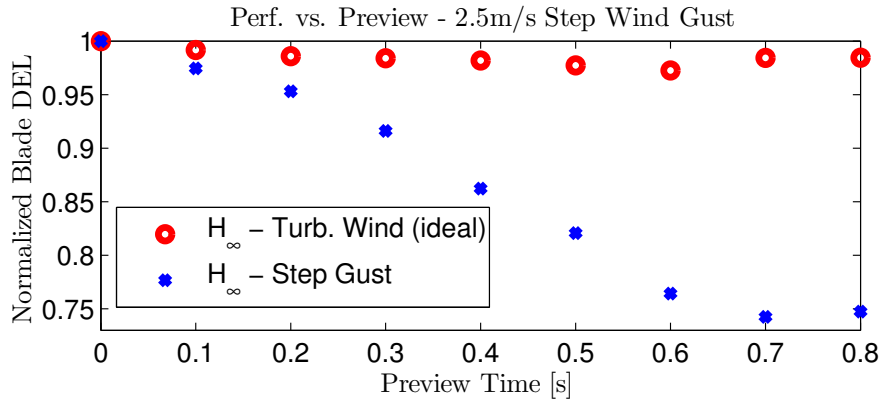


Figure 5.14: Normalized, average blade DELs vs. preview time for step and turbulent wind for  $H_\infty$  controllers on FAST simulations. Ideal three point measurements of the wind field is used.

Figure 5.14 presents the normalized, average blade damage equivalent loads on the nonlinear simulations. The normalizing factors for the step gusts and the turbulent wind conditions are 220 and 328 respectively. The reduction in blade damage equivalent loads is almost linear with small preview times with step wind gusts in step wind gusts. Similar to the rotor speed tracking performance, this improvement continues until 0.8s preview. The improvement between 0s preview and 0.8s preview are approximately 25%. This validates the correlation between rotor speed tracking and blade bending loads. However, these large improvements are not observed with the simulations under

turbulent wind. The improvement obtained in this case is approximately 3%. Even though this performance depends on the design weights, we anticipate this gap to be due to the strong spatial variation of the wind over turbine blades with realistic full-field wind trajectories. This renders the use of collective pitch control for blade load reduction less effective. Individual pitch control with preview wind information may be used to address this issue.

The tower fore-aft bending moments and the RMS rotor tracking speed errors in step and turbulent wind conditions in FAST simulations are not shown here. These results follow the same trend as the peak rotor speed errors shown in Figure 5.13. Almost linear improvements are observed at low preview times and the improvements stop at 0.8s preview.

The results presented in this section are in agreement with the results in [31] which present the worst case gains of various  $H_\infty$  preview controllers designed for the CART3. The worst-case gain of the controller with 6deg/s pitch rate limit approximately flattens out at 0.65s of preview. This is a slightly shorter preview time than the one predicted here. But reference [31] does not use a frequency-based weighting for the wind disturbances. The optimal preview time depends on the design weight choice. Results in [31] also show that there is a fundamental performance limitation imposed by the pitch rate constraints regardless of the preview time. The worst-case gain versus preview time plots flatten out at a higher gain for controllers with smaller pitch rate bounds. This agrees with the results presented in Section 5.4.1 which shows that the optimal cost with long preview is inversely proportional to the pitch rate bounds.

### Results with Realistic LIDAR Measurements

Figure 5.15 compares the performance of the  $H_\infty$  controllers with ideal measurements presented in Section 5.4.2 to their performance with realistic preview wind measurements. These results capture the error characteristics of typical continuous wave LIDARs but use the Taylor's frozen turbulence hypothesis. Specifically, wind measurement errors from spatial range weighting and projection of the horizontal wind onto the laser beam are incorporated on top of the errors caused by the rotor position prediction. The results with LIDAR models under 0.3s are not plotted since the large measurement errors from larger measurement angles from the horizon are extremely detrimental to

turbine performance. The key conclusion from Figure 5.15 is that the error characteristics of the LIDAR sensors may require a longer preview time than the ones observed with the ideal measurements. The main reason behind this behavior is the large angle between the LIDAR beam and the horizon when trying to measure wind at the 75% blade span with small preview. The LIDAR measures the projection of the three dimensional wind speed along its beam. The increased angle between the horizon and the beam reduces the contribution of the horizontal wind speed to the measurement and increases the contributions of the vertical and side-wise wind speed. Increasing the preview time allows the LIDAR to obtain measurements at the same blade span with a smaller angle with the horizon. It is observed that the performance with realistic measurement get fairly close to the ideal performance with higher preview times. It should be noted that using too long preview times can also deteriorate the turbine performance. At long preview times the range weighting errors and the errors from the frozen turbulence hypothesis can dominate the measurement errors and be detrimental to turbine performance.

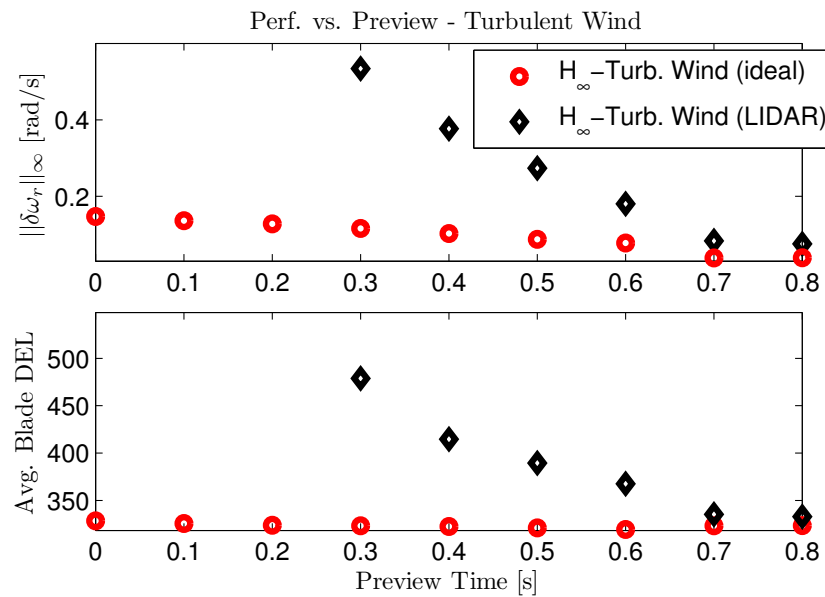


Figure 5.15: Performance metrics vs. preview time for  $H_\infty$  controller simulations in turbulent wind and realistic LIDAR sensor models on FAST

## Summary of Results

In summary, the performance of the advanced preview controllers depend on the pitch rate limits as well as the aggressiveness of the control design. The analytical formulas provide a method to predict the performance limits and trends for these controllers before any detailed control design. The simple steps taken for these predictions can be summarized as follows. A one-state nonlinear model that captures rigid-body rotor dynamics is linearized to obtain  $(a, b, c)$  parameters. The analytical results presented in Section 5.4.1 depend on a step wind gust magnitude. This gust magnitude is obtained from the frequency spectrum of realistic turbulent wind conditions for turbine site. The second parameter required for the analytical solutions, the peak blade pitch rate, is obtained from simulation of the  $H_\infty$  controllers with step wind gusts. It is important to test the final controllers in medium to high-fidelity simulations with LIDAR sensor models. It was observed that the error characteristics of these sensors may necessitate use of longer preview times than the ones predicted by the analytical formulas.

## 5.5 Preview Control for Extreme Events

In this section we present a framework that can be used to analyze the turbine performance versus preview characteristics for a given arbitrary disturbance signal as a function of time. This is in contrast to the step wind gust approximation used to derive our analytical results in Section 5.4.1. The motivation for developing this framework comes from the extreme operating conditions the turbines can face once a year or once in fifty years. Turbine structural health must be tested in the field or with simulations for these extreme conditions [45]. These conditions are described with specific disturbance inputs as a function of time in turbine certification guidelines. There is a need for a method that can be used to analyze the impact of preview on alleviating the effects of these extreme conditions. We present this framework and demonstrate an example with a 50-year extreme operating gust as described by the Germanischer Lloyd wind turbine certification standards [45] on the CART3.

A discretized version of the optimal control problem used for the analytical results for Region 3 preview control, Eq. (5.10), can be utilized to analyze turbine performance for specific wind trajectories. The infinite-dimensional optimization in Eq. (5.10) can be

converted to a finite-dimensional linear program. This approach offers two key benefits. First, a specific wind trajectory can be used to analyze the limits of performance. Second, it is possible to analyze higher order linear models. This allows the introduction of turbine structural modes and actuator models in the optimization problem.

The approach described here has close ties to the work by Boyd and Barratt [86] and Dahleh and Diaz-Bobillo [87]. Boyd and Barratt use the Youla parametrization to formulate wide classes of linear control design problems with time and frequency domain constraints as convex optimizations. Solution of the convex optimizations can be used to determine if there exists a controller that satisfies the given design constraints. The work contained in this paper is influenced by these studies of fundamental performance limits. Dahleh and Diaz-Bobillo consider the  $L_1$  optimal control problem: Find a control  $K$  that minimizes the closed loop induced  $L_\infty$  (peak) norm from disturbances to errors. Linear programming (LP) techniques are used to solve for the optimal controller. We also use  $L_\infty$  (peak) signal norms and LP techniques. The  $L_\infty$  norm of the error signal is minimized for a given disturbance signal rather than for a class of  $L_\infty$  norm bounded disturbance signals. This enables analysis of the optimal control action based on a particular wind trajectory. In addition, we focus on understanding the limits of performance. No effort has been made to synthesize feedback controllers. Implementation of the proposed control actions synthesized by LP techniques can be realized in MPC style but this is not investigated in this thesis.

We envision that the proposed approach can be employed in various ways. First, given a wind profile it is possible to analyze the optimality of various control designs. Second, the impact of the preview wind information versus controller performance can be studied in time-domain. Lastly, linear programming results can be used to develop insight about controller behavior.

The remainder of the section is structured as follows: Section 5.5.1 formulates an optimal rotor speed tracking problem with wind preview information as an LP. Section 5.5.2 uses this framework to analyze the trade-off between performance versus preview time characteristics of the NREL's CART3 [59] for a 50-year gust. This analysis is based on a low-order rotor-inertia model of CART3. We also test the performance of the  $H_\infty$  controllers designed in Section 5.4.2 on the nonlinear FAST turbine simulation package. These results are compared with the performance trade-offs computed

using the LP framework. Our results show that the  $H_\infty$  controllers that were designed without these extreme events in mind result in poor performance. The  $H_\infty$  controllers can be modified to better attenuate the effects of this 50-year gust.

### 5.5.1 Problem Formulation

The control objectives during extreme events are the same with the Region 3 control: maintaining a constant rotor speed and reducing the structural loads. Therefore the problem posed here has many similarities with the one presented in Section 5.4.1. In summary, peak over time rotor speed error minimization is considered. This is important for avoiding generator over-speed problem during an extreme gust. We rely on the correlation between the peak structural loads and the peak rotor speed tracking error for load reduction. It is assumed that a disturbance trajectory as a function of time is provided. The one-state continuous-time linear model in Section 5.4.1 is replaced with an  $n$ -state discrete-time linear model. These linear models are typically obtained from medium to high-fidelity, nonlinear turbine models that involve tower and blade structural modes, models of aeroelastic behavior and turbulent wind profiles. It is assumed that an LTI approximation is used for the periodic LTV models resulting from linearization. Some of the common LTI approximation methods are explained in Section 3.5.2.

The linear turbine model is assumed to have the following form:

$$\begin{aligned}x[k+1] &= Ax[k] + Bu[k] + B_d u_d[k] \\ e[k] &= Cx[k]\end{aligned}\tag{5.15}$$

Here  $A \in \mathbb{R}^{n \times n}$ ,  $B \in \mathbb{R}^{n \times 1}$ ,  $B_d \in \mathbb{R}^{n \times 1}$  and  $C \in \mathbb{R}^{1 \times n}$ . In words, this formulation assumes an  $n$ -state model with one disturbance input, one control input and one system output. The framework described in this section can easily be generalized to MIMO systems.  $x[k+1] \in \mathbb{R}^n$  is the turbine state,  $u[k] \in \mathbb{R}$  is the collective blade pitch,  $u_d[k] \in \mathbb{R}$  is the uniform hub-height horizontal wind speed. The signals  $x[k]$ ,  $u[k]$ ,  $u_d[k]$  and  $e[k]$  are measured relative to their trim value, e.g.  $u[k]$  is the difference between the collective blade pitch and its trim value. For our specific problem  $e[k] \in \mathbb{R}$  is the rotor speed tracking error, i.e. the difference between the current rotor speed and the rated rotor speed.

The turbine dynamics in Eq. (5.15) are assumed to be stable, i.e. all eigenvalues of the state matrix  $A$  have magnitude  $< 1$ . If the wind disturbances and collective blade pitch remain at their trim values ( $u[k] = 0$  and  $u_d[k] = 0$ ), the turbine will reach the rated rotor speed in steady state ( $e[k] \rightarrow 0$  as  $t \rightarrow \infty$ ). Wind gusts ( $u_d[k] \neq 0$ ) will impact the turbine and perturb the rotor speed from its rated value. Actuator rate limits will prevent the blades from instantaneously moving to reject this disturbance. Intuitively preview information of the wind disturbance can be used to (partially) overcome the actuator rate limitations and reduce the effect of the wind on the rotor speed error. The objective of this section is to formulate a simple optimal control problem that provides insight into the benefits and limitations of wind preview information for specific wind trajectories. This is important since the turbine performance versus trade-off characteristics depend heavily on the considered wind disturbance.

We use a model predictive controller to analyze the performance vs. preview trade-off. Let  $N > 0$  denote the number of steps of available wind preview information. Assume that the controller has access to the wind disturbance signal of interest  $u_d[k]$  for  $k \in \{1, \dots, N\}$ . Denote this wind disturbance measurements used by the controller as  $u_{dm}[k]$ . The optimal collective blade pitch angle input is calculated at each time step by solving the following linear program:

$$\begin{aligned}
 p^*(N) &:= \min_{u[1], \dots, u[T-1]} \|e\|_\infty \\
 &\text{subject to: Equation (5.15) with initial cond. } x[0], u[0], u_d[0] \\
 &u_{dm}[k] = \begin{cases} u_d[k] & \text{if } k < N \\ u_d[N] & \text{if } k \geq N \end{cases} \\
 &|u[k] - u[k-1]| \leq r \text{ for } k = 1, \dots, T-1
 \end{aligned} \tag{5.16}$$

where  $\|e\|_\infty := \max_{0 \leq k \leq T} e[k]$  is the peak rotor speed error over the window  $0 \leq k \leq T$  where  $T > N$ . This optimal control problem assumes that the current turbine state  $x[0]$  and collective blade pitch  $u[0]$  are available as measurements. The  $u_d[k]$  for  $k = \{0, 1, \dots, N\}$  is supplied by an advanced wind preview sensor such as a LIDAR. The actuator rate constraints are modeled by a bound of  $r$  (*degs*) on the change in the collective blade pitch between discrete sample times. The objective is to find the optimal collective blade pitch  $u[1], \dots, u[T-1]$  that minimizes the peak rotor speed error.  $N$  denotes the preview time in the sense that the collective blade pitch can begin responding at

time  $k = 1$  to a gust at time  $N$ . This problem formulation solves for the optimal control input over the entire horizon  $1 \leq k \leq T - 1$ , i.e. it assumes knowledge of the entire wind profile. Technically a controller with  $N$  steps of preview would only have access to  $u_{dm}[j]$  for  $1 \leq j \leq N$  at time  $k = 1$ . The wind profile beyond the  $N$ -step prediction is modeled as a persistent wind, i.e.  $u_{dm}[j]$  for  $j \geq N + 1$  is  $u_d[N]$ . The controller implements the  $u[1]$  from the calculated optimal collective pitch command. The optimization is repeated at every time step with the new measurements.

The response of the system in Eq. (5.15) can be written in matrix form as:

$$\begin{aligned}
 \begin{bmatrix} e[1] \\ e[2] \\ e[3] \\ e[4] \\ \vdots \\ e[T] \end{bmatrix} &= \begin{bmatrix} 0 & 0 & 0 & \dots & 0 \\ CB & 0 & 0 & \dots & 0 \\ CAB & CB & 0 & \dots & 0 \\ CA^2B & CAB & CB & \ddots & 0 \\ \vdots & \vdots & \vdots & \ddots & 0 \\ CA^{k-1}B & CA^{k-2}B & CA^{k-3}B & \dots & CB \end{bmatrix} \begin{bmatrix} u[0] \\ u[1] \\ u[2] \\ u[3] \\ \vdots \\ u[T-1] \end{bmatrix} + \\
 &\begin{bmatrix} 0 & 0 & 0 & \dots & 0 \\ CB_d & 0 & 0 & \dots & 0 \\ CAB_d & CB_d & 0 & \dots & 0 \\ CA^2B_d & CAB_d & CB_d & \dots & 0 \\ \vdots & \vdots & \vdots & \ddots & 0 \\ CA^{k-1}B_d & CA^{k-2}B_d & CA^{k-3}B_d & \dots & CB_d \end{bmatrix} \begin{bmatrix} u_{dm}[0] \\ u_{dm}[1] \\ u_{dm}[2] \\ u_{dm}[3] \\ \vdots \\ u_{dm}[T-1] \end{bmatrix} + \quad (5.17) \\
 &\begin{bmatrix} CA \\ CA^2 \\ CA^3 \\ \vdots \\ CA^k \end{bmatrix} x[0]
 \end{aligned}$$

Let  $\bar{e}$  denote the stacked vector of  $e[1], e[2], \dots, e[T]$  that appears in Equation (5.17). Similarly, let  $\bar{u}$  and  $\bar{u}_{dm}$  denote the stacked vectors of  $u[k]$  and  $u_{dm}[k]$  for  $1 \leq k \leq T - 1$ . Define  $M_1$  and  $M_2$  as the Toeplitz matrices that multiply  $\bar{u}$  and  $\bar{u}_{dm}$  in Equation (5.17). Define  $M_3$  as the matrix that multiplies  $x[0]$  in Eq. (5.17). Now the optimization

described in Equation (5.16) can be formulated as:

$$\begin{aligned}
& \min_{\bar{u}, \gamma} \gamma \\
& \text{subject to: } -\gamma \leq M_1 \bar{u} + M_2 \bar{u}_{dm} + M_3 x[0] \leq \gamma \\
& \quad -r\mathbf{1} \leq M_4 \bar{u} \leq r\mathbf{1} \\
& \quad u_{dm}[k] = \begin{cases} u_d[k] & \text{if } k < N \\ u_d[N] & \text{if } k \geq N \end{cases}
\end{aligned} \tag{5.18}$$

where  $\gamma$  is a slack variable,  $\mathbf{1} \in \mathbb{R}^T$  is a vector of ones, and  $M_4$  is the difference operator given by the matrix in Equation (5.19).

$$M_4 = \begin{bmatrix} 1 & 0 & 0 & \dots & 0 \\ -1 & 1 & 0 & \dots & 0 \\ 0 & -1 & 1 & \dots & 0 \\ \vdots & \vdots & \vdots & \ddots & \vdots \\ 0 & 0 & \dots & -1 & 1 \end{bmatrix} \tag{5.19}$$

This problem has a linear cost subject to linear equality constraints. This is a linear programming problem and more details can be found in the textbook by Vandenberghe and Boyd [88]. Linear programs (LPs) are convex problems and efficient software exists to solve problems with thousands of constraints and decision variables.

### 5.5.2 Analysis of a 50-Year Gust

This section uses the linear programming framework presented in Section 5.5.1 to analyze the performance versus preview characteristics for a 50-year gust. Preview information is used to overcome the performance limitations imposed by pitch rate constraints. The wind turbine considered for this analysis is the three-bladed Controls Advanced Research Turbine (CART3) [59] located at the National Wind Technology Center (NWTC). A one-state LTV model of the turbine is obtained from a higher complexity nonlinear model in NREL's FAST [51] code. The linearization is obtained at uniform hub-height wind speed of  $18m/s$ . The trim rotor speed is  $3.881rad/s$  and the trim blade pitch angle is  $16.5deg$ . Since the rotor dynamics do not have a strong dependence on rotor position, the LTV system matrices are averaged over one rotor period to obtain an LTI

model. The resulting one-state model is:

$$\begin{aligned}\dot{\delta}_{\omega_r}(t) &= a\delta_{\omega_r}(t) + b\delta_{\beta}(t) + c\delta_v(t) \\ e(t) &= \delta_{\omega_r}(t)\end{aligned}\tag{5.20}$$

where  $\delta_{\omega_r}(t)$  is the rotor speed error in  $rad/s$ ,  $\delta_{\beta}(t)$  is the difference between collective pitch angle and trim pitch in  $deg$ , and  $\delta_v(t)$  is the uniform hub-height wind perturbation in  $m/s$ . The numerical values of these parameters are  $a = -0.2771$ ,  $b = -0.0527$  and  $c = 0.0731$ . The blade pitch actuators of CART3 can be modeled with first-order transfer functions with  $30 rad/s$  bandwidth:

$$\dot{\delta}_{\beta}(t) = -30\delta_{\beta}(t) + 30\delta_{\beta_{cmd}}(t)\tag{5.21}$$

We combine the actuator model with the one-state linear model of CART3 in Eq. (5.20). This two-state model is discretized using the zero-order-hold method at a sampling time of  $T_s = 0.05s$ . The resulting discrete-time turbine model is:

$$\begin{aligned}\begin{bmatrix} \delta_{\omega_r}[k+1] \\ \delta_{\beta}[k+1] \end{bmatrix} &= \begin{bmatrix} 0.9862 & -0.0014 \\ 0 & 0.2231 \end{bmatrix} \begin{bmatrix} \delta_{\omega_r}[k] \\ \delta_{\beta}[k] \end{bmatrix} + \begin{bmatrix} 0.0036 & -0.0013 \\ 0 & 0.7769 \end{bmatrix} \begin{bmatrix} \delta_v[k] \\ \delta_{\beta_{cmd}}[k] \end{bmatrix} \\ e[k] &= \begin{bmatrix} 1 & 0 \end{bmatrix} \begin{bmatrix} \delta_{\omega_r}[k] \\ \delta_{\beta}[k] \end{bmatrix}\end{aligned}\tag{5.22}$$

The wind condition investigated for performance versus preview trends is a 50-year extreme wind gust. Chapter 4 of the Germanischer Lloyd certification standards [45] defines this wind profile as:

$$v(h, t) = V_{avg}(h) - 0.37V_{gust} \sin\left(\frac{3\pi t}{14}\right) \left(1 - \cos\left(\frac{2\pi t}{14}\right)\right)\tag{5.23}$$

where  $V_{avg}(h)$  is the average wind speed at height  $h$ ,  $0 < t < 14 s$  is the time and the  $V_{gust}$  is the gust amplitude given as :

$$V_{gust} = \frac{6.4\sigma_u}{1 + 0.2\frac{R}{\Lambda}}\tag{5.24}$$

where  $\sigma_u$  is the standard deviation of the turbulent wind speed fluctuations and  $\Lambda$  is the turbulence scale parameter.  $\Lambda$  is the minimum of 0.7 times of hub height or  $21 m$ . The numerical values used for these parameters are  $V_{avg} = 18 m/s$ ,  $\sigma_u = 0.18$ ,  $\Lambda = 21 m/s$  and  $R = 20 m$ . The resulting wind gust is shown in Figure 5.16.

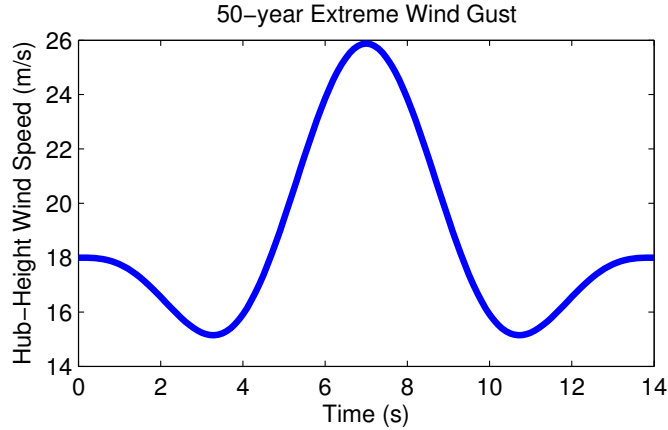


Figure 5.16: A 50-year extreme gust as defined by IEC-61400-1

We assume a  $T_{prev}$  seconds or  $N := \frac{T_{prev}}{T_s}$  time-steps of preview information is available where  $N$  is assumed to be an integer. The optimization problem in Eq. (5.16) is solved for a window  $T = N + N^*$  of time steps where  $N^*$  is the number of steps sufficient for one full rotor rotation at its rated speed. The wind speed after  $N$  time steps preview window is assumed to be constant, i.e.  $u_d[k] = u_d[N]$  for  $N < k \leq N^*$ . The first time step of the optimal pitch input solution is implemented, and the optimization is repeated with the newly available preview data and the initial conditions from the last time step. The CART3 has a blade pitch rate limit of  $18deg/s$  but this analysis is conducted for a pitch rate limit of  $6deg/s$ . At the sample time of  $T_s = 0.05s$ , the  $6deg/s$  rate limit is equivalent to a discrete-time rate bound of  $r = 0.3deg$  per sample time. The choice of using  $6deg/s$  pitch-rate limits was explained in 5.4.1. In summary, controllers designed on this low order model may use higher pitch rates on higher-fidelity simulations.

The linear program in Equation (5.16) is solved for the one-state turbine model using SeDuMi [89] in MATLAB. Solutions are obtained for preview times of  $T_{prev} = 0, 0.1, 0.2, \dots, 2.0$  seconds. It is assumed that the turbine is initially at trim, i.e.  $\delta_{\omega_r}[0] = 0$ ,  $\delta_{\beta}[0] = 0$  and  $\delta_v[0] = 0$ . Results with preview times larger than  $2s$  yield same results as the  $2s$  preview case. The top plot in Figure 5.17 shows the ultimate performance limits obtained from the linear programs as a function of the time. Performance improvements

are obtained until 1.7s of preview. The best performance is approximately 5.5 times better than the performance with no preview. It is important to keep the peak tracking error,  $\|\delta_{\omega_r}\|_{\infty}$ , under  $0.1164\text{rad/s}$  for CART3 to avoid the generator from overspeeding and sustaining physical damage. The performance with no preview is sufficient for avoiding the rotor overspeed.

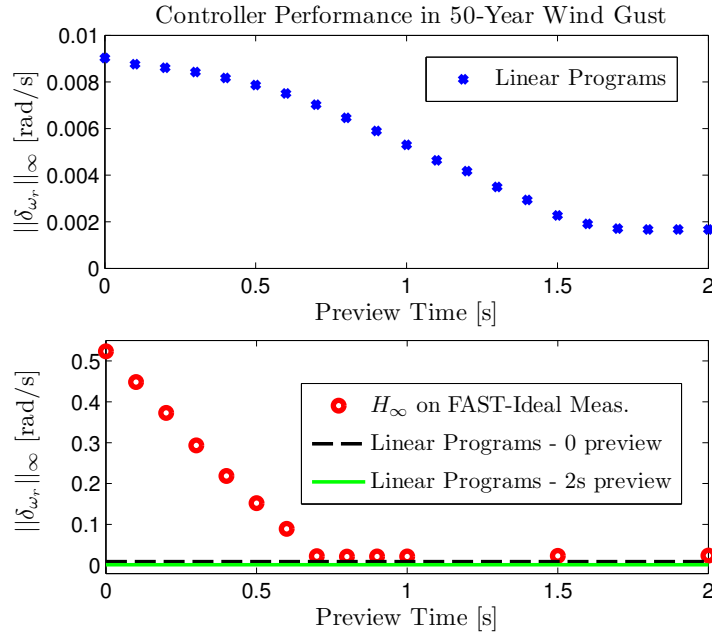


Figure 5.17: Peak Positive Rotor Speed Error with varying preview wind amounts

The bottom plot in the Figure 5.17 presents the performance of the  $H_{\infty}$  controller on FAST simulations. These are the same  $H_{\infty}$  controllers used in Section 5.4.2. The red circles show the performance of these controllers with ideal preview measurements of the average hub-height wind speed across the rotor. The green solid and black dashed lines show the ultimate performance limits predicted by the linear programs with no and 2s preview. The  $H_{\infty}$  controllers with preview less than 0.4s are not able to avoid the generator overspeed problem. The performance of these controllers improve until 0.8s preview. Even with a long preview time the performance is worse than the performance limits that can be achieved with no preview. There are two possible explanations to the trends observed in this figure. First, it is possible that the  $H_{\infty}$  controllers are poorly designed to handle this extreme gust event. Second, the two-state linear model

used for analysis may not be accurately capturing the turbine dynamics accurately that occur in peak gust scenarios. The following procedure can be followed to investigate this problem. First, the MPC controller that rely on linear programs can be implemented on the FAST code. If large tracking errors are observed with MPC controllers on FAST, the accuracy of the linear model can be further investigated. If the tracking errors are small, this would imply that the  $H_\infty$  controllers are poorly designed. The  $H_\infty$  controllers can be modified to have higher disturbance rejection in the frequency range of the spectra of the extreme gust.

### 5.5.3 Generalizations

The optimization problem presented in Equation (5.16) can be generalized in various ways to represent other turbine control problems of interest. First, this problem can be generalized to MIMO systems. This allows analyzing problems such as individual pitch control. A more detailed description of the wind field can also be used. Second, blade, tower and gearbox bending loads can be incorporated into the constraints and/or cost function. This generalization would be useful for a more precise formulation of the structural load reduction problems. The peak norm, i.e.  $\|y\|_\infty$  norm, could be used to measure the peak bending load. However, some initial investigations have indicated that the total variation as  $TV = \sum_{n=0}^{k-1} |y[n+1] - y[n]|$  is better suited for measuring fatigue. The total variation is a measure of the variation of a signal from one time step to the next one. Minimization of this quantity results in smoother bending loads and reduced variations. In the ideal case, zero total variation corresponds to a constant load and hence zero fatigue. Hence there is a good correlation between minimization of the total variation and the damage equivalent loads that are commonly used for evaluation of the performances of controllers for load attenuation. Optimizations involving TV in the constraints and/or objective function can be formulated as LPs. To summarize, the LP framework can be used to investigate the effect of preview time on more complicated wind turbine control problems involving constraints and objective functions that depend on rotor speed tracking, bending loads, and/or blade pitch deflection and rate limits.

## 5.6 Conclusions

Our results for optimal Region 2 control show that simultaneous power capture improvements and gearbox load reductions can be obtained with the use of preview. We also show that the standard control law  $K\omega_r^2$  is not Pareto optimal in turbulent wind conditions. In other words, there exists a control input for which power is increased and loads are reduced relative to the standard control law. Furthermore the distance between the Pareto optimal front and the  $K\omega_r^2$  law increases with increasing turbulence intensities.

It is seen that the use of preview information in Region 2 control laws is a promising concept. In the ideal case a 6% extra power can be captured with the similar gearbox load levels seen with the standard law. Preview allows the controller to speed up the slow responding rotor before the onset of the gust such that when the gust hits, the turbine reaches the optimal tip speed ratio for power capture. These gusts carry a large amount of energy and it is important to capture as much of this energy as possible. The 6% increase in power capture is a significant amount for wind energy industry. For a 100MW wind farm operating at 35% capacity factor, a 6% increase in power corresponds to an extra US\$738,000 profit per year at a cost of energy of US\$0.04 per kilowatt-hour [90].

Another important Region 2 control result is the strong trade-off between power capture and gearbox loads in high turbulence levels. The evaluation of the economic benefits of the preview control is more challenging to determine because currently there are no models exist in the literature that can estimate the economic benefits of structural load reduction. Therefore it is not possible to conclude if some extra power capture can be economically justified if there is an increase in the gearbox loads. Developing models that relate structural fatigue and peak load reduction to turbine costs is an important open area of research in wind turbine control literature both for Region 2 and 3 control research.

Our Region 3 results investigated the relationship between turbine performance, preview time and blade pitch rate limits. Three three key conclusions can be drawn from these results. First, performance improves linear with small preview times. Second,

there is a fundamental preview time beyond which no additional performance improvement can be obtained. Third, this fundamental preview time is proportional to the step gust magnitude and inversely related to pitch actuator rate limit. The conclusions were validated with more realistic CART3 nonlinear simulations. The medium-fidelity simulations showed similar trends for rotor speed tracking and tower structural loads. However, it was also observed that the error characteristics of the preview wind sensors can play an important role in turbine performance. Thus longer preview times may be required than those predicted from the low-fidelity model. Unfortunately evaluating the economic benefits of improved control performance in Region 3 is not possible due to lack of economic models for structural load reduction.

We have provided a framework that can be used to analyze turbine performance limits during extreme gust events. We have analyzed an example 50-year gust case. Results show that the preview requirements for these extreme cases can be different than the preview requirements for Region 3 control.

## Chapter 6

# Conclusions and Recommendations

This thesis considered two aspects of wind turbine control. The first aspect is the automated tuning of advanced  $H_\infty$  multivariable controllers. In Chapter 4 we propose a preliminary control design framework to tune first-order design weights. The objective was to improve a combination of time and frequency domain performance metrics such as damage equivalent loads, peak loads and the damping of tower modes. The optimization was observed to converge to a local optima successfully while improving performance objectives. These mathematical optimization tools can reduce the burden of design weight selection from control engineers in industry. Simplification of this design process is important for transition of advanced multivariable controllers to industry.

The second aspect we considered is the use of preview wind measurements in turbine closed-loop controllers. Our research in Chapter 5 shows that different amount of preview times are required in Region 2, Region 3 and extreme wind conditions. This is because the preview wind information is used to address different control challenges in these operating conditions. The following questions were investigated for each operating condition: How much preview is necessary? How much performance improvement can be obtained? We have used various tools from the optimal control literature to quantify these ultimate performance limits given any controller. These performance limits are important to decide if the use of these sensors can be justified from an economic point

of view.

In Region 2 the preview is used to overcome the slow rotor speed response to control due to the large rotor inertia. A nonlinear optimal control problem formulation is presented to study the Pareto optimal trade-off between the power capture maximization and gearbox load reduction objectives in this region. This formulation also allows investigating the impact of the wind turbulence levels on this trade-off. The presented framework is used to analysis the preview time requirements and the optimal performance bounds for the NREL's CART3 turbine. It was seen that long preview times that push the boundaries of the continuous wave LIDARs are required in this region. A simultaneous performance increase in power capture maximization and gearbox load reduction is possible with the use of preview wind measurements. The performance benefits of preview increase with higher wind turbulence.

Preview wind measurements are used to overcome the blade pitch-rate limits in Region 3 operation and during extreme wind events. This thesis provided analytical formulas based on a one-state rigid body rotor-inertia model that can be used to predict the preview time requirements in Region 3 operation. These formulas also predict the minimum rotor speed tracking error achievable as a function of the preview time. There are three key observations in these formulas. First, rotor speed tracking performance improves linearly with small preview times. Second, there is a fundamental preview time beyond which no performance improvement is obtained. Third, this fundamental preview time is proportional to the magnitude of a step wind gust that can be used to approximate the frequency spectra of the wind fluctuations at the turbine side. The fundamental preview time is inversely proportional to the blade pitch-rate limits. A medium-fidelity model of the CART3 turbine is used to validate the trends observed in the provided analytical formulas.  $H_\infty$ -optimal multivariable controllers designed for this model validated these trends. It is also observed that the preview time requirements in Region 3 control are significantly shorter than the Region 2 operation. These short preview times pose challenges for continuous wave LIDARs. It is seen that the error characteristics of these sensors may necessitate longer preview times than what is found with ideal measurements. Finally, this thesis provided a numerical method to extend these results to analyze the preview time requirements and the performance bounds during extreme wind events.

The results presented in this thesis leave several open topics for future research. These areas are:

- **Optimization and controller structures for Region 3 controller auto-tuning:** We used a simple gradient based nonlinear optimization method for auto-tuning. This approach ignores the specific properties of the cost and constraint functions. For instance, the optimization cost included damage-equivalent load calculation via rainflow cycle counting in time-domain [91]. This is a non-integrable, non-smooth function that can be challenging for generic gradient based optimization tools. Specific tools for such functions can be investigated to improve performance.

The auto-tuned controller was based on a linear turbine model obtained at a single operating condition. It is known that variations in wind speed and blade pitch angle lead to model variations. One common approach to address this problem is the use of linear, parameter-varying (LPV) control techniques. There exists various turbine Region 3 LPV control approaches in literature that use blade pitch angle as the scheduling parameter. Incorporating these LPV design approaches in our auto-tuning tools has a potential to further improve turbine performance.

Another control design challenge in industry is the transition between Regions 2 and 3. This transition is challenging due to two reasons. First, advanced multi-variable controllers have a large number of abstract states that are hard to relate to physical turbine variables. This brings state initialization challenges. Second, the distinction between these regions are based on wind speed, which is a low quality measurement with anemometers. One solution is to work with a controller structure that can operate both in Regions 2 and 3. A linear controller is the easiest approach, but has its challenges. The Region 2 control aim is to make the rotor speed track a constant multiple of the wind speed. However, this is a low quality measurement with anemometers. One potential approach is to use of a LIDAR for reliable wind speed measurements. This controller can track the desired rotor speed in Region 2 while keeping it constant in Region 3. The tuning of the parameters of this unified controller can be done with the optimization tools investigated in this thesis.

- **Turbine preview control:** Our research assumed a specific preview wind measurement location and pattern. We have used three point wind measurements at the 75% blade span of the CART3 turbine blades. The average of these three measurements were fed into the controller. This decision was based on the knowledge that most of the power generation is obtained at the outer sections of the blades. However, the optimal measurement location or the pattern is not known. This issue is further complicated by the measurement errors. The error characteristics of preview wind sensors should also be considered when investigating the optimal measurement location and patterns. The question 'what to measure' is an important future research direction to investigate.

The second research direction of interest is the use of physically motivated cost functions in optimal preview control design. We have used various abstract mathematical cost functions in place of actual turbine performance metrics of interest. In Section 5.3 we have used signal two-norm of the generator torque command to approximate the damage-equivalent loads. An approximation that has a higher correlation with the damage-equivalent loads would improve the applicability of this research. In Section 5.4 we have only used the peak rotor speed error in our optimal control problem formulation. We have relied on the correlation between peak loads and the peak rotor speed tracking error. However, peak loads are only one aspect of the load reduction. Fatigue minimization is also important in turbine design. Similar to the Region 2 problem, introduction of a realistic approximation to damage-equivalent loads in this problem formulation is important to analyze for performance versus preview characteristics.

Third, we have only considered the impact of preview on performance during normal operating conditions. The benefits of preview in extreme operating cases should also be investigated. Extreme cases such as 50-year gusts or sudden wind direction changes can drive the turbine design. It is important to investigate how much of the effects of these extreme situations can be attenuated with preview wind measurements.

Lastly, there is a need for cost models that relate the peak loads and fatigue in tower, blades and gearbox to a monetary value. Different controllers can involve

trade-offs between these loads as well as the power capture. The controllers that yield the minimum structural cost and the maximum power capture can be chosen with the help of these cost models. This also allows expressing the performance improvements obtained with preview in terms of an economic value. This can answer the question if the use of expensive preview sensors is justified.

- **Experimental verification of theoretical results:** We have verified several of our results in Chapters 4 and 5 through medium-fidelity simulations. However, field testing is important for the ultimate verification of the applicability of these results. University of Minnesota's 2.5 MW Clipper Liberty C96 turbine is a potential test bed for these experiments, but several steps will need to precede. First, a medium to high-fidelity turbine model should be built. This is useful for simulation testing of algorithms on this specific turbine. Second, an implementation and safety system should be developed. The implementation system would allow using experimental controllers and be responsible for smooth transitions between the default and these controllers. The safety system would be responsible for overseeing certain measurements that are key to turbine health such as the rotor speed or structural loads. Emergency stop procedures would be triggered in case of an anomaly. These steps are currently being pursued.

# References

- [1] DOE Office of Energy Efficiency and Renewable Energy. Inside the wind turbine. [http://www1.eere.energy.gov/wind/inside\\_a\\_wind\\_turbine.html](http://www1.eere.energy.gov/wind/inside_a_wind_turbine.html), 2012.
- [2] Clipper turbine from dutch hill/cohocton wind farm near cohocton, new york. <http://www.flickr.com/photos/40765798@N00/2802139997/>, 2008.
- [3] A.D. Wright, P. Fleming, and J. van Wingerden. Refinements and tests of advanced controller to mitigate fatigue loads in the controls advanced research turbine. In *49th AIAA Aerospace Sciences Meeting and Exhibit*, 2011.
- [4] Ryan Wisser and Mark Bolinger. 2011 wind technologies market report. Technical report, U. S. Department of Energy, 2012.
- [5] U. S. Department of Energy. 20% Wind Energy by 2030: Increasing Wind Energy's Contribution to US Electricity Supply. Technical report, U. S. Department of Energy, Washington, DC, 2008.
- [6] Hermann-Josef Wagner and Jyotirmay Mathur. *Introduction to Wind Energy systems*. Springer, 2009.
- [7] Tony Burton, David Sharpe, Nick Jenkins, and Ervin Bossanyi. *Wind Energy Handbook*. John Wiley & Sons, 1st edition, 2001.
- [8] E. A. Bossanyi. The design of closed loop controllers for wind turbines. *Wind Energy*, 3:149–163, 2000.
- [9] L.Y. Pao and K. Johnson. A tutorial on the dynamics and control of wind turbines and wind farms. In *Proceedings of American Control Conference*, pages 2076–2089, St. Louis, Missouri, 2009.

- [10] J.F. Manwell, J.G. McGowan, and A.L. Rogers. *Wind Energy Explained: Theory, Design, and Applications*. John Wiley & Sons, 2010.
- [11] Clipper Windpower Vestas Wind Systems A/S. Liberty 2.5 mw product brochure. <http://www.clipperwind.com/productline.html>, 2010.
- [12] Jason H. Laks, Lucy Y. Pao, and Alan D. Wright. Control of wind turbines: Past, present, and future. In *Proceedings of American Control Conference*, pages 2096–2103, St. Louis, Missouri, 2009.
- [13] S. Suryanarayanan and A. Dixit. Control of large wind turbines: Review and suggested approach to multivariable design. In *Proc. of the National Conference on Control and Dynamic Systems*, Mumbai, India, 2005.
- [14] A. Dixit and S. Suryanarayanan. Towards pitch-scheduled drive train damping in variable-speed, horizontal-axis large wind turbines. In *IEEE Conference on Decision and Control*, pages 1295–1300, 2005.
- [15] K.E. Johnson, L.J. Fingersh, M.J. Balas, and L.Y. Pao. Methods for increasing region 2 power capture on a variable-speed wind turbine. *Journal of solar energy engineering*, 126:1092, 2004.
- [16] Jan-Willem Van Wingerden. *Control of Wind Turbines with 'Smart' Rotors: Proof of Concept and LPV Subspace Identification*. PhD thesis, Delft University of Technology, 2008.
- [17] K. Selvam, S. Kanev, J. W. van Wingerden, T. van Engelen, and M. Verhaegen. Feedback-feedforward individual pitch control for wind turbine load reduction. *International Journal of Robust and Nonlinear Control*, 19(1):72–91, 2008.
- [18] Karl A. Stol and Mark J. Balas. Periodic disturbance accommodating control for blade load mitigation in wind turbines. *Journal of Solar Energy Engineering*, 125(4):379–385, 2003.
- [19] K.A. Stol, W. Zhao, and A.D. Wright. Individual blade pitch control for the controls advanced research turbine (CART). *Journal of Solar Energy Engineering*, 128:498, 2006.

- [20] A.A. Ozdemir, P.J. Seiler, and G.J. Balas. Performance of disturbance augmented control design in turbulent wind conditions. *Mechatronics*, 2011.
- [21] K.E. Johnson, L.Y. Pao, M.J. Balas, and L.J. Fingersh. Control of variable-speed wind turbines: standard and adaptive techniques for maximizing energy capture. *Control Systems Magazine, IEEE*, 26(3):70–81, Jun. 2006.
- [22] K.E. Johnson and L.J. Fingersh. Adaptive pitch control of variable-speed wind turbines. *ASME Journal of Solar Energy Engineering*, 130, 2008.
- [23] M. J. Grimble. Horizontal axis wind turbine control: Comparison of classical, LQG and  $H_\infty$  designs. *Dynamics and Control*, 6(2):143–161, 1996.
- [24] Alan D. Wright and Mark J. Balas. Design of controls to attenuate loads in the controls advanced research turbine. *ASME Journal of Solar Energy Engineering*, 126(4):1083–1091, 2004.
- [25] E. A. Bossanyi. Individual blade pitch control for load reduction. *Wind Energy*, 6(2):119–128, 2003.
- [26] E. A. Bossanyi. Further load reductions with individual pitch control. *Wind energy*, 8(4):481–485, 2005.
- [27] Karl A. Stol and Mark J. Balas. Full-state feedback control of a variable-speed wind turbine: A comparison of periodic and constant gains. *Journal of Solar Energy Engineering*, 123(4):319–326, 2001.
- [28] M. Geyler and P. Caselitz. Robust multivariable pitch control design for load reduction on large wind turbines. *Journal of Solar Energy Engineering*, 130(3):031014, 2008.
- [29] B. Connor, S.N. Iyer, W.E. Leithead, and M.J. Grimble. Control of a horizontal axis wind turbine using  $H_\infty$  control. In *Control Applications, 1992., First IEEE Conference on*, volume 1, pages 117–122, September 1992.
- [30] M.L. Lima, J.L. Silvino, and P. de Resende.  $H_\infty$  control for a variable-speed adjustable-pitch wind energy conversion system. In *Industrial Electronics, 1999.*

- ISIE '99. Proceedings of the IEEE International Symposium on*, volume 2, pages 556–561, 1999.
- [31] J. Laks, L. Pao, A. Wright, N. Kelley, and B. Jonkman. Blade pitch control with preview wind measurements. In *48th AIAA Aerospace Sciences Meeting and Exhibit*, pages AIAA–2010–251, 2010.
- [32] J. Laks, L. Pao, and A. Wright. Combined Feed-forward/Feedback control of wind turbines to reduce blade flap bending moments. In *47th AIAA Aerospace Sciences Meeting*, pages AIAA–2009–687, 2009.
- [33] Jason Laks, Lucy Y. Pao, Eric Simley, Alan Wright, and Neil Kelley. Model predictive control using preview measurements from lidar. In *49th AIAA Aerospace Sciences Meeting*, pages AIAA–2011–813, 2011.
- [34] A. A. Kumar and K. A. Stol. Simulating MIMO Feedback Linearization Control of Wind Turbines Using FAST. In *46th AIAA Aerospace Sciences Meeting and Exhibit*, 2008.
- [35] A.D. Wright, K.A. Stol, and L.J. Fingersh. Progress in implementing and testing state-space controls for the controls advanced research turbine. In *43rd AIAA Aerospace Sciences Meeting and Exhibit*, pages 1–13, 2005.
- [36] J. B. Freeman and M. J. Balas. An investigation of variable speed horizontal-axis wind turbines using direct model-reference adaptive control. In *1999 ASME Wind Energy Symposium, 18 th, AIAA, Aerospace Sciences Meeting and Exhibit, 37 th, Reno, NV*, pages 66–76, 1999.
- [37] Karl A. Stol. *Dynamics Modeling and Periodic Control of Horizontal-Axis Wind Turbines*. PhD thesis, University of Colorado at Boulder, Boulder, Colorado, 2001.
- [38] A. D. Wright. Modern control design for flexible wind turbines. Technical report, National Renewable Energy Laboratory, 2004.
- [39] A.D. Wright. *Control Design for Flexible Wind Turbines*. PhD thesis, University of Colorado, Boulder, 2003.

- [40] A. D. Wright, L. Fingersh, and M. J. Balas. Testing state-space controls for the controls advanced research turbine. *ASME Journal of Solar Energy Engineering*, 128(4):506–515, 2006.
- [41] A. Wright and K. Stol. Designing and testing controls to mitigate dynamic loads in the controls advanced research turbine. Technical Report NREL/CP-500-42490, NREL, 2008.
- [42] A.D. Wright, L.J. Fingersh, and K. A. Stol. Field testing controls to mitigate fatigue loads in the controls advanced research turbine. In *47th AIAA Aerospace Sciences Meeting and Exhibit*, 2009.
- [43] A.D. Wright, L.J. Fingersh, and K. A. Stol. Testing further controls to mitigate loads in the controls advanced research turbine. In *48th AIAA Aerospace Sciences Meeting and Exhibit*, 2010.
- [44] IEC 61400-1: Wind turbines part 1: Design requirements, 2005.
- [45] Guideline for the certification of wind turbines, 2010.
- [46] E.H. Dowell and K.C. Hall. Modeling of fluid-structure interaction. *Annual Review of Fluid Mechanics*, 33(1):445–490, 2001.
- [47] Y. Bazilevs, M.C. Hsu, I. Akkerman, S. Wright, K. Takizawa, B. Henicke, T. Spielman, and TE Tezduyar. 3d simulation of wind turbine rotors at full scale. part i: geometry modeling and aerodynamics. *International Journal for Numerical Methods in Fluids*, 65(1-3):207–235, 2011.
- [48] Y. Bazilevs, M.C. Hsu, J. Kiendl, R. Wüchner, and K.U. Bletzinger. 3d simulation of wind turbine rotors at full scale. part ii: fluid–structure interaction modeling with composite blades. *International Journal for Numerical Methods in Fluids*, 65(1-3):236–253, 2011.
- [49] R.W. Clough and J. Penzien. *Dynamics of structures*, volume 19. McGraw-Hill, 1975.
- [50] L. Meirovitch. *Dynamics and Control of Structures*. Wiley New York, 1990.

- [51] Jason M. Jonkman and Jr. Marshall L. Buhl. *FAST User's Guide*. National Renewable Energy Laboratory, Golden, Colorado, 2005.
- [52] A. C. Hansen. *User's Guide to the Wind Turbine Dynamics Computer Programs YawDyn and AeroDyn for ADAMS version 11.0*. Mech. Eng. Dept. University of Utah, Golden, Colorado, 1998.
- [53] Matt Churchfield and Sang Lee. *Overview of the Simulator for Offshore Wind Farm Application SOWFA*. National Renewable Energy Laboratory, Golden, Colorado, 2012.
- [54] B.J. Jonkman. *TurbSim User's Guide*. National Renewable Energy Laboratory, Golden, Colorado, 2009.
- [55] R. E. Wilson, S. N. Walker, and P. Heh. Technical and user's manual for the FAST\_AD advanced dynamics code. Technical report, Oregon State University, 1999.
- [56] M.L. Buhl Jr and A. Manjock. A comparison of wind turbine aeroelastic codes used for certification. In *44th AIAA Aerospace Sciences Meeting and Exhibit*, pages AIAA-2006-786, 2006.
- [57] Dayton A. Griffin. WindPACT turbine design scaling studies technical area 1-composite blades for 80-to 120-meter rotor. Technical report, National Renewable Energy Laboratory, 2001.
- [58] D. J. Malcolm and A. C. Hansen. WindPACT turbine rotor design study. Technical report, National Renewable Energy Laboratory, 2002.
- [59] Cart3 fast model, personal communication with a. wright, 2011.
- [60] ZephIR Ltd. ZephIR technical specification. <http://www.yourwindlidar.com/technical-specification-zephir>. Accessed: 09/30/2012.
- [61] Eric Simley, Lucy Y. Pao, Rod Frehlich, Bonnie Jonkman, and Neil Kelley. Analysis of Wind Speed Measurements using Continuous Wave LIDAR for Wind Turbine Control. In *49th AIAA Aerospace Sciences Meeting*, pages AIAA-2011-263, 2011.

- [62] R. B. Stull. *An introduction to boundary layer meteorology*. Springer, 1988.
- [63] W. Johnson. *Helicopter Theory*. Princeton University Press, 1st edition, 1980.
- [64] K. A. Stol, M. J. Balas, and G. Bir. Floquet modal analysis of a teetered-rotor wind turbine. *Journal of Solar Energy Engineering*, 124:364, 2002.
- [65] G.S. Bir, A.D Wright, and C.P. Butterfield. Stability analysis of a variable-speed wind turbine. In *AIAA Aerospace Sciences Meeting and Exhibit*, pages AIAA Paper 97-0965, 1997.
- [66] M.H. Hansen. Improved modal dynamics of wind turbines to avoid stall-induced vibrations. *Wind Energy*, 6:179-195, 2003.
- [67] Karl A. Stol, H.-G. Moll, G. Bir, and H. Namik. A comparison of multi-blade coordinate transformation and direct periodic techniques for wind turbine control design. In *Proceedings of the 47th AIAA/ASME*, pages AIAA-2009-479, Orlando, Florida, 2009.
- [68] D.J. Malcolm. Modal response of 3-bladed wind turbines. *Journal of Solar Energy Engineering*, 124:372, 2002.
- [69] G. Bir. Multi-blade coordinate transformation and its applications to wind turbine analysis. In *AIAA Wind Energy Symposium*, pages AIAA-2008-1300, Reno, Nevada, 2008.
- [70] G.S. Bir. *User's Guide to MBC3: Multi-Blade Coordinate Transformation Code for 3-Bladed Wind Turbines*. National Renewable Energy Laboratory, Golden, Colorado, 2010.
- [71] V.A. Riziotis, S.G. Voutsinas, E.S. Politis, and P.K Chaviaropoulos. Aeroelastic stability of wind turbines: the problem, the methods and the issues. *Wind Energy*, 7:373-392, 2004.
- [72] R. Coleman and A. Feingold. Theory of self-excited mechanical oscillations of helicopter rotors with hinged blades. Technical report, NASA, 1958.

- [73] Kemin Zhou, John C. Doyle, and Keith Glover. *Robust and Optimal Control*. Prentice Hall, 1st edition, 1996.
- [74] S. Skogestad and I. Postlethwaite. *Multivariable Feedback Control: Analysis and Design*. John Wiley, 1996.
- [75] G. Balas, R. Chiang, A. Packard, and M. Safonov. *Robust Control Toolbox*. MathWorks, 2010.
- [76] D. Bertsekas. *Nonlinear Programming*. Athena Scientific, 1999.
- [77] J. Nocedal and S.J. Wright. *Numerical Optimization*. Springer, 1999.
- [78] Jr. Marshall L. Buhl. *MCrunch User's Guide*. National Renewable Energy Laboratory, Golden, Colorado, 2008.
- [79] The Mathworks. *Matlab Optimization Toolbox User's Guide*, 2009.
- [80] A.A. Ozdemir, P. Seiler, and G.J. Balas. Design tradeoffs of wind turbine preview control. *Control Systems Technology, IEEE Transactions on*, 21(4):1143–1154, 2013.
- [81] A. Körber and R. King. Nonlinear model predictive control for wind turbines. In *Proceedings of the 2011 European Wind Energy Conference*, 2011.
- [82] A. Körber and R. King. Model predictive control for wind turbines. In *Proceedings of the 2010 European Wind Energy Conference*, 2010.
- [83] M. Soltani, R. Wisniewski, P. Brath, and S. Boyd. Load reduction of wind turbines using receding horizon control. In *IEEE International Conference on Control Applications*, pages 852 –857, 2011.
- [84] A.E. Bryson and Y.C. Ho. *Applied optimal control: optimization, estimation, and control*. Ginn and Company, 1969.
- [85] Peter Seiler, Ahmet Arda Ozdemir, and Gary J. Balas. Performance limits with preview information and actuator rate constraints. In *American Control Conference*, 2012.

- [86] S.P. Boyd and C.H. Barratt. *Linear controller design: limits of performance*. Prentice-Hall, 1991.
- [87] M.A. Dahleh and I.J. Diaz-Bobillo. *Control of uncertain systems: a linear programming approach*. Prentice-Hall, 1994.
- [88] S.P. Boyd and L. Vandenberghe. *Convex Optimization*. Cambridge University Press, 2004.
- [89] Jos F. Sturm. Using sedumi 1.02, a matlab toolbox for optimization over symmetric cones. Technical report, Tilburg University, 2001.
- [90] L.Y. Pao and K.E. Johnson. Control of wind turbines: Approaches, challenges and recent developments. *IEEE Control Systems Magazine*, 31(2):44–62, 2011.
- [91] Secil Ariduru. Fatigue life calculation by rainflow cycle counting method. Master's thesis, Middle East Technical University, 2004.